

6.5 Data Recovery After Removal of Contaminated Data

Data recovery statistics were prepared for each site after removal of contaminated data. These were calculated for the entire 24-h period and then separately for the nighttime distributions for three sites, Oroville (close to the foothills of the Sierra Nevada), Davis (in the southwestern corner of the Sacramento Valley), and Arbuckle (on the western side of the Sacramento Valley). During the daytime, data collection rates are typically about ninety percent to heights of a few kilometers. At night, these rates drop somewhat just above the nighttime boundary layer. At greater heights (above 3 or 4 km) there is little in the way of a diurnal signature. Figures 7.1a,b shows the comparison for Arbuckle for low-resolution (5-km range) and high-resolution (2.5-km range) modes, respectively. Comparison of high- and low-resolution modes for the full diurnal cycle and the nighttime-only cycle, shows comparable differences (10% to 20%) in both modes in the lower half of each profile. Because of the similarity of the recovery rates at the 3-km height and the observation that birds typically fly below 3 km (Appendix A), the differences can be attributed primarily to bird contamination. Figures 7.2a,b show results for Oroville that indicate a much larger reduction of almost 50% in the lowest 3 km; above 3 km, the recovery rates are almost identical. Inspection of individual days, using the graphical tools described in Appendix G, show a much higher prevalence of bird echoes from sites close to the eastern foothills. Figures 7.3a,b in mid-valley at Davis show a reduction intermediate between Arbuckle and Oroville.

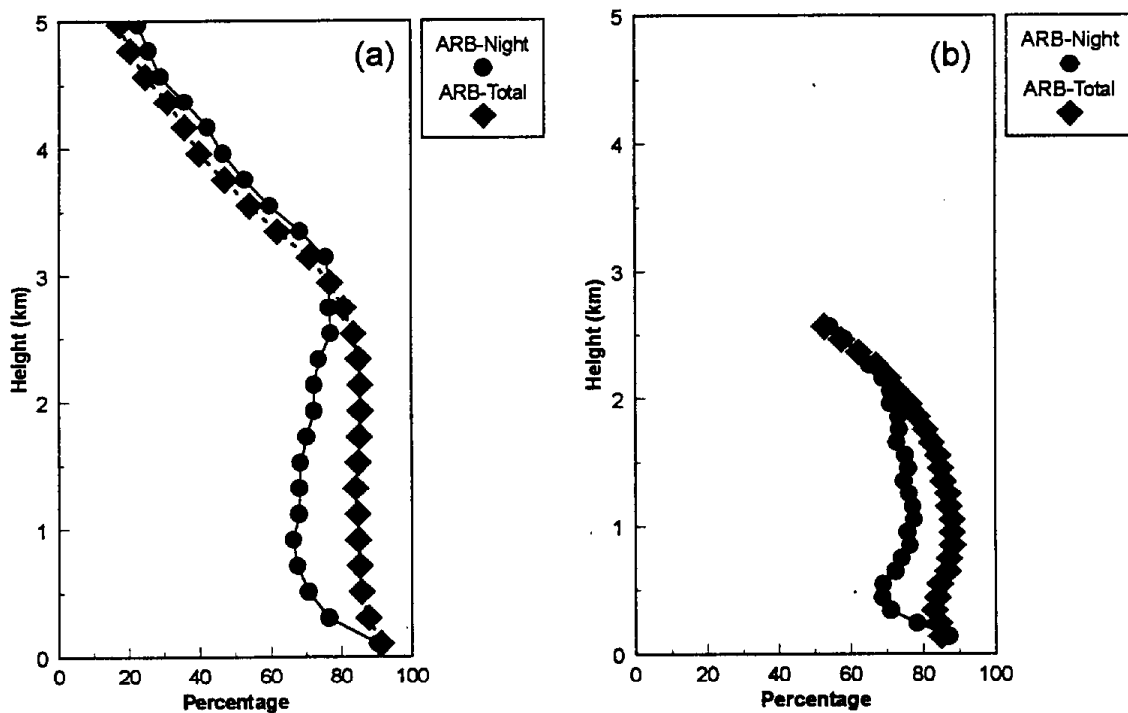


Figure 7.1 Profiler recovery rates as a function of elevation above ground level for Arbuckle (ARB) and separated by low-resolution (a) and high-resolution (b) modes and nighttime (Night) and full diurnal period (Total).

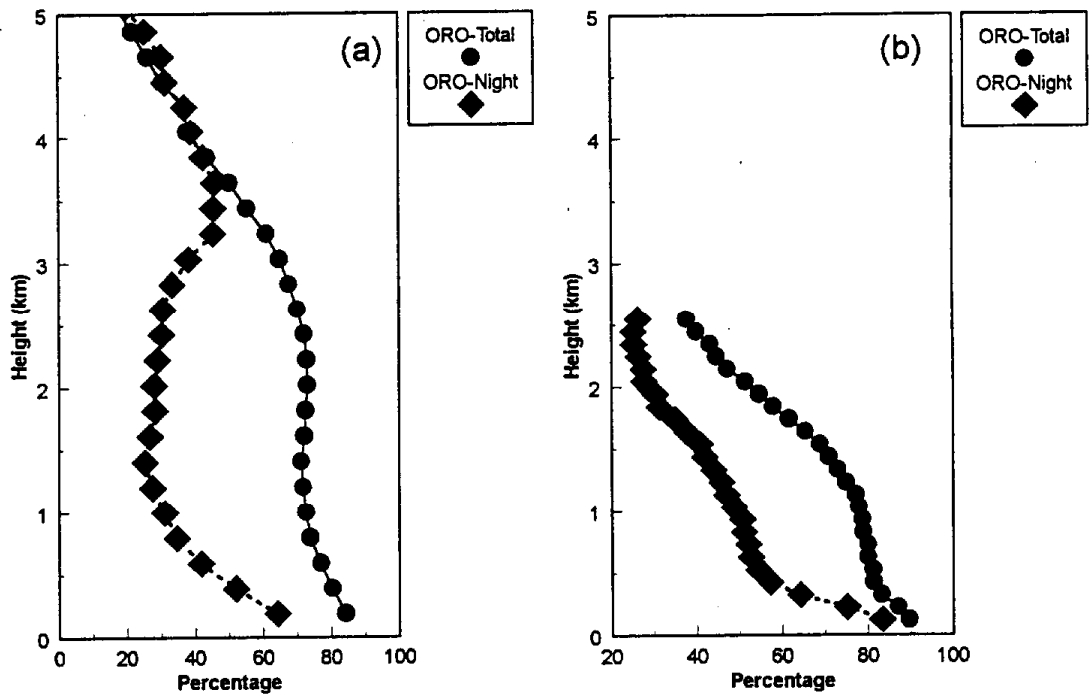


Figure 7.2 Profiler recovery rates as a function of elevation above ground level for Oroville (ORO) and separated by high- and low-resolution modes and nighttime (Night) and full diurnal period (Total).

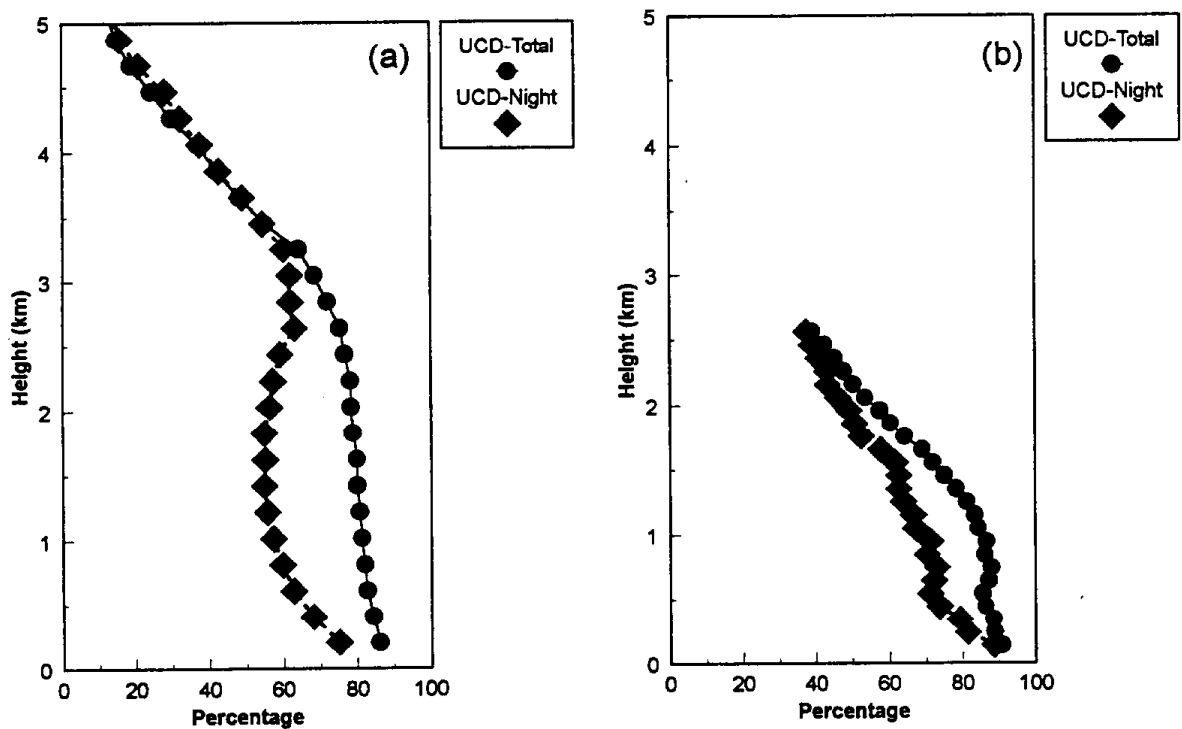


Figure 7.3 Profiler recovery rates as a function of elevation above ground level for Davis (UCD) and separated by high- and low-resolution modes and nighttime (Night) and full diurnal period (Total).

7 WIND DISTRIBUTIONS

7.1 Introduction

Several tasks related to the generation of wind distribution statistics. We sought in these to separate different meteorological regimes relative to the observation of high and low ozone occurrences. In particular, we examined data from the NCT (Northern California Transport) and NCCT (North Central Coast Transport) portion of our study to demonstrate how these data could be used. We found that both scatter plots of wind speed and direction on x-y plots were useful as well as speed distributions as a function of directional class interval and stratified according to the presence of synoptic scale ridges and troughs (corresponding generally to high and low ozone periods, respectively). We have included these latter data in this section; the scatter plots are voluminous and can be viewed from the data base in the workstation environment.

7.2 Discussion of Results

Results from all eleven wind profiler sites are presented in the graphs at the end of this section. As discussed previously, there were a total of eight wind profilers deployed during NCT and three of them were moved south in late August. Table 4 presents summaries of the time period of operations, total days available, case days, range resolution, and first level (above ground level) heights for each site. Data were stratified according to pressure patterns at mid-level (500-hPa) in the atmosphere: a ridge pattern is normally characterized by sinking air (conducive to clear skies) and warm, stagnant air near the surface; a trough pattern is associated usually with rising air (conducive to cloud formation) and disturbed weather. The 500-hPa ridge and trough cases were chosen for their longest persistence so that we would be able to analyze as similar conditions as possible in each case. The period of the trough case was July 15-20 and the period of the ridge case was September 14-24. The NCCT Study which occurred very late summer and early fall and consisted of the HOL, MOS and BEA sites (see the map in Fig. 1) were actually separated into low and high ozone cases rather than ridge and trough because there were no persistent ridging and troughing over the area during this study. The ozone for NCCT Study was measured at Pinnacles National Monument. Daily peak ozone concentrations were used to segregate days into high ozone cases (8.5 pphm or greater) and low ozone cases (6.0 pphm or less). It should be noted that we have not specifically examined violation days but rather the meteorological factors associated with relative differences of high and low cases as a demonstration of the utility of profiler technology.

Table 5 presents an overall summary of wind statistics for the eight sites for which the statistics for the ridge (high ozone) and trough (low ozone) cases were available. For all of the ridge cases in the NCT Study, high ozone (8.5 pphm) occurred on about 60% of those classified as ridge cases. Table 5 lists wind speed averages and maxima as well as the first and second peaks (if there were any predominant ones) in wind directions. The three height levels of wind statistics considered were the second gate of the wind profilers (about 300 m above the surface), about 1 km and about 2 km ASL. Level 1 is essentially always in the mixed layer, certainly during the day, level 2 would usually be in the mixed layer by afternoon (a transition level) and level 3 would normally be above the mixed layer. This does not, however, imply that level 3 is in the free, synoptically-driven atmosphere at all sites. Because the Sierra Nevada Mountains immediately to the east are about 3 km in elevation and the Coastal Range immediately to the west is about 1.5 km in elevation, the level 3 winds could certainly

be strongly influenced by the nearby terrain at some sites. Table 6 displays the results of the same statistics with the separation according to morning (0700-1200 PDT) and afternoon (1300-1800 PDT) cases. We will not discuss the summary results presented in this tables as they are self-explanatory. However, we will use bar charts (Appendix D) as the basis for the interpretation of the results because these provide the most complete summary of wind distribution characteristics.

We begin this brief, overview discussion of the bar chart frequency distributions with the Sacramento Valley portion of the NCT study (Appendix D). The charts are ordered from the most southern site to the most northern site (see Fig. 1) with each site separated by the three levels and by the ridge and trough cases. The charts comprise data from 0700 to 1800 PDT only because of sparse nighttime data, especially at the upper levels, after eliminating bird echo contamination. ARB and RAN are not included because they were not operable for either the ridge or trough case or both. TRN is not included because the winds at this site were nearly identical to those at TRS. The discussion follows the order of the charts.

Table 4 Wind Profiler Run Summary

Site	Run period (No. of days)	Ridge case (No. of days)	Trough case (No. of days)	Resolution		First level height (ASL,m)	Begin-End Day
				High(m)* ¹	Low(m)* ²		
ORO	156	11	6	100	200	178	5/30-11/1
ARB	103	no	6	100	200	194	5/16-8/26
PLG	170	11	6	100 * ³	200	154	5/16-11/1
UCD	128	11	6	100	200	156	6/27-11/1
TRS	142	11	5	100	200	188	6/13-11/1
TRN	60	no	6	100	200	148	6/28-8/26
DEL	140	11	5	100	200	130	6/16-11/1
RAN	82	no	6	100	200	182	6/6-8/26
HOL* ⁶	59	12	9	60 * ⁴	200	292	9/7-11/4
MOS* ⁶	71	11	8	60 * ⁴	200	153	8/26-11/4
BEA* ⁶	49	10	6	100	200 * ⁵	603	8/29-10/16

*¹ : high resolution, 700 ns, 25 gates.

*² : low resolution, 2800 ns, 25 gates.

*³ : 29 gates.

*⁴ : 400ns.

*⁵ : 30 gates.

*⁶ : high ozone (ridge) and low ozone (trough) case.

Table 5 Wind Speed and Wind Direction

site	Ridge Case (High Ozone)						Trough Case (Low Ozone)					
	First * ¹		Second * ²		Third * ³		First		Second		Third	
	ws a/m	wd pk	ws	wd	ws	wd	ws	wd	ws	wd	ws	wd
ORO	2/7	150 300	4/9	60	3/11	60	3/11	150	4/9	150	3/9	190
PLG	2/9	200 330	2/11	330	4/9	330	3/9	150	3/7	200	2/11	200
UCD	5/11	330	3/9	330	3/11	330	3/9	200	3/7	250 300	2/7	200
TRS	3/11	250	3/9	22.5	2/9	300	5/11	250	2/7	300	2/5	23
DEL	3/9	330	3/9	300	4/11	330	3/11	250	4/7	250	2/11	200
HOL	2/9	300	2/11	23	3/11	23	2/9	300	4/11	300	4/12	250
MOS	3/7	250	3/7	23	6/11	330	3/11	250	3/11	250	5/16	300
BEA	4/11	330	3/11	330	6/11	330	2/7	23	2/8	23	2/11	23

* a/m : average /maximum (m/s and degrees); * pk : peak or predominant direction
 *¹: Second gate(~300m); *²: ~1000m level; *³: ~2000m level.

Table 6 Morning and Afternoon Wind

site	Ridge Case			Trough Case		
	First	Second	Third	First	Second	Third
	ws/wd (m/pk)	ws/wd (m/pk)	ws/wd (m/pk)	ws/wd (m/pk)	ws/wd (m/pk)	ws/wd (m/pk)
ORO(Mor)	6/330,110	8/45	8/210,45	8/150	8/160,350	9/190,20
(Aft)	6/300,210	8/330,150	8/300,60	10/150,240	8/160	9/180,330
TRS(Mor)	11/240,330	8/no	8/300,90	10/250	4/no	4/no
(Aft)	10/240	6/no	8/no	10/230	6/no	4/no
PLG(Mor)	8/no	8/no	8/330,210	8/150	6/190,350	8/180,350
(Aft)	8/no	10/no	8/no	8/180	4/180	7/200

* m/pk : Maximum/peak (m/s;degrees).
 * Mor : Morning (07:00-12:00).
 * Aft : Afternoon (13:00-18:00).

7.3 Data Stratified By Presence Of Upper-Level Ridge Or Trough

In the following site-by-site description for the NCT Study, reference is made to Appendix D which presents stacked bar charts which describe the frequency of occurrence of winds by directions and speeds, equivalent to wind roses but selected by meteorological regime (ridges and troughs).

7.3.1 DEL

The ridge case at DEL, level 1, show a strong preference for stronger north-northwesterly winds. This represents the turning of the winds coming from San Francisco Bay through the Sacramento Delta and into the south Central Valley. Later discussions will reveal that other sites also show a general tendency for northerly-component flow in the ridge case. The shallowness of this flow is shown in DEL level 2 which reveals much more evenly distributed wind directions.

The DEL trough case, level 1, shows a definite tendency for westerly winds, becoming less definite at level 2 and fairly evenly distributed at level 3.

7.3.2 TRS

Moving north to the TRS ridge case, level 1, we note frequent and relatively strong west-southwesterly winds and somewhat less frequent winds from the north-northwest. The west-southwesterly flow is the on-shore wind from San Francisco Bay, moving through the Sacramento Delta and turning slightly north at the TRS site as the air enters the Central Valley. This flow is very shallow. The northerly winds, which are much deeper, represents a combination of morning drainage from the Sacramento Valley to the north combined with the general tendency for northerly flow in the ridge case. Most of the time these northerlies lie above the shallow sea breeze. The trough case shows a peak of strong winds in the west-southwesterly direction. This flow is much stronger and more persistent in than the ridge case.

As with DEL, level 1, trough case, the north-northeasterly winds at TRS are very light and very infrequent. Level 2 shows much lighter winds, well-distributed in wind direction, while level 3 shows a peak in light winds in the north-northeasterly direction. The reason for this peak is not clear because the 2-km level is probably too high for valley drainage.

7.3.3 UCD

The UCD site level 1, ridge case, shows a significant tendency for moderate northerly winds which represents a combination of Sacramento Valley morning drainage and the general tendency for northerly flow in the ridge case mentioned above. UCD level 2 also shows this northerly tendency, but somewhat less frequent than level 1. At level 3 we see that the wind directions are well-distributed.

For the UCD trough case at level 1, a weak peak indicates south-southwesterly winds. However, this flow is rather shallow because at level 2, this peak totally disappears, and at level 3 there are two very weak peaks, one for north-northeasterly winds and the other for the south-southwesterly winds. These directions are consistent with morning down-valley channeled flow and afternoon up-valley flow. As with TRS, if this is the case, this terrain-influenced flow is very deep and should be the subject for further analysis.

7.3.4 PLG

PLG is near the center of the Sacramento Valley and for the ridge case, level 1, the winds are light and uniformly distributed in direction. At levels 2 and 3 there is a slight tendency for moderate north-northwesterly flow, which, as with the other valley sites, may be indicative of very deep morning drainage down the valley and the general ridge-induced northerly-component flow.

At level 1 at PLG for the trough case, there is a definite peak in the south-southeasterly direction representing moderate winds. There remains a weak tendency for southerly flow at levels 2 and 3, but there is also another peak of weak winds in the north-northeasterly direction at both of these levels. Again, this north-northeasterly flow could represent a deep, morning valley drainage.

7.3.5 ORO

The ORO ridge case, level 1, does not show a well-defined peak, but there is a hint of two weak peaks with light south-southeasterly winds and west-northwesterly winds. The south-southeasterly winds represent afternoon up-valley flow and the west-northwesterly winds correspond to nighttime, down-valley drainage flows. At levels 2 and 3 there is a broad tendency for northerly and northeasterly winds which are likely to be the combination of prevalent down-valley drainage and ridge-influenced synoptic flow.

The ORO trough case, levels 1 and 2, show a very strong peak in the south-southeasterly direction. This is an extension of the strong sea breeze into the valley and channeled by the terrain. At level 3 this peak is weaker and shifts to south-southwesterly, probably reflecting a decreasing channeling effect at this higher level.

7.4 Morning and Afternoon Flows during NCT

For TRS, PLG and ORO, we compare the morning and afternoon transport patterns using the same bar chart format (Appendix E). The morning is defined as 0700-1200 PDT and the afternoon is for the period 1300-1800 PDT. These results illustrate the diurnal variation of the transport. All of the results are presented for level 1 which is close to the level of maximum transport and for the ridge case for which the terrain influence is greater than the trough case.

At TRS in the morning, the main peak of fairly strong winds is north-northwesterly. This peak disappears in the afternoon indicating that this northerly flow is a drainage flow toward the south, out of the Sacramento Valley. The secondary peak in the morning of west-southwesterly winds becomes the major peak in the afternoon as the sea breeze increases with the valley heating.

At PLG the morning and afternoon wind direction distributions are very broad with no definite peak. This is similar to the distributions for the entire day discussed above. These results indicate that the diurnal and, therefore terrain influence, is very small or non-existent. Likely this is because PLG is located near the center of the Sacramento Valley, well distanced from the mountains.

The ORO site presents a rather complex and subtle pattern. In the morning there are small peaks representing weak southeasterly winds and another small peak of slightly stronger

north-northwesterly winds. The north-northwesterly wind is probably the morning drainage down the Sacramento Valley. The southeasterly wind is more difficult to explain in the morning ridge case because it is surprising to see southerly component flow so early in the day. By afternoon, the continued southerly flow, moderate in speed, is the up-valley flow due to the combination of heating in the upper Sacramento Valley and the intrusion of the highly modified ocean air by late afternoon. The moderate west-northwesterly winds are a surface reflection of the general higher-level northerly flow in the ridge case with an upslope (toward the Sierra Nevada foothills) component.

7.5 Wind Roses for the NCT Sites

The use of stacked bar charts proved most useful for us in stratifying winds according to synoptic meteorological or ozone concentration data rather than wind roses as shown in Appendices D and E. Preliminary analysis of the profiler data, however, can benefit from a quick look and wind distributions. For this reason, we implemented a wind scatterplot display capability in our workstation development effort: the clustering of winds on such a display gives an indication of any preferred wind distribution.

7.6 Summary of NCT Wind Distribution Results

The summarized wind data reveal the following general conclusions:

- There is a general tendency for northerly-component flow above the boundary layer in the ridge case.
- In the trough case, there is general southerly-component flow.
- The flow is stronger at all levels in the trough case compared to the ridge case and the flow tends to be channeled in the boundary layer by the nearby significant terrain features.
- In the ridge case, the wind patterns in the boundary layer at sites within the valley are significantly influenced by diurnal heating patterns of the nearby terrain while in the trough case, the diurnal patterns do not appear significant. A general diurnal pattern throughout most of the valley is a northerly drainage flow in the morning (amplified by the northerly synoptic flow in the ridge case), and a southerly up-valley flow in the afternoon.
- At sites near the passes to the Pacific Ocean, the diurnal patterns are not important in either the trough or ridge case as the on-shore ocean breeze is continuous throughout the day. The flow from the ocean into the valley is stronger in the trough case than in the ridge case and, in both cases, it is very shallow.
- In the center of the valley and in the ridge case, the winds at most levels are light and variable throughout the day with little indication of diurnal patterns.
- The sea breeze penetrates to UCD by around midday in the ridge case and to ORO late in the afternoon. This sea breeze is highly modified and is in nearly the same direction as the already existing up-valley flow at each of these sites.

The summaries presented illustrate the usefulness of distributed wind profilers in this complex terrain region. The transport patterns can be described in great spatial, vertical and temporal detail well beyond the capabilities of rawinsondes and beyond the realm of reasonable aircraft deployment.

7.7 Discussion of the Results from the North Central Coast Transport (NCCT) Study

The NCCT Study took place during September and October 1991 to describe, in particular, the transport path(s) of ozone or its precursors into the Pinnacles National Monument. Three wind profilers were moved from NCT Study sites in late August to MOS, HOL and BEA (see the map in Fig. 1). Historically, the ozone readings are the highest during these two months in this basin. The two-month period was too short to include several-contiguous days of ridge and trough conditions, so the wind profiler data were divided into high (≥ 8.5 pphm) and low ozone (≤ 6 pphm) cases measured at the Pinnacles monitoring site. There were 13 days of high ozone and 9 days of low ozone at Pinnacles during the NCCT period for MOS and HOL and 10 days of high ozone and 6 days of low ozone for BEA. BEA stopped operating after October 15.

The results are presented Appendix F, in bar charts identical to the NCT presentations discussed above. The discussion that follows and the plots are in order from the coast (MOS) to the most inland and southern site (BEA). As with the NCT results, most of the discussion is based on the bar charts rather than wind roses because they do not change the conclusions reached from the bar charts.

7.7.1 MOS

At this coastal site, level 1, high ozone, there are two distinct sets of peaks, moderate westerly flow and light to moderate northeasterly flow. The westerly flow is the prevalent on-shore, daytime pattern, but the northeasterly winds are indicative of the wind pattern in a NCT ridge case discussed above. Levels 2 and 3 at MOS during high ozone at Pinnacles also show two distinct peaks, but these are centered around north, again indicative of a ridge situation. The north-northwesterly winds at level 3 are moderate to strong.

The wind distributions at MOS during low ozone are considerably different from the high ozone composite. The level 1 westerly peak is significant and the speeds are moderate. There is no significant northerly flow. At level 2 there are moderate to strong winds from south to west-northwesterly and at level 3 the winds are moderate to strong in the west-southwesterly to north-northwesterly directions. There is a very small peak in the north-northeasterly direction.

7.7.2 HOL

During high ozone events at Pinnacles, HOL exhibits significant peaks of moderate winds from the northwest direction and a very light wind from the north-northeasterly direction. A small, light-wind peak is also evident from the southeast quadrant. At levels 2 and 3 for the high ozone case, the winds direction peaks are centered more in the northerly direction and are stronger than at level 1.

By contrast, for the low ozone case at level 1, there are small peaks centered in the northwesterly direction which is indicative of a channeling of the on-shore flow from Monterey Bay into the Salinas Valley. At level 2 this west-northwesterly peak is very pronounced and the winds are

quite strong. At level 3 the peaks are much less pronounced from the northwesterly direction, but the winds remain strong.

7.7.3 BEA

At BEA during high ozone and at level 1, there is a significant frequency of strong winds from the northerly direction with a weak peak from the south-southeasterly direction. Levels 2 and 3 show the same tendencies in the wind direction as level 1. This northerly flow is consistent with the pattern during NCT ridge conditions. For the Pinnacles low ozone cases, the BEA wind profiler site at level 1 shows winds that are mostly light from the north-northeast. This light-wind north-northeasterly peak extends up to level 3, but at this level there are small, moderate wind peaks from the southwest. This northeasterly wind could be daytime upslope flow into the Gabilon Range.

7.8 Summary of NCCT Study Results

In brief summary of the wind distributions found in the NCCT Study, we reached the following conclusions:

- There is a marked contrast between the high and low ozone cases at all three NCCT Study sites.
- The high ozone case exhibits less on-shore flow than the low ozone case and a significant indication of transport parallel to the coast toward the southwest and flow down the Santa Clara Valley from the southern portion of San Francisco Bay. This is strong indication of direct transport of pollutants from the south San Francisco Bay Area into the North Central Coast region and on to Pinnacles National Monument.
- In the low ozone situation, the on-shore breeze from Monterey Bay is much more pronounced than during high ozone cases, and this relatively clean air is channeled southeastward toward Pinnacles.
- The high ozone case shows the northerly-component tendency associated with the NCT ridge conditions discussed above, but, for the NCCT Study low-ozone case, the southerly-component flow prevalent during the trough cases in the NCT study did not appear during NCCT Study.

8 BOUNDARY-LAYER STRUCTURE AND PROPERTIES

8.1 Mixing Layer Depths

Of all the variables that can be used to describe the structure of the convectively driven planetary boundary layer (PBL), the most critical parameter for use in air pollution or dispersion modeling is the height of the mixed layer, h . Unfortunately, h is not always easy to predict on a day to day basis. For example, the boundary-layer scheme of a commonly used mesoscale model overpredicted mixing depths in the San Joaquin Valley by a factor of two on certain days (Seaman; private communication, 1992).

Growth of the mixed layer comes about from the absorption of solar radiation at the surface and the resulting positive heat flux into the boundary layer. However, heat can also enter the PBL through horizontal advection or by entraining warmer air from above the PBL. In addition, subsidence in the overlying free troposphere may inhibit growth of the mixed layer. The idea of using remote sensors to study the evolution of the convective boundary layer began in the early 1970's (see Richter et al., 1974; Frisch and Clifford, 1974). A comparison of mixing depths measured by a variety of remote sensors and *in-situ* platforms is given by Kaimal et al. (1982).

At ETL we have developed a technique for estimating mixing depths using the profiles of radar reflectivity recorded by the 915-MHz radar. Radar reflectivity measurements in the form of backscattered power or signal-to-noise ratio (*SNR*) can be related to the refractive index structure function parameter of turbulence theory, C_n^2 . This parameter gives us information on the strength of turbulence measured within the radar sampling volume. Observations by Ochs and Lawrence (1972) and Beecher (1988) as well as theoretical models (e.g., Fairall, 1991) give a consistent picture of C_n^2 behavior in the unstable boundary layer. As height increases, C_n^2 first decreases in the surface layer, levels off in the mixed layer, increases to a peak value at the inversion capping the mixed layer, and then decreases to free tropospheric values. Our technique, then, is to locate the peak in radar C_n^2 corresponding to the capping inversion. Since for this measurement we are not concerned with the value of C_n^2 , we simply use time series of range-corrected *SNR*.

Examples of this technique are shown elsewhere and in White and Fairall (1991) and White (1993) as well as Gaynor et al. (1994). At selected sites, we used rawinsonde measurements of the inversion height for reference. The absolute errors between the radar and rawinsonde were found to be comparable to the pulse resolution of the radar.

The obvious advantage of using the radar for remote detection of mixing depth is the greatly enhanced temporal resolution. During extreme convective conditions, such as those encountered in the southeastern U.S. during spring and summer, the mixing depth can increase by several hundred meters in a span as short as one hour. Transitions such as this would more than likely be missed by conventional rawinsonde spacing. Unmanned operation of the profiler also allows the user to collect extended time series with little effort.

There are some important limitations to this technique. During the night, only the lowest portion of the PBL is continuously turbulent; the height to which mixing occurs is usually on the order of a few tens of meters. Consequently, nocturnal mixing depths are often below the minimum

detectable range of the 915-MHz radar (100-150 m). The problem of nocturnal mixing-depth detection is well suited to the use of an acoustic sounder. In fact for the limited range required for this application, a relatively inexpensive single-axis sodar could be used in conjunction with the radar. At one of the sites (UCD), we operated a sodar next to the radar. Analysis of the reflectivity data from the sodar indicated the existence of a ground-based temperature inversion below 100 m beginning as early as 1700 PDT on certain days. This important feature cannot be identified in the radar mixing-depth analysis because of the radar's minimum detectable range.

Secondly, as the convective boundary layer heats up, the inversion at the top of the mixed layer erodes. In many cases, this leads to a reduction in the turbulence at the altitudes adjacent to the inversion. The highest value of radar reflectivity may then come from some other region within the PBL or perhaps even from above the PBL. An example of this scenario is depicted in the radar reflectivity plot shown in Appendix G (Lewis et al., 1994; pg. 30). Here, mixing depths averaged to 30-minute resolution are superimposed on a color plot of range corrected *SNR*. In the time period between 1510 and 1630, the mixing-depth algorithm picks heights corresponding to sporadic regions of locally enhanced turbulence *in* the mixed layer instead of the more coherent but weaker layer at the *top* of the mixed layer. By about 1630, the maximum backscatter is again from the capping inversion, which has increased its altitude to about 1700 m. By 1730, the mixed layer collapses.

Finally, the presence of PBL clouds confuses the issue. For example, when cumulus clouds exist in a convectively driven PBL, there is no clear cut definition of the mixing depth. Also, we find that the increased radar reflectivity due to increased turbulence in clouds is comparable to the signals received from the inversion capping the mixed layer. Perhaps more relevant is the decrease in radar reflectivity occurring near cloud top. This information becomes even more useful when combined with an algorithm to estimate the lifting condensation level (LCL) or when the radar is collocated with an instrument such as a ceilometer, which actually measures cloud base. For example, ETL has used a radar and ceilometer mounted on a ship to estimate cloud depths in a study of trade wind cumulus clouds (Chertock et al., 1993). On the other hand, when cloud top coincides with the inversion, as in the case of a stratocumulus topped marine boundary layer, the received signals from the inversion are enhanced (White et al., 1991).

8.2 Four Dimensional Velocity Fields Obtained From Profilers

8.2.1 Methodology

The profilers measure the temporal evolution of the wind speed and direction at single locations. With well-located sites, it is possible to generate four dimensional wind fields over the region. We define the two dimensional interpolation model that grids the array in the horizontal at any vertical level. A somewhat more sophisticated technique includes the terrain and uses a mass-conserving model. This technique is important when data are sparse temporally and/or spatially and/or when vertical profiles are not available. The wind profiler data implicitly include the terrain effects in the flow because of the profiler's strategic locations relative to important terrain features, their relatively high time resolution (1-h averages), and the fact that they provide high-vertical-resolution profiles. The same type of spatial interpolation was applied to the mixing depth height as detected by the profilers. It should be noted, however, that no data existed over the mountainous terrain surrounding the Central Valley so that the interpolated wind field should not be assumed to be valid over those regions. We minimized the possible errors of misinterpolating the data over the slopes of the Sacramento Valley by confining the study area to a rectangle defined by the 8 profiler locations (Figure 1). Travis North and Travis South are located near the mouth of the valley while Pleasant Grove and UC Davis are closer to the middle of the Sacramento Valley. The other four sites are located on the perimeter (Delta Island to the south, Rancho Seco to the east, Oroville to the north, and Arbuckle to the west).

8.2.2 Spatial interpolation

The spatial interpolation scheme calculates a value of wind speed and wind direction at each point of a 15 X 19 X 26 grid. The horizontal resolution is about 10 km and the vertical resolution is 100 meters. The lowest layer is calculated by using the hourly-averaged wind speed and direction from the surface meteorological network collocated with the profiler network. Then, at each grid height, the values are linearly interpolated from the two closest profiler heights.

8.3 Four-Dimensional Wind Fields And Mixing Depth Heights

In this section we show the temporal and spatial evolution of the wind fields and mixing depth heights for 2 days. The first day is typical of a ridge case with high ozone concentrations (Figs. 8 and 9 and Appendix H). The second day is typical of a trough case with low ozone concentrations (Figs 10 and 11 and Appendix I). The first plot of each group is the diurnal temporal and spatial evolution of the mixing depth as computed from the profiler reflectivity, between 1000 PDT and 1800 PDT. The hourly wind field plots that follow include 5 layers: surface, 500 meters (ASL), 1000 meters (ASL), 1500 meters (ASL), and 2000 meters (ASL). The reference vector defines the wind speed derived at each grid point. At each level, a streamline is drawn, representing the hypothetical path of a massless particle placed in the field at the San Francisco location. The sites used in the layer interpolation are symbolized by black dots located at the given layer. If a site is not used in the layer interpolation (flag or no data) the black dot is not displayed. The winds interfering with the topography are not displayed. The header defines the Julian day and time (PDT) of the plot. The corresponding mixing depth surface is displayed as a "transparent" isosurface in the volume. Note that the vertical axis is strongly exaggerated.

Julian Day 191

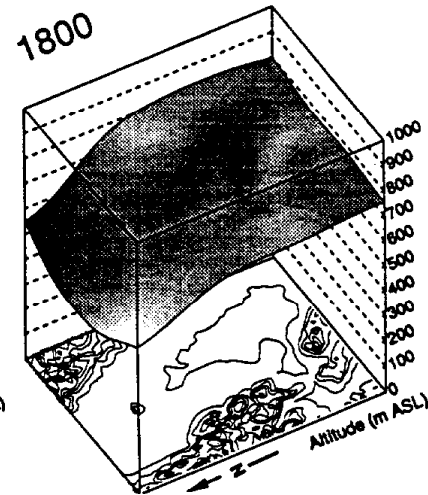
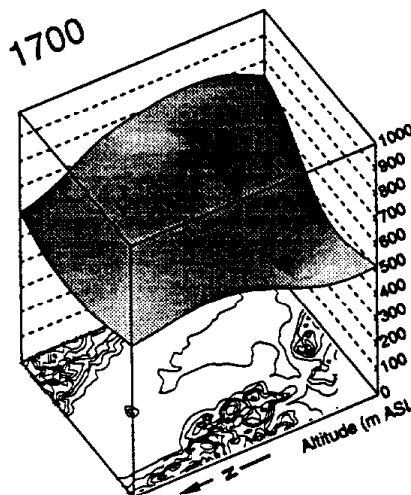
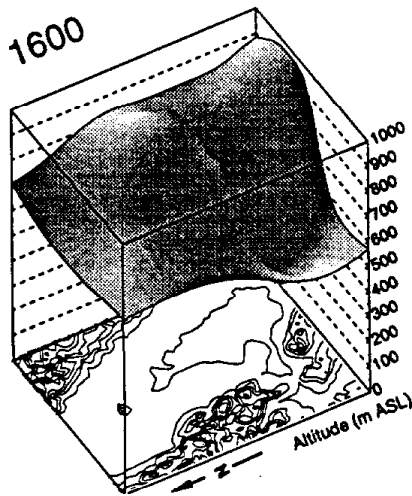
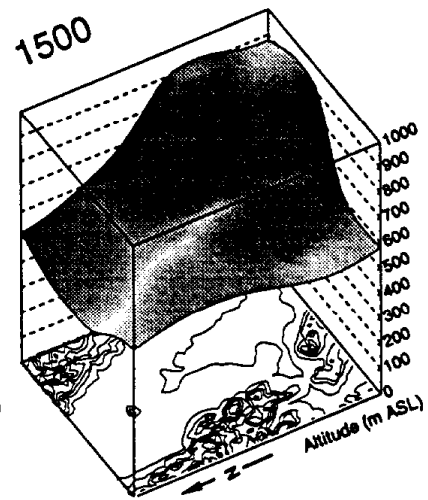
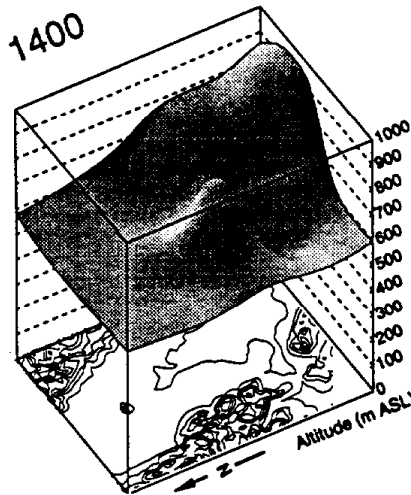
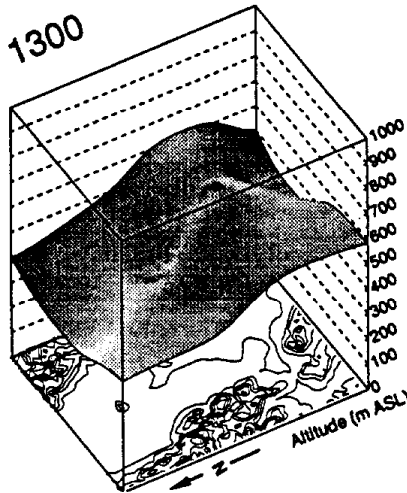
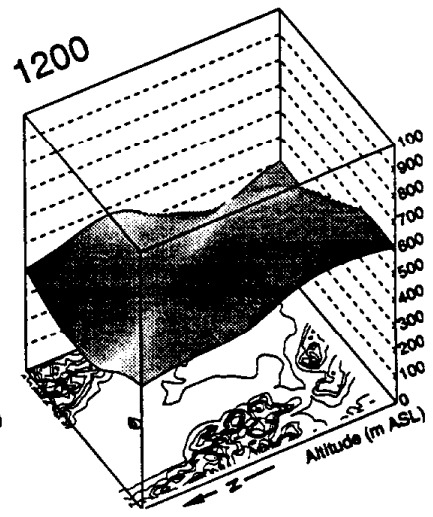
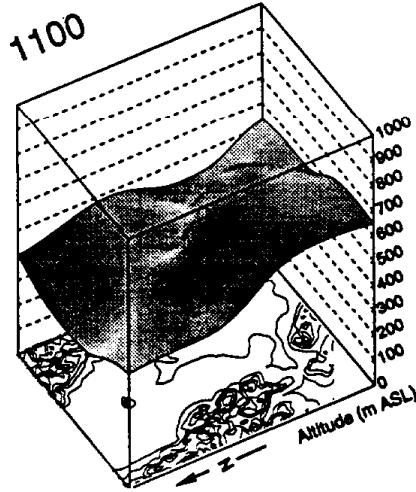
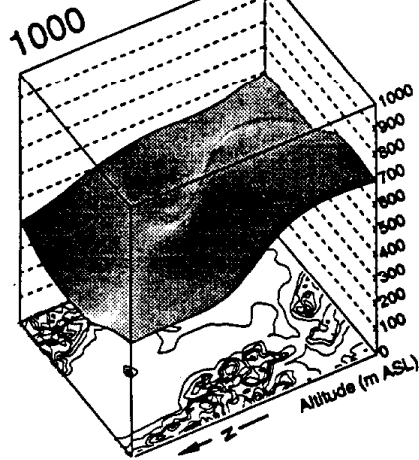


Figure 8. Typical ridge case- Mixed Layer isosurfaces: 10 July 1991 (Julian Day 191)

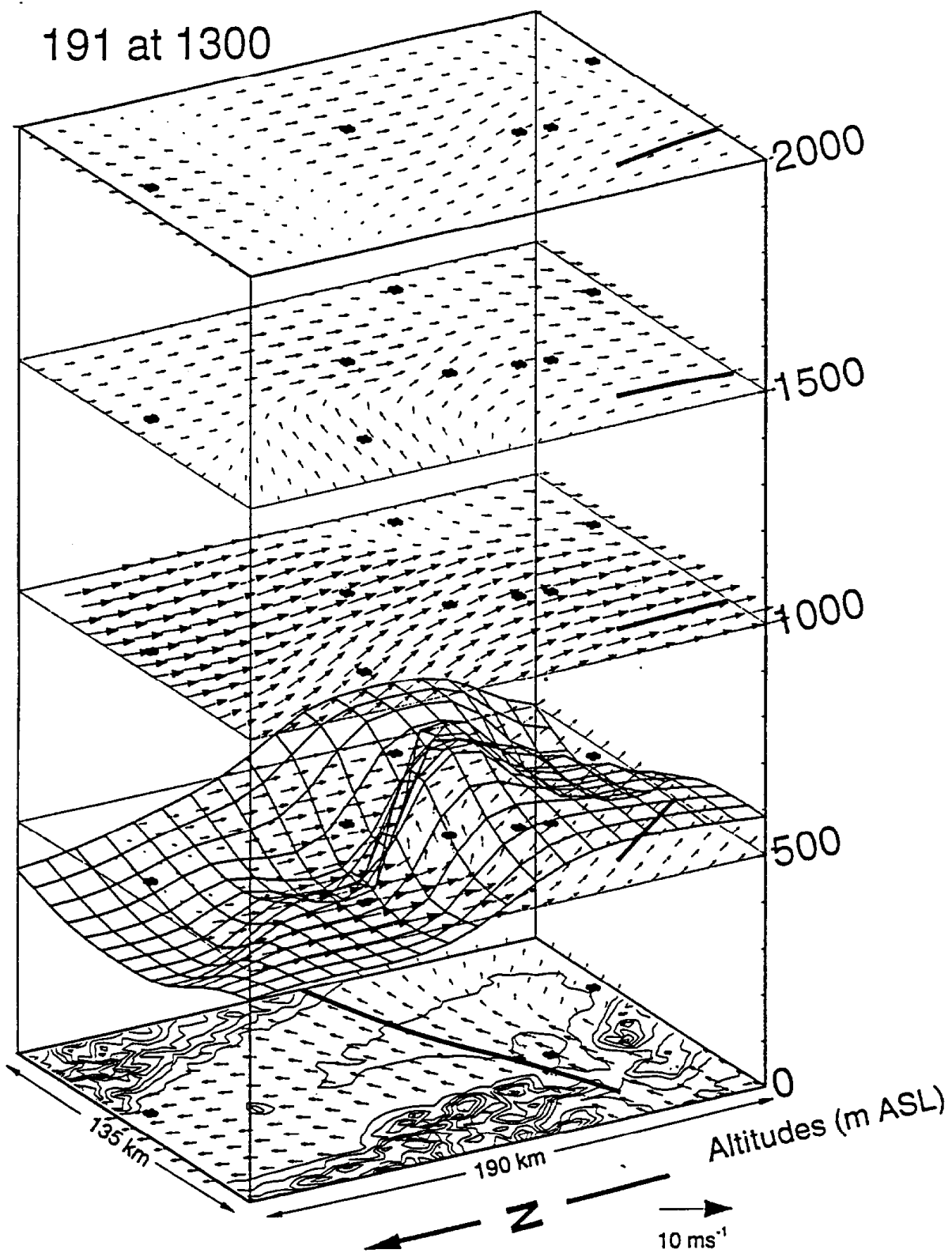


Figure 9. Typical ridge case- Wind fields and isosurface at 1300 PDT, (Julian Day 191)

Julian Day 201

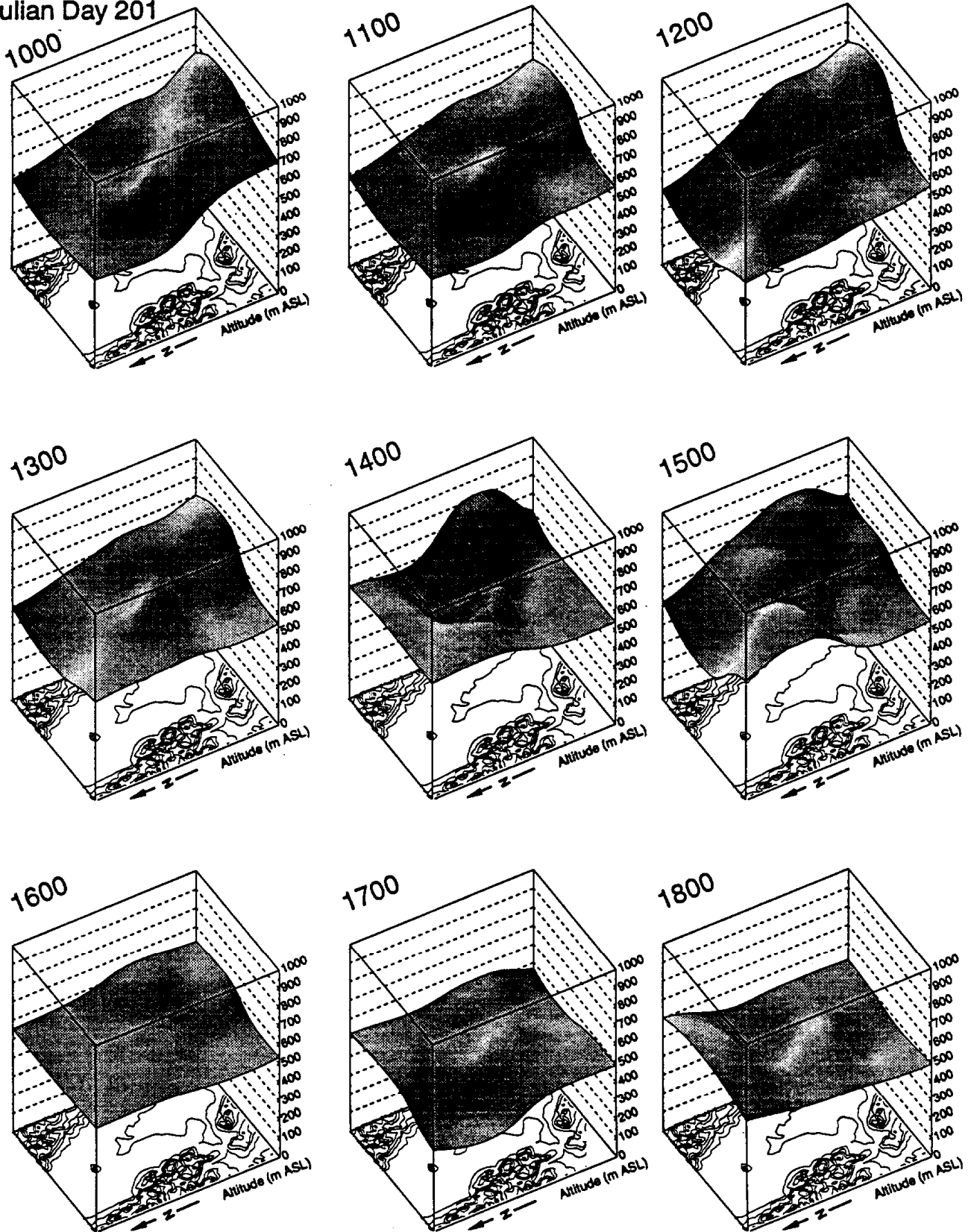


Figure 10. Typical trough case-Mixed Layer isosurfaces: 20 July 1991 (Julian Day 201)

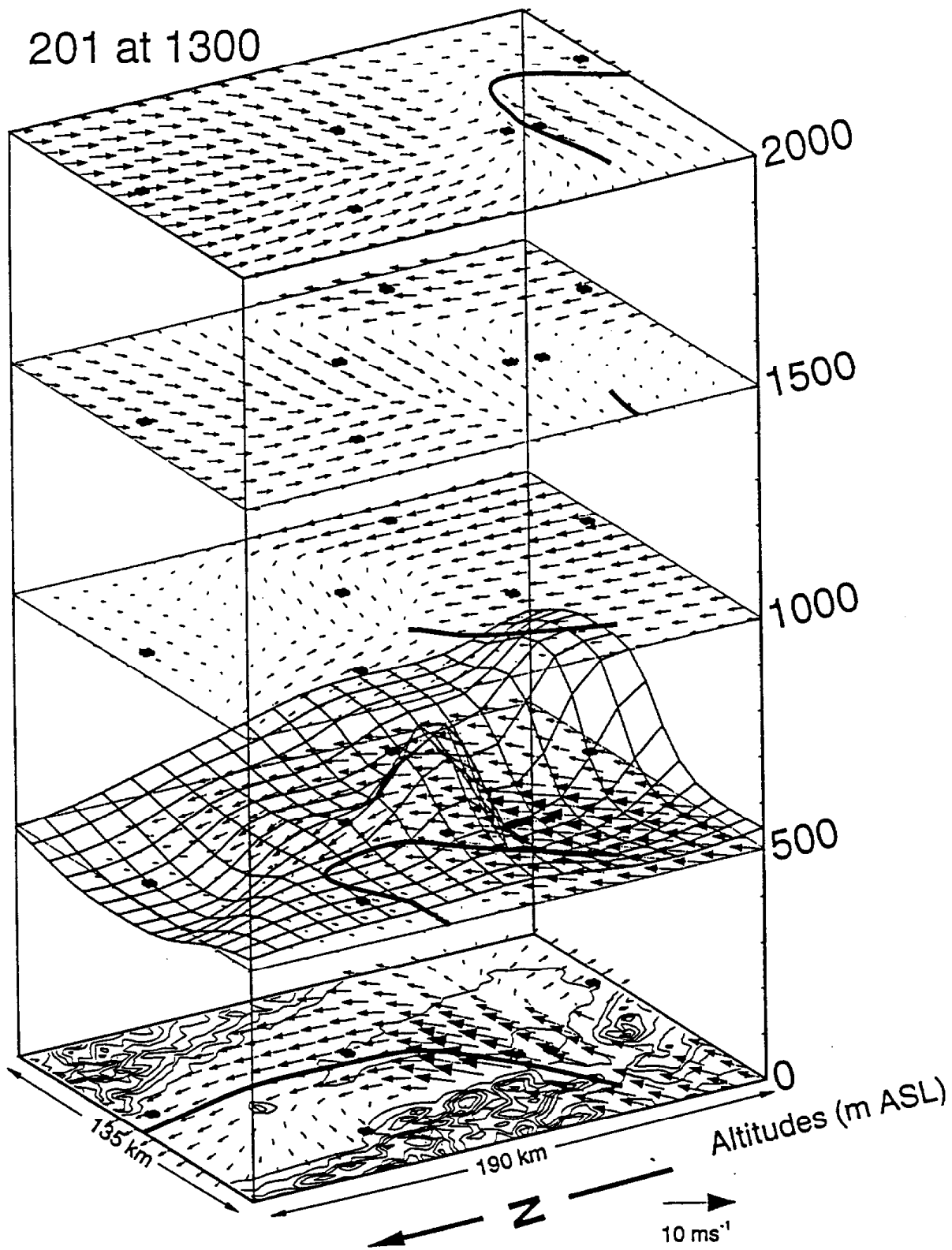


Figure 11. Typical trough case- Wind fields and isosurface at 1300 PDT, (Julian Day 201)

8.4 Development Of An Expert System For Mixing Depth Analysis

In developing an algorithm for detecting mixing depths, we originally thought it might be useful to employ some of the expert system techniques developed at Pennsylvania State University for other meteorological analyses. However, upon analyzing the radar reflectivity data as described in Task 2.3, we found that simple time filters removed much of the noise caused by non-atmospheric targets and turbulent "hot" spots. In the current approach, we analyze the profile of reflectivity measured by each of the radar's high spatial resolution beams (one vertical axis and two off-vertical axes) and extract the height at which the maximum range-corrected *SNR* was recorded. This operation produces a time series to which we apply a simple median filter in time. The desired level of smoothing is obtained by varying the length of the filter (10 minutes, 1 hour, etc.). Longer filtering periods produce smoother results.

Note that we must use the short-time resolution moments rather than the hourly averaged data for the mixing-depth analysis. Nearly instantaneous profiles, such as those obtained from aircraft, show that mixed-layer capping inversions are often characterized by very sharp gradients in temperature and moisture. Averaging tends to wash out these identifying features. The same is true with the radar C_n^2 profile -- preaveraging will reduce our ability to detect the capping inversion.

8.5 Analysis Of Dispersion Variables

An ongoing area of wind profiler research is the development of techniques whereby meteorological variables affecting dispersion of pollutants can be directly measured. Although the mixed layer depth can be deduced in simple meteorological situations, other important dispersion variables include the variance of fluctuations in the wind in the vertical and horizontal as well as the vertical gradient of the horizontal wind (wind shear). These parameters are necessary to characterize the dilution of pollutants as they are transported over longer distances and are not available from routine measurement systems. Evaluating the utility of the 915-MHz radar in providing estimates of these variables has been an ongoing research effort at ETL (see Gossard, 1990; White and Fairall, 1991; White et al., 1991). This problem is quite complex due to the nature of the measurement. For example, information about turbulence is available in the raw data recorded by the profiler but is complicated by a number of atmospheric factors and by the fact that the radar measurements are derived from a time-average (the radar dwell time is about 30 seconds in any given direction) and a relatively large spatial sampling volume in the atmosphere compared to direct turbulence measurement systems. The radar sample is thus a combination of a spatial average over the volume illuminated by the radar beam, and a temporal average over the radar dwell time. Any turbulence information in the raw radar data is obscured by these time and space averages.

We could also address the calculation of the vertical velocity variance in the following manner. Suppose we use a time series of vertical velocities measured by the radar's high-resolution, vertical beam to get an estimate of vertical velocity variance. The variance we calculate contains information on the turbulent fluctuations existing at time scales equal to or greater than the dwell time (roughly 30 s for the most commonly used radar operating parameters) and on spatial scales greater than the radar sampling volume (on the order of 100 m or greater). Thus, the calculation underestimates vertical velocity variance by neglecting small-scale turbulence. However, all is not lost. Information on the smaller scales is contained in the Doppler spectral width (one of the routinely recorded parameters from the wind profiler). White and Fairall (1991) found that including spectral width in radar vertical

velocity variance calculations was necessary in order to obtain realistic profiles of vertical velocity variance in a daytime, convectively driven boundary layer. For this technique to work effectively, the radar sampling volume must be reduced in size by using a shorter pulse and a narrower beam. Some progress has been made in this area by using shorter pulses and by designing a radar antenna that produces a narrower beam (and hence smaller sampling volume).

8.6 Examination Of Boundary Layer Turbulence Variables

An important physical result of turbulence is the random variations it creates in the refractive index of the fluid, which are responsible for the scattering of electromagnetic radiation. These variations are often characterized by the refractive index structure parameter, C_n^2 , which measures the variability of temperature and humidity at spatial scales of a fraction of a meter. Radars provide information on C_n^2 through the intensity of the received backscattered signal. Large values of C_n^2 indicate the presence of strong vertical gradients of humidity and/or temperature together with significant turbulence necessary to produce mixing of air parcels. The situation of a moist, cool marine layer underlying a warm, dry subsidence inversion produces an optimum situation for the use of radars to detect the base of the subsidence inversion. However, the more difficult task of producing calibrated values of C_n^2 requires knowledge of the performance characteristics of the radar system components including the transmitter, receiver, and antenna as well as the signal gain that results during Doppler signal processing. Because numerical models that use higher order turbulence parameterizations can calculate profiles of C_n^2 directly, radar-measured profiles may provide a useful data set for model testing and validation.

As a first step in this effort to develop new model validation data sets, we designed an experiment to calibrate radar C_n^2 measurements using measurements of C_n^2 made on a tower. The experiment was performed at the Boulder Atmospheric Observatory (BAO) in Erie, Colorado. The fixed 300-m tower located at the site was instrumented with a sonic anemometer/thermometer and an infrared fast hygrometer at the 250-m level to provide in situ measurements of temperature and humidity fluctuations which were converted to C_n^2 . We then compared the tower C_n^2 measurements with radar reflectivity measurements to obtain a calibration factor. Details of the experiment and preliminary results are summarized by White et al. (1994).

Another important microturbulence variable is the rate at which turbulent kinetic energy (TKE) is removed from the flow at small scales due to dissipation, ϵ . For example, many mesoscale numerical models use parameterizations of ϵ to calculate turbulence effects, including mixing lengths. These calculations within the model affect the predicted dispersion of pollutants without any real test of their efficacy. Because ϵ is such an important variable, the theory and practice of using spectral width recorded by a radar for its calculation have received considerable attention (e.g., Frisch and Clifford, 1974; Gossard, 1990). The essence of this technique lies in the effect of mean wind and turbulence on the signal recorded by the wind profiler. Were turbulence not present within the radar sampling volume, one would measure a sharply defined Doppler-shifted radio frequency proportional only to the mean wind component along the axis of the radar beam. However, within the relatively large radar sampling volume, turbulent motions will result in a variety of Doppler shifts from different portions of the volume. The more vigorous and random these motions the greater will be the range of Doppler shifts recorded in a single radar spectrum. Thus, the width of the Doppler spectrum, recorded routinely by the wind profiler system will characterize the strength of the velocity variations at each height. The application of this technique to data collected with the 915-MHz radar is discussed briefly

by White and Fairall (1991). If other objects, such as birds, are moving through the radar beam at speeds substantially different from the mean motion of the air, then a much wider Doppler spectral width results. Because this width greatly exceeds that expected from normal atmospheric motions, it provides the basis for a test to eliminate data contaminated by bird motions. Even in the absence of bird echoes, however, the calculation of ϵ from the width of the Doppler spectrum is somewhat complicated. As pointed out by Gossard (1990), several factors contribute to the width of the Doppler spectrum other than turbulence. The most important of these factors for the portable 915-MHz system is the contribution due to a finite beamwidth. For a wind component transverse to a finite radar beam, a range of vertical velocities is sensed over the width of the beam, even if the wind is perfectly uniform. This contribution to the spectral width may well exceed the contribution due to turbulence (Gossard, 1990). Accurate estimates of ϵ depend on the successful removal of the contamination. Although a removal technique is proposed (Gossard, 1990), it is likely that more accurate retrievals of ϵ could be obtained from radars with narrower beams. The data set obtained from the BAO tower used to calibrate radar measurements of C_n^2 will also allow us to compare tower measurements of ϵ with radar-derived estimates in both daytime and nighttime conditions.

Yet another potential use for 915-MHz radar data is diagnosing the profiles of the fluxes of heat, moisture, and momentum. Such profiles could be used to test numerical model results or to be used in data assimilation schemes to improve the performance of models used to calculate transport and dispersion of pollutants. For example, one technique is to combine RASS temperature profiles with radar vertical velocity measurements to infer heat fluxes (Angevine et al., 1993). Another possibility is to calculate the relevant fluxes from the values of the structure function parameters for temperature, C_T^2 , and humidity, C_q^2 (e.g. Panofsky and Dutton, 1984). These micrometeorological structure function parameters can be calculated from radar measurements of C_n^2 (Wesely 1976). We are currently evaluating the application of 915-MHz radar data to these techniques using the aforementioned data set collected at the Boulder Atmospheric Observatory.

In summary, as new techniques are developed to exploit the measurement capabilities of 915-MHz wind profilers, the existing data base obtained in the Northern and Southern California Transport Studies may prove invaluable in future modeling exercises.

9 LOCAL FLOW REGIMES

9.1 Nighttime Drainage Winds

This section summarizes a series of tethered measurements made in the Kings River and North Fork of the Feather River canyons to examine the structure of the nighttime drainage winds and the transport of aged pollutants back into the San Joaquin and Sacramento Valleys. Measurements were made within the Kings River canyon during August 1990 and within the North Fork of the Feather River Canyon during August 1991. Both of these experiments revealed persistent, strong drainage winds within these canyons during the nighttime hours, suggesting that drainage winds are a significant facet of Sierra Nevada meteorology.

Although nighttime drainage winds may be responsible for the return of a substantial portion of aged pollution from the mountain slopes and valleys, only limited observations exist of nighttime drainage winds along the western slopes and canyons of the Sierra Nevada. Measurements made by Morgan (personal communication) during September 1979 along the Kings River canyon documented both the strength and depth of the daytime thermally driven upslope and nighttime downslope drainage winds in that region. Morgan found that daytime upcanyon winds became fully established by 1600 PDT extending to heights of 1500 m with maximum speeds of 7 ms^{-1} at 300 m. By 2200 PDT the upcanyon wind ceases and a downcanyon wind begins. The downcanyon winds continue through the night completely filling the canyon (1300 m depth) with speeds of approximately 3 ms^{-1} . Model simulations do not adequately describe these drainage flows from the Sierra Nevada. For example, in the simulations described by Kessler and Douglas (1989), drainage winds are confined to the lowest 50 m AGL in some cases or are nonexistent in the first 750 m ASL in other cases. The only nighttime easterly winds from the Sierra Nevada appear to come from the model-computed inertial rotation of daytime upslope winds over the higher terrain of the Sierra Nevada. Without better observations of terrain-associated flows and their subsequent incorporation into models, those models are unlikely to be substantially improved.

9.1.1 Kings River Canyon

During the 1990 SJVAQS/AUSPEX field program, ETL carried out a special series of measurements in the Kings River canyon. The site was located along the Kings River, 2 km downstream from where the North Fork of the Kings River joins the Kings River and just upstream from where the Kings River enters Pine Flat Reservoir (Fig. 12). The Kings River canyon is located within a V-shaped valley that extends for a distance of 65 km from near the crest of the Sierra Nevada Mountains to the San Joaquin Valley. The depth of the canyon near the measurement site was 1200 m with a width of over 12 km (Fig. 13). Three nights of measurements (8/11-12, 8/13-14, 8/15-16) took place at this site.

The evolution and strength of the drainage winds within the Kings River canyon was quite similar during the three nights of measurements. Clear skies and weak ambient winds persisted during the three experiment nights. For the first two experiment nights, the east to west surface pressure gradient across the Sierra Nevada Mountains was weak and in the same direction as the Archimedean forces resulting from the cooling of the air near the surface. On the third measurement night, these gradients had reversed and strengthened, directly opposing the Archimedean forces. This may have

accounted for the slight delay in the onset time of the drainage on this night and the slightly weaker drainage observed when compared with the previous two nights. In general, the three nights of tethersonde measurements showed that upcanyon winds persisted throughout the depth of the canyon in the early evening hours (prior to 2200 PDT) with maximum speeds greater than 5 ms^{-1} . Also prior to 2200 PDT, a weak surface-based inversion begins to form in the lowest 50 m. Between 2200 and 2230 PDT the winds shift abruptly from upcanyon to downcanyon throughout the region of the canyon sampled by the tethersonde. Maximum heights attained with the tethersonde were usually just less than 1 km. The downcanyon winds remained relatively unchanged throughout the night with maximum speeds of 3 to 4 ms^{-1} . The stability within the canyon generally increased throughout the night. By 0800 PDT, solar heating had completely destroyed the nocturnal inversion although the downcanyon winds remained within the canyon.

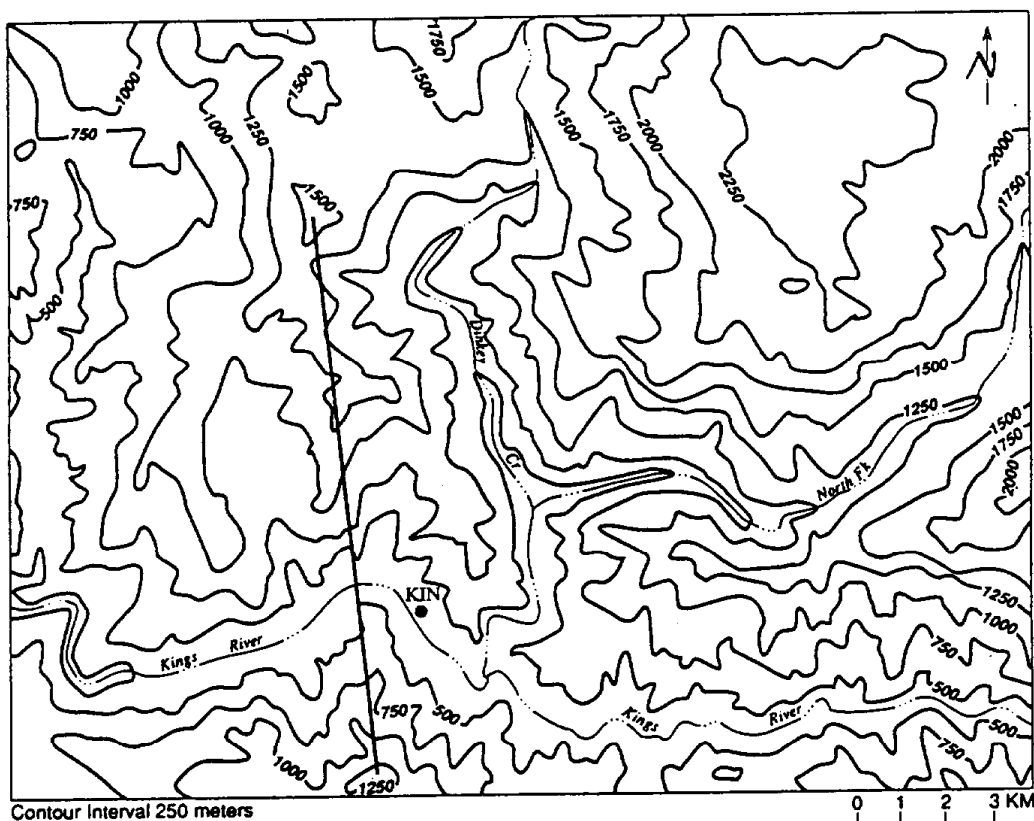


Figure 12. Topography of study region along the Kings River. The tethersonde was located at the site denoted by 'KIN'.

The nighttime drainage down the Kings River canyon represents a tremendous volume of air being advected into the San Joaquin Valley and likely accounts for the return of a large percentage of the polluted air advected up the canyon during the daytime hours. Using a technique developed by King (1989), the average nighttime volume flux within the canyon was estimated at $10.3 \times 10^6 \text{ m}^3\text{s}^{-1}$. Considering that the drainage typically lasts 10 hours during that time of year, $3.7 \times 10^{11} \text{ m}^3$ of air flows down the canyon and into the San Joaquin Valley on a typical drainage night. Morgan (personal communication) calculated the volume of air in the San Joaquin Valley, assuming the top to be the typical inversion height of 450 m, as $11.4 \times 10^{12} \text{ m}^3$. The volume of air entering the San Joaquin Valley from the Kings River canyon represents 3.2% of the total valley volume. Unfortunately, no measurements were made of this drainage flow as it entered the San Joaquin Valley. A Doppler sodar operating at Piedra, along the Kings River approximately 5 km below the Pine Flat Dam, measured only weak drainage in the lowest several hundred meters. It is likely that the trajectory of the Kings River drainage carried the flow north of this site towards the Fresno area.

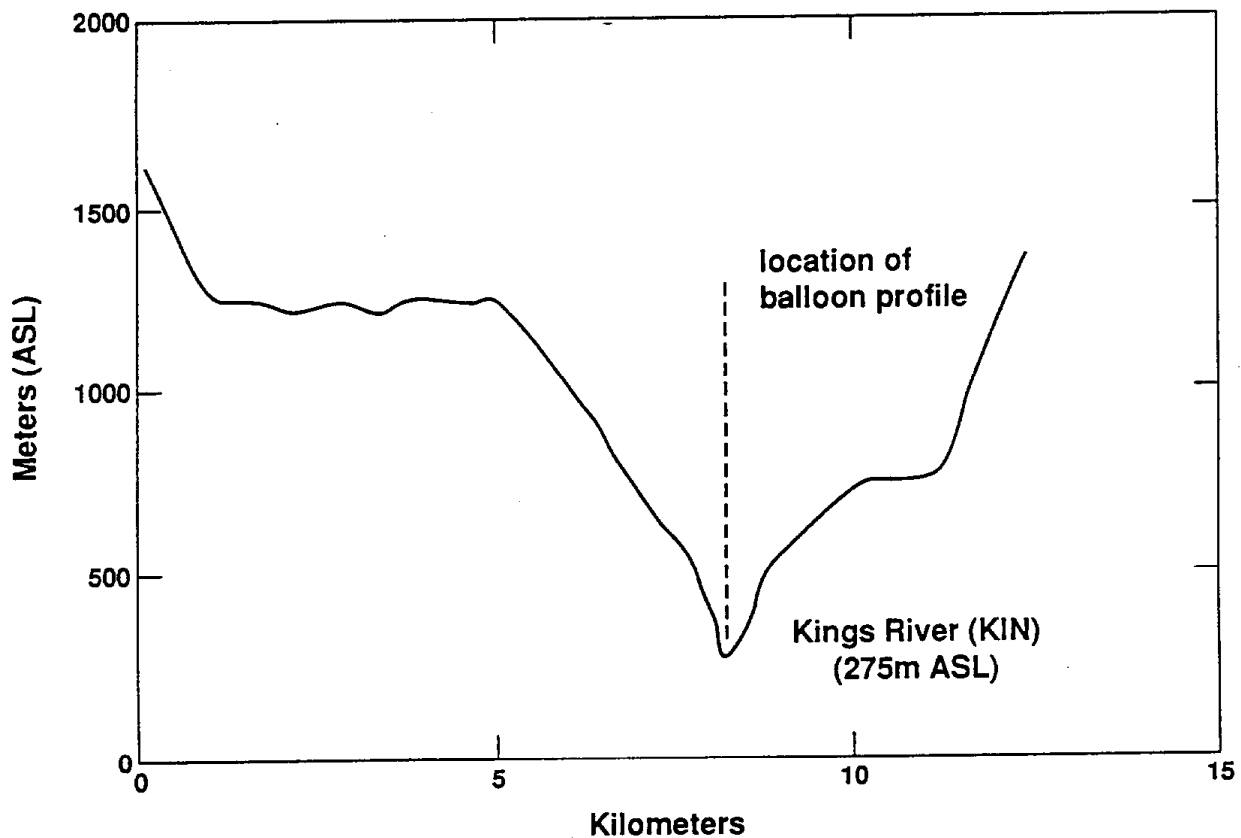


Figure 13. Kings River canyon cross-section. The location of the cross-section is indicated on Fig. 12. The approximate path of the balloon profile is indicated by the dashed line.

9.1.2 North Fork of the Feather River Canyon

During the August 1991 audit of the NCT Oroville (ORO) profiler site, coincident measurements of drainage winds along the North Fork of the Feather River were made over two consecutive nights (8/20-21, 8/21-22). Averaged profiler measurements of nighttime winds at ORO had revealed the presence of persistent northeasterly winds in the lowest km during the late night and early morning hours. The ORO site was directly in line with any drainage winds that would exit both the North Fork of the Feather River and the Middle Fork of the Feather River canyons, northeast of the site. The airsheds of both of these canyons were comparable. The tethersonde profiles were made to document the strength and depth of these flows along the North Fork of the Feather River canyon.

The measurement site was located approximately 30 km upstream from where the North Fork of the Feather River enters Lake Oroville. The valley is V-shaped with steep sidewalls for a distance of 60 km. Approximately 10 km upstream from the site the North Fork of the Feather River merges with the East Branch of the North Fork of the Feather River. Approximately 20 km upstream from this intersection, both canyons open up into relatively large, flat basins. At the measurement site (Fig. 14), the canyon was 1380 m deep and 8.5 km wide (Fig. 15).

On both experiment nights, tethersonde profiling began at 2100 PDT, and continued at two-hour intervals throughout the night. Strong drainage winds and turbulence forced the cancellation of these flights after 0800 PDT on August 21 and after 0600 PDT on August 22. As with the data obtained in the Kings River canyon, the drainage measured on both experiment nights behaved quite similarly. Clear skies and weak ambient winds dominated on both experiment nights. Cross-mountain surface pressure gradients were quite weak on both experiment nights with upper level ridging over the Great Basin. The 2100-PDT profiles revealed upcanyon winds with maximum speeds of up to 5.5 ms^{-1} . The 2200 profiles also showed upcanyon winds throughout the depth of the canyon although strengths had weakened considerably. On August 22, the 2320-2340 PDT tethersonde descent showed that the winds had switched to a downcanyon direction in the lowest 400 m with speeds less than 2 ms^{-1} . The 0100 profile on both nights showed similar conditions with drainage winds to a depth of 900 m and maximum speeds to 4 ms^{-1} . The winds in the lowest 100 m of the canyon were generally light and variable. The surface-based inversion had increased to a depth of 200 m with a strength of 2°C . Through the rest of the night and into the early morning hours, drainage wind maximum speeds continued to increase while the stability within the canyon decreased becoming adiabatic by early morning. These adiabatic conditions likely resulted from the shear-induced mixing created by the strong drainage winds channeled within the canyon. By early morning, maximum drainage wind speeds exceeded 10 ms^{-1} . Profiling was discontinued at this time as the balloon could not operate in these strong wind conditions.

These drainage winds were also observed at the ORO profiler site, located approximately 10 km west of the base of the Sierra Nevada foothills. The North Fork of the Feather River canyon lies to the northeast of this site while the Middle Fork of the Feather River lies to the east-northeast. Wilczak et al. (1992), using profiler winds averaged over a 27-day period (31 July-26 August, 1991), observed northeasterly winds at ORO extending to depths of 1 km during the morning hours. These were most likely drainage winds exiting these two river canyons. The ORO profiler data from the mornings of August 21 and August 22, 1991 also showed evidence of drainage winds within the lowest km with speeds to 4 ms^{-1} .

9.1.3 Comparison of the Kings River and the North Fork of the Feather River drainages.

Both similarities and differences existed in both the evolution and structure of the nighttime boundary layer at the Kings River and North Fork of the Feather River sites. The most obvious similarity was the rapid switch from upcanyon to downcanyon winds throughout the

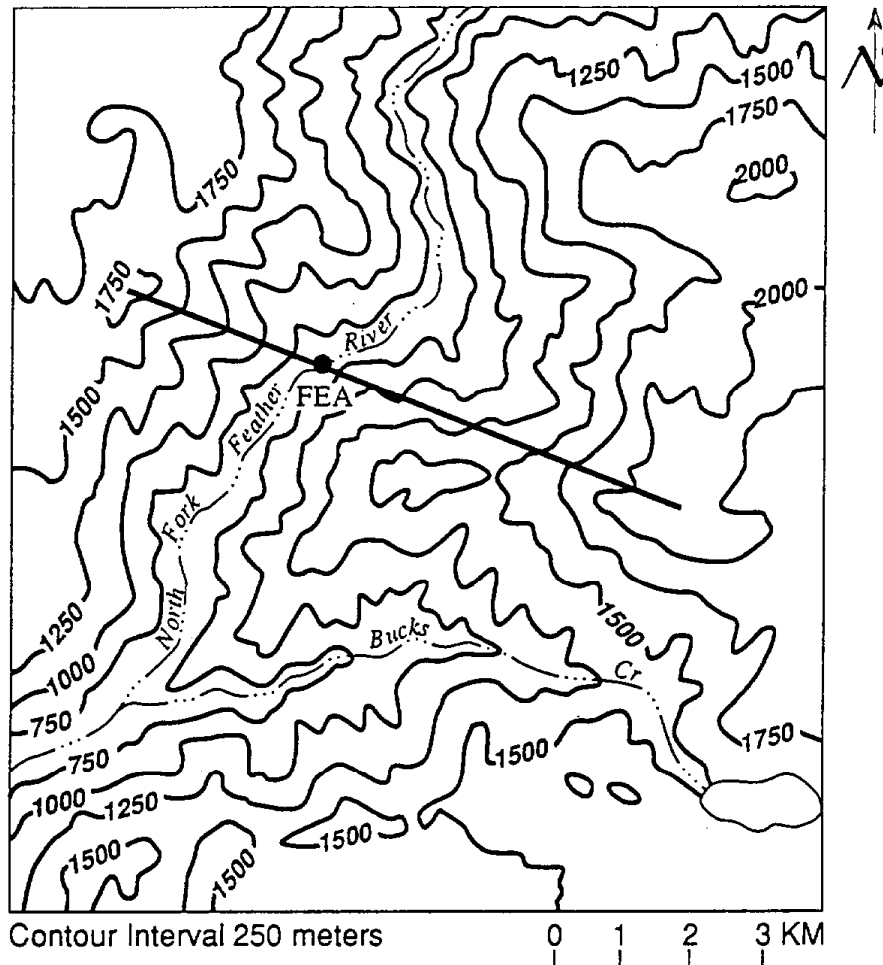


Figure 14. Topography of the study area along the North Fork of the Feather River. The tethersonde was located at the site denoted by 'FEA'.

depth of the canyon at both sites. This switch was observed to occur over periods as short as 20 minutes. In the earliest stages of drainage wind at both sites, a weak surface-based inversion often formed with winds remaining generally light and variable in the lowest 100 m until several hours after the drainage had begun. After this time, drainage winds extended from the bottom to the top of the river canyon. A major difference between the sites lies in the strength of the drainage. At the Kings River canyon site, the drainage quickly established itself with maximum speeds of 3 to 4 ms^{-1} . These winds remained relatively unchanged through the rest of the night and into the early morning hours. In

contrast, drainage wind maximum speeds within the North Fork of the Feather River canyon increased nearly linearly throughout the night, reaching speeds exceeding 10 ms^{-1} by early morning. The stability within the two canyons also evolved differently. While the stability within the lowest 100 m of the Kings River Canyon generally increased throughout the night, the stability within the North Fork of the Feather River canyon initially increased with the onset of drainage but quickly became neutral as the drainage intensified. The differences between the two canyons appears to be related to the size and shape of the drainage source regions. As discussed earlier, the Kings River canyon consists of a V-shaped valley from near the crest of the Sierra Nevada Mountains down to Pine Flat Reservoir. In contrast, the North Fork of the Feather River canyon consists of a V-shaped valley in the lower part of the airshed and a large flat basin in the upper part of the airshed. As described by Neff (1990), these elevated, gently sloping drainage areas are more effective sources of volume flux than the interiors of steep valleys. In a well-drained valley, such as the Kings River canyon, once the downcanyon flow sets up and attains a reasonably steady state, the rate of cooling of the valley atmosphere becomes small (Whiteman, 1990). This is because the air carried down the valley is replaced by potentially warmer air from aloft and a balance is maintained between the inflow of the warmer air and the cooling produced by diabatic processes. In a large basin with a small outflow region, such as the upper part of the North Fork of the Feather River, moderate rates of cooling can continue throughout the night as a smaller amount of warmer air is entrained from above.

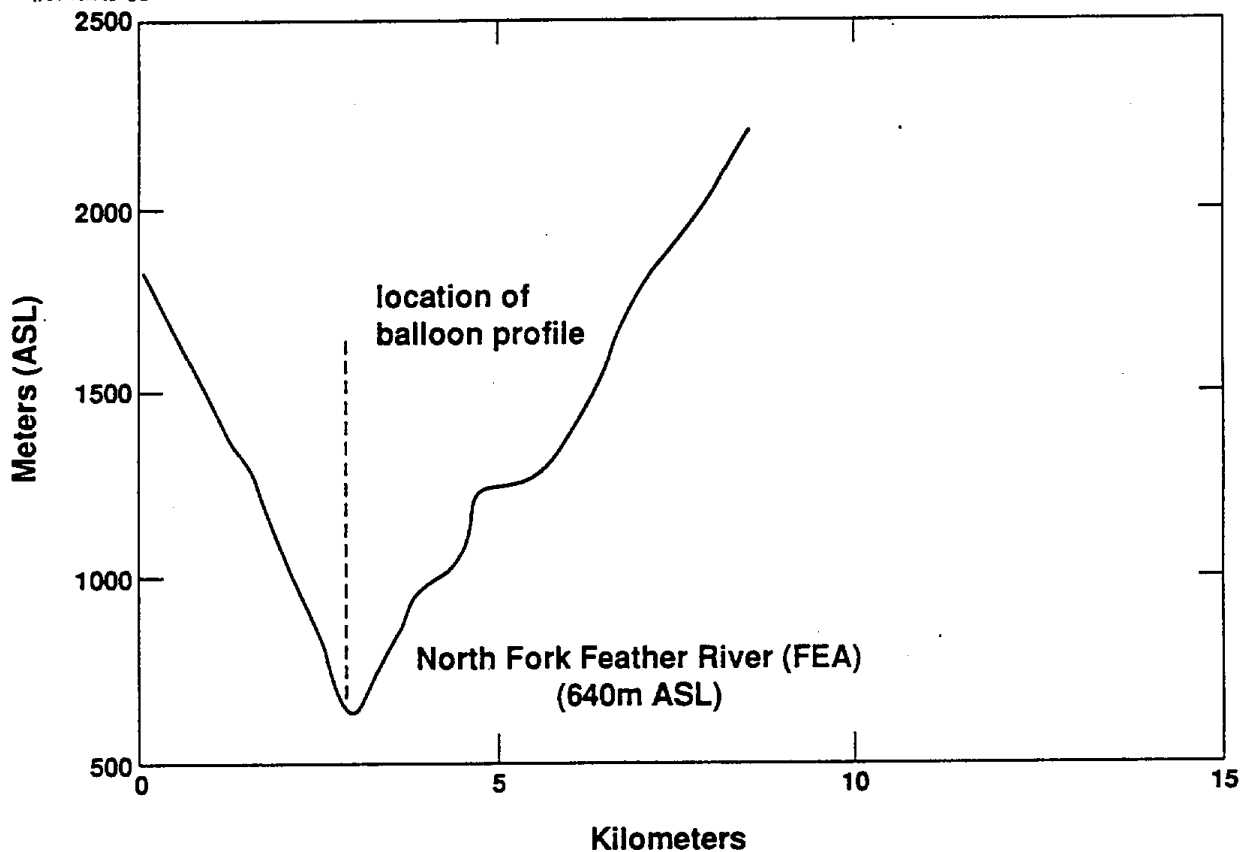


Figure 15. North Fork of the Feather River cross-section. The location of the cross-section is indicated on Fig. 14. The approximate path of the balloon profile is indicated by the dashed line.

9.1.4 Relationship of drainage winds to the recirculation of pollutants.

This study has documented the existence of deep, strong drainage flows channeled through two different river canyons on the western slope of the Sierra Nevada Mountains. Several of these canyons drain into the east sides of the San Joaquin and Sacramento Valleys. The profiler located near Oroville documented the depth and strength of one of these drainages as it exited into the Sacramento Valley. Considering the large volume of air transported by these drainages, a substantial portion of the polluted air advected into the mountains by the daytime upslope winds may be returned to the valleys during the nighttime and early morning hours. The results suggest that current simulations may not correctly model these drainage flows. A substantial improvement in these models may occur with the incorporation of these terrain-associated flows.

10 ANALYSIS: NORTHERN CALIFORNIA TRANSPORT STUDY

This section examines the response of ozone transport from one basin to another to significant mesoscale events. In particular transport between the San Francisco Bay Area and the Sacramento Valley are investigated. Summer and early fall synoptic weather patterns in California are often conducive to high ozone levels, especially near heavily populated areas. These conditions include high pressure ridges aloft, light winds, low subsidence inversions, and strong insolation. This section examines the relationship between synoptic-scale and mesoscale atmospheric influences on ozone levels in the San Francisco Bay Area (SFBA) and the Sacramento Valley.

10.1 The San Francisco Bay Area and the Sacramento Valley

The surface synoptic-scale meteorology of this region during the summer and early fall is dominated by the semi-permanent subtropical high over the eastern Pacific Ocean and a persistent thermal trough within the Central Valley. The unequal heating of the land and water surfaces generates a flow of marine air through the Carquinez Strait and other passageways. The Carquinez Strait represents an area where the air flows unobstructed from the SFBA into the Central Valley. Synoptic patterns are typically weak at 500 mb although the forcing from aloft is sometimes sufficient to influence the timing and intensity of the mesoscale airflow. In general, troughs at 500 mb increase the depth of the marine layer (subsidence inversion base rises) and the influx of marine air into the Central Valley, while ridges at 500 mb, coupled with the surface high, produce a deep layer of light winds and a large area of subsidence. This subsidence lowers the inversion base, thus decreasing the depth of the marine layer. The subsidence also inhibits convective activities and enhances atmospheric photochemistry due to clear skies. During the months of July, September, and October, 1991, more than 50% of the days recorded 500-mb height anomalies greater than 15 m, with the largest percentages during September and October.

The number of violations of the State of California Air Quality Standard for ozone for the period 1 July through 31 October '91 in both the San Francisco Bay Area and the Sacramento Valley fell below the number normally observed during that period. In the Sacramento Valley, 62 ozone violations occurred during the 4-month period, with a maximum reading of 19 pphm on 30 July at the Folsom monitoring site. Nineteen of these events occurred during July, 12 in August, 17 in September, and 14 in October. As discussed previously, the three months with the most violations also represent those months with positive height anomalies at 500 mb. The SFBA recorded 22 ozone violations during the same 4-month period, with a maximum reading of 14 pphm on 2 July at the Livermore monitoring site. Only one of these violations occurred during the month of August, with 5 events in July, 10 in September, and 6 in October. The majority of violations in the Sacramento Valley occurred at the Folsom site, located east of Sacramento at an elevation of 66 m ASL. This site is located at the base of the Sierra Nevada foothills along the American River. Ozone levels at this site equaled the maximum for the Sacramento Valley on 58% of the events. The Auburn site, also located in the Sierra Nevada foothills at an elevation of 395 m ASL, equaled the daily maximum during 26% of the events. This percentage may have been higher as ozone data were not available from this site after 22 September. In the San Francisco Bay Area, the Livermore site recorded a large majority of the ozone violations, equaling the maximum for the SFBA on 64% of the events. The site, at an elevation of 148 m, is located east of the San Francisco Bay area within a nearly closed basin. Other ozone exceedences

typically occurred in the southern part of the SFBA. These events occurred when the marine layer could not penetrate the Livermore Valley because base of the subsidence inversion was below the elevation of openings in the topography surrounding the Livermore Valley.

10.2 Data Sources for the SFBA - Sacramento Valley Study

A number of sources were tapped to establish the synoptic-scale and mesoscale data bases for this study. Information on the thermal structure of the atmosphere above the SFBA were obtained from the 00 GMT rawinsonde soundings from Oakland for the period 1 July - 22 October 1991. Surface pressure data were obtained from the National Meteorological Center (NMC) 00 GMT surface analyses. Upper level (500 mb) features were analyzed using the 00 GMT 500-mb analyses. Ozone data were obtained from the California Air Resources Board and included hourly averages from 21 stations in the Sacramento Valley Air Basin and 22 stations in the SFBA Air Basin. Mesoscale winds within the Sacramento Valley were obtained from the network of eight 915 MHz wind profilers, with a horizontal spacing of approximately 50 km (Fig. 1), obtaining hourly wind profiles from 100 m to 5 km. Mixing heights within the Sacramento Valley were derived from profiler data as described in Section 8.1.

10.3 Meteorological Influence on Ozone Levels in the SFBA and the Sacramento Valley

This section examines the mesoscale and synoptic-scale meteorological parameters which determine near-surface ozone concentrations in both the SFBA and the Sacramento Valley Air Basins. As discussed earlier, the state of the atmosphere has a significant effect on the amount of pollution at a particular site. In this section, various statistical techniques are used to identify those meteorological parameters. A statistical significance level of 0.01 was chosen for the statistical tests in Section 10 of this report. Table 7 lists the meteorological variables used in the statistical analysis. The variables BASEIN, STRIN, and DTDZ were all determined from the 00 GMT Oakland rawinsonde. The SFBA will be examined first, followed by the Sacramento Valley. The results for the two areas will be compared to identify similarities and differences. For all of the following statistical analyses, days were categorized according to maximum ozone levels for that day. Group 1 days represent those days where the maximum ozone level remained below 8 pphm while Group 2 days represent those days where the maximum ozone level equals or exceeds the state standard of 10 pphm. Those days with maximum ozone levels of 8 or 9 pphm were eliminated from the analysis to provide some separation between the groups.

The first part of the statistical analysis examines the differences between the means of the meteorological parameters in the two groups. Results are shown in Table 8. A t-test was utilized to determine the probability that a difference at least as large as the one observed would occur if the two population means were equal. This probability was chosen as 0.01. The results showed that significant differences existed between the ozone groups for the variables DELPRS, TROFST, TROF, RIDG, and BASEIN. The results suggest that high ozone days in the San Francisco Bay Area would be characterized by 500-mb ridging either over or to the west of the area, accompanied by a well-developed surface thermal trough through the Central Valley with a strong pressure gradient between Reno and Sacramento ($P_{\text{Reno}} > P_{\text{Sacramento}}$), and a shallow marine layer in the SFBA.

Table 7 Meteorological variables used in the statistical analysis.

Variable Name	Description
BASEIN	Represents the depth of the mixed layer, the depth of the marine layer, and the height of the base of the subsidence inversion.
STRIN	Represents the temperature difference between the top and base of the inversion(°C).
DTDZ	Represents the temperature gradient within the subsidence inversion (°C/km).
DELPCS	Pressure difference (mb) between the coast just northwest of San Francisco and Sacramento.
DELPRS	Pressure difference (mb) between Reno, Nevada and Sacramento.
TROFST	Represents a measure of the strength of the thermal trough. $((P_{Reno} + P_{Coast})/2) - P_{Sacramento}$
RIDG	RIDG = 0 if no ridge exists at 500 mb between 120-130 longitude and 35-40 latitude. RIDG = 1 if a ridge does exist in this region.
TROF	TROF = 0 if no trough exists at 500 mb between 120-130 longitude and 35-40 latitude. TROF = 1 if a trough does exist in this region.

Next, in order to quantify the strength of the association between the various meteorological parameters and the ozone levels, a correlation analysis was undertaken. The results are shown in Table 9. The correlation coefficients were then examined along with scatterplots. This ensures that no nonlinear relationships exist between the meteorological variables and the ozone levels. Statistically significant correlations existed between the ozone levels and the meteorological variables DELPRS, TROF, RIDG, TROFST, and BASEIN. A significance level of .01 was chosen for this analysis. This means that the probability that a correlation coefficient of at least the indicated value can be obtained when there is no linear association is less than .01. The results show that ozone levels in the San Francisco Bay Area are affected by the presence of a ridge or trough at 500 mb, the strength and presence of a surface thermal trough through the Central Valley, and the depth of the marine layer. In particular, the highest ozone levels will be observed with a 500-mb ridge lying over or west of the San Francisco Bay Area, a strong thermal trough in the Central Valley, and a shallow marine layer.

Table 8 Comparison of means of the meteorological parameters for the two ozone groups. Ozone values are from the SFBA.

	GROUP 1 ($O_3 < 8$ PPHM)	GROUP 2 ($O_3 > 9$ PPHM)
DELPRS	0.06	5.1
DELPCS	3.81	3.24
TROFST	1.94	4.18
TROF	0.36	0.05
RIDG	0.14	0.64
BASEIN	406.01	101.45
STRIN	6.85	5.95
DTDZ	16.27	17.08

A multiple regression analysis was next used to determine the relative importance of each of the independent variables for determining ozone levels. A stepwise selection procedure was chosen for this analysis. In this procedure, the first variable considered for entry into the regression equation is the one with the largest positive or negative correlation with the dependent variable. The second variable is selected based on the highest partial correlation. If it passes entry criteria, it also enters the equation. Now, the first variable is examined to see whether it should be removed according to the removal criteria (minimum F value). Variables not in the equation are examined for entry while variables in the equation are examined for removal. The results of the procedure showed that the variable DELPRS accounted for 51% of the variance in ozone levels. The variables DELPRS and BASEIN accounted for 55% of the variance while the variables DELPRS, BASEIN, and DELPCS accounted for 57% of the variance in SFBA ozone levels. Large colinearities existed between the variable DELPRS and several of the other meteorological variables. A correlation coefficient of $-.43$ existed between DELPRS and TROF while a correlation coefficient of $.53$ existed between DELPCS and RIDG. The reason for this interrelationship appears to be that a 500-mb trough tends to cool the Sacramento Valley, thus decreasing the intensity of the thermal low, and in turn decreasing the magnitude of the pressure difference between Sacramento and Reno. Just the opposite effect occurs with the presence of a 500-mb ridge, with strong heating of the Sacramento Valley intensifying the thermal low, thus increasing the pressure difference between Sacramento and Reno. A strong colinearity also existed between the meteorological variables DELPRS and BASEIN ($r = -.58$) with shallow marine layers associated with large pressure differences between Sacramento and Reno ($P_{\text{Reno}} > P_{\text{Sacramento}}$). This colinearity seems to be associated with the interrelationship between 500-mb ridging, the depth of the marine layer, and the pressure difference between Sacramento and Reno. In addition to its effect on heating in the Sacramento Valley, 500-mb ridging also creates a shallower marine layer than normally observed with no ridge situations. Much different results are obtained by leaving the variable DELPRS out of the multiple regression analysis. The variable TROFST accounted for 40% of the variability in ozone levels in the SFBA, TROFST and DELPCS accounted for 53%, and TROFST, DELPCS, and BASEIN accounted for 57% of the variance. These results show that ozone levels in the SFBA are controlled by the strength of the thermal trough, coast-inland pressure gradients, and the depth of the marine layer. The variables TROFST and BASEIN are in turn controlled by TROF and RIDG. During the entire 4-month study, the pressure difference between the coast and Sacramento remained positive ($P_{\text{Coast}} > P_{\text{Sacramento}}$) and showed a strong linear relationship ($r = .54$) with only one other meteorological

variable, the strength of the marine inversion (STRIN). The reason for this relationship is that as temperatures equalize between the coast and inland, either from a frontal passage or strong heating along the coast, pressures tend to equalize also. A weak subsidence inversion is also associated with frontal passages and strong heating along the coast. As discussed earlier, the selection of meteorological variables has been arbitrary to some extent and it is unlikely that all relevant variables have been identified. In addition, non-linear relationships may exist between the meteorological variables and ozone concentrations. Only linear relationships were examined in this analysis. This may account for the relatively low amount of variance explained by the meteorological variables.

Table 9 Correlation matrix using ozone data from the SFBA.

	O ₃	DEL-PRS	DEL-PCS	TROF	RIDG	BAS-EIN	STRIN	DT-DZ	TROFST
O ₃	1.00								
DELPRS	.72	1.00							
DELPCS	-.23	-.13	1.00						
TROF	-.39	-.43	.00	1.00					
RIDG	.51	.53	-.14	-.37	1.00				
BASEIN	-.57	-.58	.02	.44	-.38	1.00			
STRIN	-.08	-.02	.54	-.08	.08	-.19	1.00		
DTDZ	.03	.04	.15	-.07	.11	.06	.40	1.00	
TROFST	.63	.94	.21	-.43	.47	-.56	.16	.09	1.00

As in the analysis for the San Francisco Bay Area, differences between the means of the meteorological parameters for the two ozone groupings were examined for the Sacramento Valley area. Results are shown in Table 10. For this analysis, statistically significant differences existed between the ozone groups for the variables RIDG, TROF, DELPRS, and TROFST. The results suggest that high ozone days in the Sacramento Valley would be characterized by 500-mb ridging, accompanied by a well-developed thermal trough through the Central Valley, with a large pressure difference between Reno and Sacramento ($P_{\text{Reno}} > P_{\text{Sacramento}}$).

Table 10 Comparison of the means of the meteorological parameters for the two ozone groups. The ozone data are from the Sacramento Valley.

	GROUP 1 (O ₃ < 8 pphm)	GROUP 2 (O ₃ > 9 pphm)
DELPCS	3.59	3.71
DELPRS	-0.42	2.45
TROFST	1.59	3.08
TROF	0.52	0.13
RIDG	0	0.41

Results of the correlation analysis are shown in Table 11. Statistically significant correlations existed between the Sacramento Valley ozone levels and the meteorological variables DELPRS, TROF, RIDG, and TROFST. The results show that ozone levels in the Sacramento Valley are affected by a ridge or trough at 500 mb and the by the strength and presence of a thermal trough through the Central Valley. Highest ozone levels will be observed with a 500-mb ridge either over or west of the Sacramento Valley and a strong surface thermal trough through the valley. Mixing depth data from both the UCD and PLG sites showed no correlation with the maximum ozone levels measured in the Sacramento area. Although the data set was somewhat limited (26 cases), mixing depths from RAN showed a weak negative correlation (-0.41) with maximum ozone levels measured in the Sacramento area. This may be because the RAN site was located in the same proximity to the foothills as the Folsom and Auburn sites where most of the high ozone values were measured.

Table 11 Correlation matrix using ozone data from the Sacramento Valley.

	O ₃	DELPCS	DELPRS	TROFST	TROF	RIDG
O ₃	1.00					
DELPCS	.07	1.00				
DELPRS	.42	-.17	1.00			
TROFST	.45	.19	.93	1.00		
TROF	-.39	-.08	-.38	-.40	1.00	
RIDG	.46	-.05	.48	.46	-.35	1.00

A multiple regression analysis was used to determine the relative importance of each of the independent meteorological variables for determining ozone levels in the Sacramento Valley. The stepwise selection procedure showed the variable RIDG as the most important variable, accounting for 21% of the variance in ozone levels, while the variables RIDG and TROFST accounted for 29% of the variance. The variables RIDG, TROFST, and TROF accounted for 32% of the variance in ozone levels. The results show that the strength of the thermal trough and the presence of either 500-mb ridging or troughing have the largest influence on ozone levels in the Sacramento Valley. As discussed earlier, all of the relevant meteorological variables may not have been selected for the analysis, which may help explain the relatively low amount of variance explained.

Since the presence of 500-mb troughs or ridges seem to have a dominate influence on the other meteorological variables and the ozone levels, average values of these variables were compared for trough and ridge cases. The results are shown in Table 12. Significant differences existed between the cross-mountain pressure gradient, the thermal trough strength, the height of the base of the subsidence inversion, and the ozone levels. The results show that the presence of a 500-mb trough or ridge has a profound influence on the meteorological parameters that control ozone levels.

A comparison of maximum ozone levels for the 114 day study period for the San Francisco and Sacramento areas shows a correlation coefficient of .60. Although the linear relationship between the two areas is statistically significant, a much stronger relationship was expected, considering the relative proximity of the two areas. Major differences do, however, exist in both topography and meteorology. During the summer months, the San Francisco Bay Area is almost always under the influence of only

slightly modified marine air. This includes a cool, moist marine layer capped by a relatively strong inversion, almost constant west to northwest flow, and a high frequency of low-level stratus, especially during the morning and evening hours. In contrast, the Sacramento Valley is characterized by a deeper mixed layer, diurnally varying wind conditions, hot afternoon temperatures, and generally clear skies. During times of low mixing depths, the topography of the SFBA inhibits the ventilation of pollutants and acts to trap the pollutants near the surface. Also, shallow mixing depths are associated with clear skies, thus allowing the formation of ozone within the lower atmosphere. The strong relationship between surface trough strength in the Sacramento Valley and high ozone values may be explained by the fact that the pressure gradient induces flow from the west that may transport pollutants from the San Francisco Bay Area into the Central Valley. The counter gradient on the eastern side of the valley acts to decelerate these winds, trapping the transported and locally produced pollutants within the valley. The clear skies allow the chemical reactions to proceed which produce ozone.

Table 12. Comparison of means of meteorological variables and ozone levels for trough and ridge cases.

	500-mb Trough	500-mb Ridge
DELPCS	3.51	3.55
DELPRS	-0.38	4.15
TROFST	1.58	3.86
BASEIN	486.03	147.89
STRIN	6	7.33
DTDZ	15.18	17.78
SAO3	7.94	11.82
SFO3	5.68	9

To examine the possibility of transport of ozone from the SFBA into the Sacramento Valley during high ozone events in the Sacramento Valley, profiler winds from the TRS and UCD sites were examined for the months of July through October. Winds obtained at 200 m, 1000 m, and 2000 m above ground level were summarized as speed distributions as a function of directional class interval for all high ozone days ($O_3 > 9$ pphm) in the Sacramento Valley for the time period between 1300 and 1800 PDT. Transport of ozone from the SFBA into the Sacramento Valley would be indicated by winds from the southwest quadrant in the lowest km at both sites. Results show that for TRS, nearly all of the winds at the 200-m level are from the southwest quadrant during high ozone days in the Sacramento Valley. Winds at 1 km possess a more northerly component, reflecting the presence of upper level ridging during these high ozone events. The UCD site had similar results with winds at 200 m largely from the southwest quadrant turning more northerly at 1 km. Winds at 2 km were well distributed from all directions.

Occasionally during high ozone events (> 9 pphm), values in the San Francisco Bay Area exceed those in the Sacramento Valley. This occurred during 15% of the events during the study period. A statistical analysis was carried out to examine differences in the means of the meteorological parameters during those events. The only significant difference observed occurred when comparing the strength of the marine inversion over Oakland with the high ozone events. During times when San

Francisco Bay area ozone levels exceeded those in the Sacramento Valley, the mean inversion strength was 2.9°C. During the events when Sacramento Valley levels exceeded those in San Francisco, the mean inversion strength was 8.3°C. If the inversion strength at Oakland is taken to be representative of the subsidence inversion strength in general, with the strong heating in the Sacramento Valley, a weak inversion would most likely be mixed out by the strong convection resulting in reduced pollution levels. In the San Francisco Bay area, the weak inversion would trap the pollutants, resulting in elevated readings when compared with those in the Sacramento Valley.

As done previously for transport from the SFBA into the Sacramento Valley, to examine the possibility of transport of ozone from the Sacramento Valley into the SFBA during high ozone events in the SFBA, profiler winds from the DEL and TRS sites were examined for the months of July through October. Winds obtained at 200 m, 1000 m, and 2000 m above ground level were summarized as speed distributions as a function of directional class interval for all high ozone days ($O_3 > 9$ pphm) in the SFBA for the time period between 1300 and 1800 PDT. Transport into the SFBA from the Sacramento Valley would be indicated by east to northeast winds at the TRS site and easterly winds at the DEL site. At TRS, the largest percentage of winds in the lowest km during high ozone days in the SFBA were from the south to west with a relative absence of winds from the east to northeast. Similarly at DEL, only a very small percentage of the winds in the lowest km possessed an easterly component with the majority of the winds coming from the northwest quadrant. Results from both of these sites suggest that the contribution of ozone from the Sacramento Valley to high ozone events in the SFBA is minimal.

10.4 Sacramento Valley Wind Fields Derived From Profiler Data

In this section, the array of previously described lower tropospheric wind profilers in the Sacramento Valley are used to examine the mesoscale wind fields under different meteorological and pollution conditions. Both vector plots at constant levels and time-height cross sections of winds are examined.

Using data from the TRS, UCD, PLG, ORO, and DEL wind profilers (Fig. 1), vector plots of the 00 GMT (1700 PDT) winds at the 300, 800, 1300, and 1800 m levels were constructed for various meteorological and pollution conditions. Winds at the 300 m level were the lowest, consistently available winds from the profiler array that still provided data within the layer where the major transport of pollutants would occur. To obtain winds between the profiler sites, a simple inverse distance algorithm was used for interpolating the data. To derive a vector value in a zone where no data exists, the vector value at each profiler site is weighted by the inverse of the distance between that site and the zone to which you are interpolating (see page 35). The weighting maximizes the influence of the winds at the sites closest to the interpolation zone and lessens the influence of those sites furthest away. For this data set, the algorithm in the interpolation package was optimized using a vendor-set exponent of 3.5.

Vector plots were constructed for four different situations; 1) all cases where the maximum ozone level exceeded 9 pphm in the Sacramento Valley (Fig. 16), 2) all cases where the maximum ozone level remained less than or equal to 8 pphm in the Sacramento Valley (Fig. 17), 3) all cases where a 500-mb ridge persisted either over or to the west of California (Fig. 18), and 4) all cases where a 500-mb trough persisted either over or to the west of California (Fig. 19). Results for situations 1 and 2 are shown in Figs. 16 and 17. A comparison of the two figures shows that winds

entering the Sacramento Valley through the Carquinez Straits (just southwest of TRS) at the 300 m level vary only slightly between the two situations with winds approximately 1 ms^{-1} higher for the low ozone case. An examination of the coast to Sacramento pressure difference helps to explain why. For both high ozone and low ozone cases the average DELPCS was 3.7 mb. Since this pressure difference most likely drives the winds through the Carquinez Straits into the Sacramento Valley, the winds should be similar. Major differences in the vector wind fields occurs once the southwesterly flow enters the Sacramento Valley. Most notable is the rapid deceleration of the winds upon entering the valley. This rapid deceleration appears to be associated with the strength of the thermal trough. As the winds enter the center of the valley they begin to encounter a counter pressure gradient causing the rapid deceleration. A comparison of Reno - Sacramento pressure differences (DELPRS) for high and low ozone cases shows a DELPRS of 3.1 mb for high ozone cases and 0.5 mb for low ozone cases. Another area of interest is the region of diffluence just east of the Carquinez Straits. The diffluence in this region seems to be related to both topographic and thermal effects. For the high ozone cases (Fig. 16) the region of highest ozone typically occurs along the foothills directly east of UCD. This is also the area (Sacramento) with the largest population density in the Sacramento Valley. The combination of these factors, possible transport of pollutants from the San Francisco Bay area, a large population density, and weak winds may all lead to the high ozone values observed in this area. The black lines on each of the vector plots represent streamlines originating in the middle of the Carquinez Straits. Both the high and low ozone cases show that at the 300 m level, a parcel of air passing through the Carquinez Straits would pass just south of TRS, over UCD, and then continue north through the central portion of the Sacramento Valley. Major differences exist in the wind field above 300 m. While winds for the low ozone cases maintain their southerly component at all levels, high ozone case winds turn northerly with height. For high ozone cases, air passing through the Carquinez Straits flows directly towards the Sacramento area between the 300 and 800 m levels. Strong convective mixing within the valley could bring this air, possibly laden with ozone and ozone precursors, near the surface.

The results from cases with a 500-mb ridge (Fig. 18) are remarkably similar to high ozone cases while cases with a 500-mb trough (Fig. 19) are remarkably similar to the low ozone cases. This is because high ozone cases normally occur with the presence of 500-mb ridging while low ozone cases normally occur with 500-mb troughs.

A similar analysis was done using time-height wind vector plots for both high and low ozone cases. Wind profiler data from TRS, PLG, and UCD were used for this analysis. Results in general show that in the lowest km, low ozone cases have persistent south to southwest winds with little diurnal variation. In contrast, high ozone cases show large diurnal variations, with regions of northerly flow during the late night and morning hours and south to west flows in the afternoon and evening. Winds at TRS are consistently from the southwest in the lowest 300 m for both high and low ozone cases (Figs. 20 and 21). The large diurnal variations at UCD (Fig. 22) and PLG (Fig. 23), for the high ozone cases, could result in the recirculation of aged pollutants within the valley. The persistence is defined as the ratio of the vector mean wind speed to the scalar wind speed (a wind from a constant direction has a persistence of 1, and a randomly distributed wind direction has a persistence of zero) (Wilczak, et al., 1992). For both high and low ozone cases, the persistence of the winds in the lowest 300 m were typically 80%.

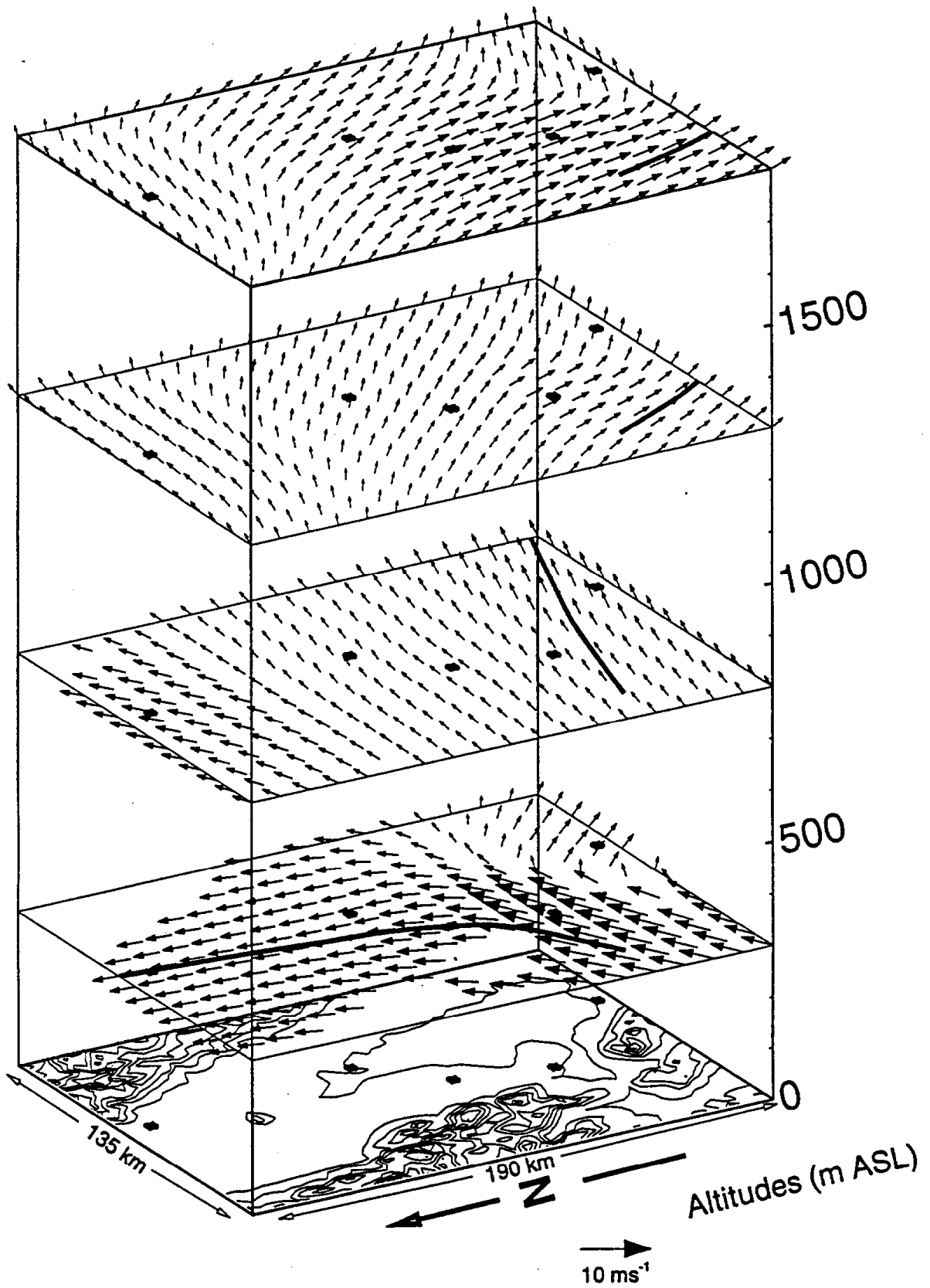


Figure 16. Vector winds for high ozone cases at 1700 PDT derived from profiler data.

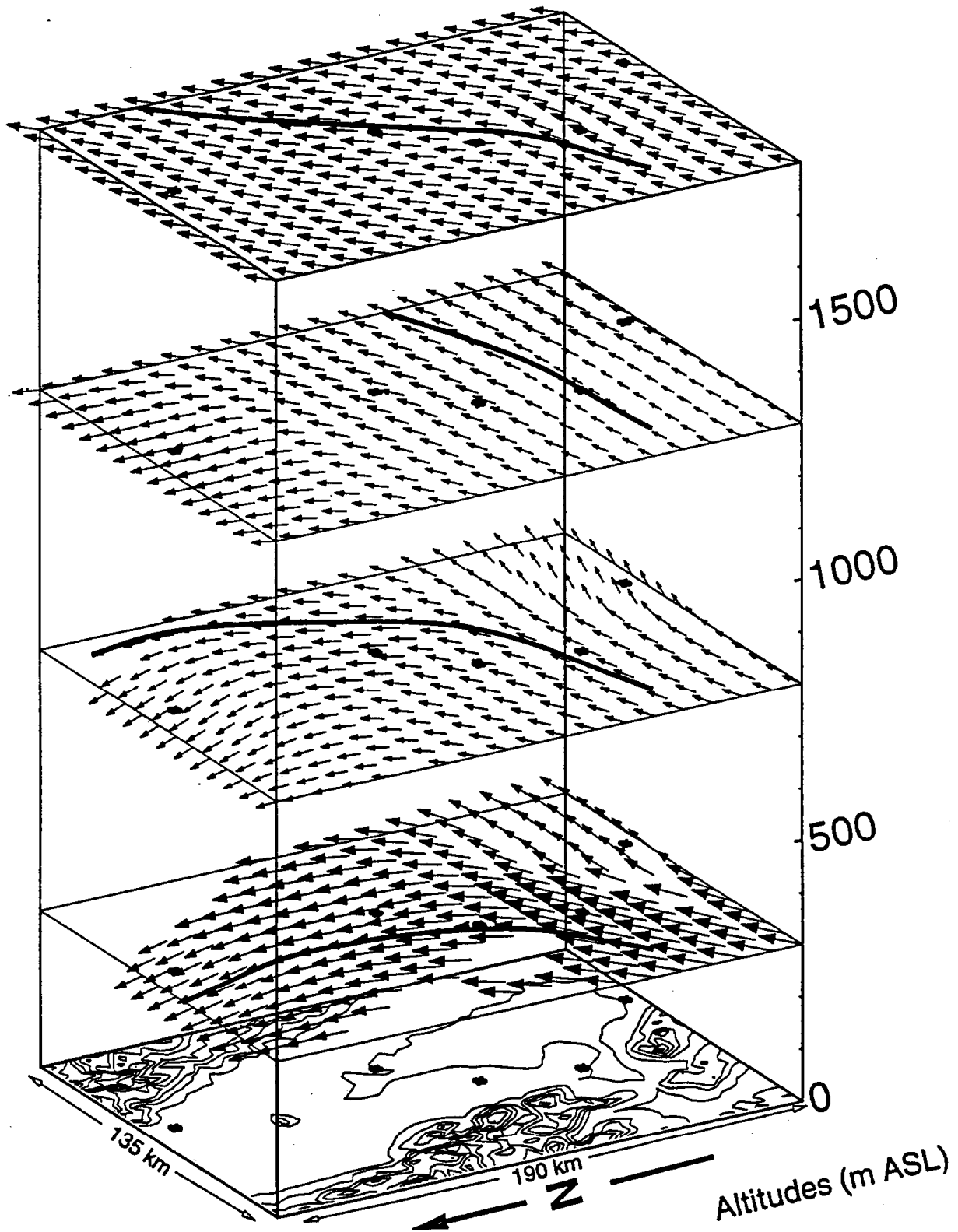


Figure 17. Vector winds for low ozone cases at 1700 PDT derived from profiler data.

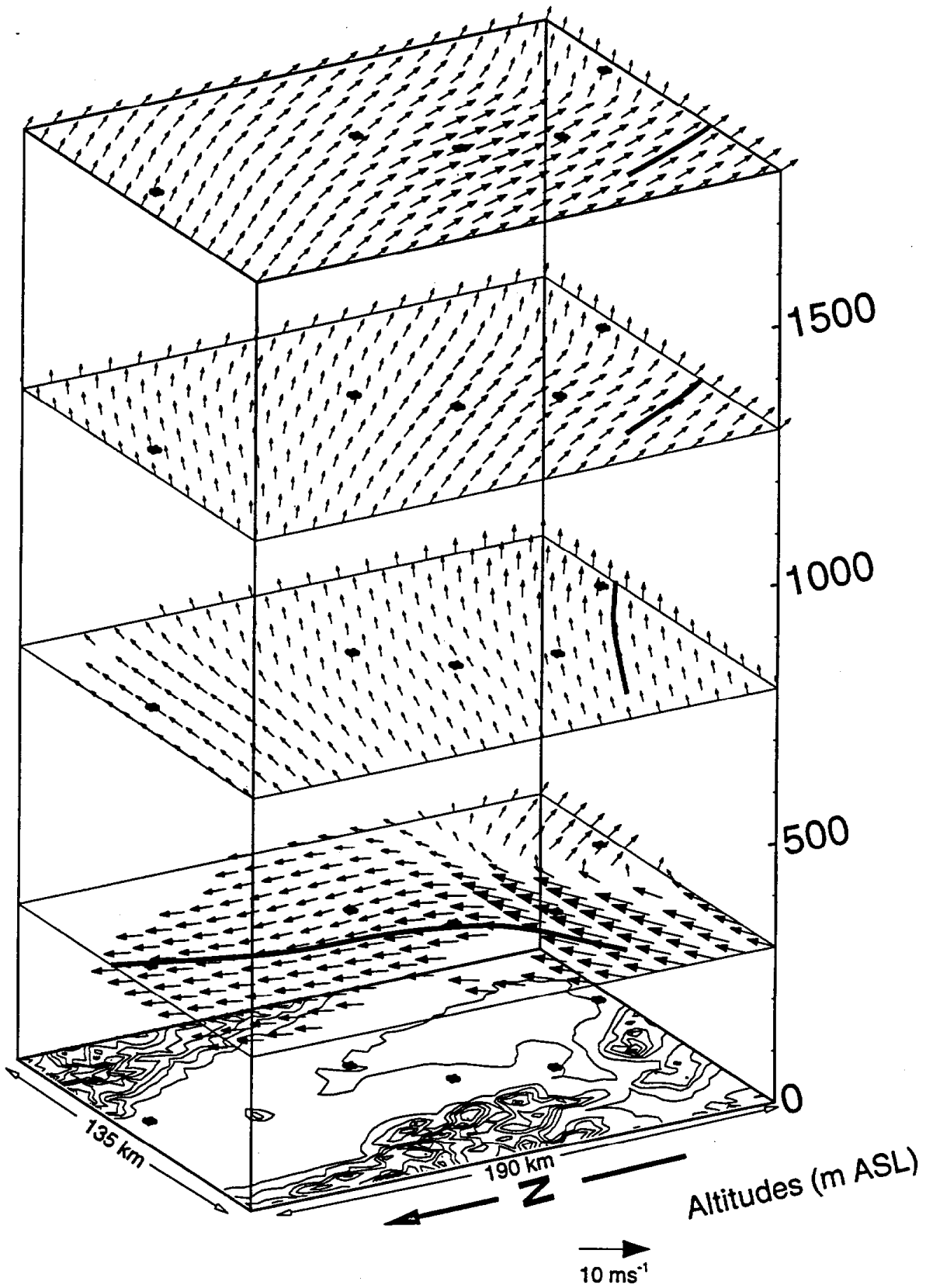


Figure 18. Vector winds for 500-mb ridge cases at 1700 PDT derived from profiler data.

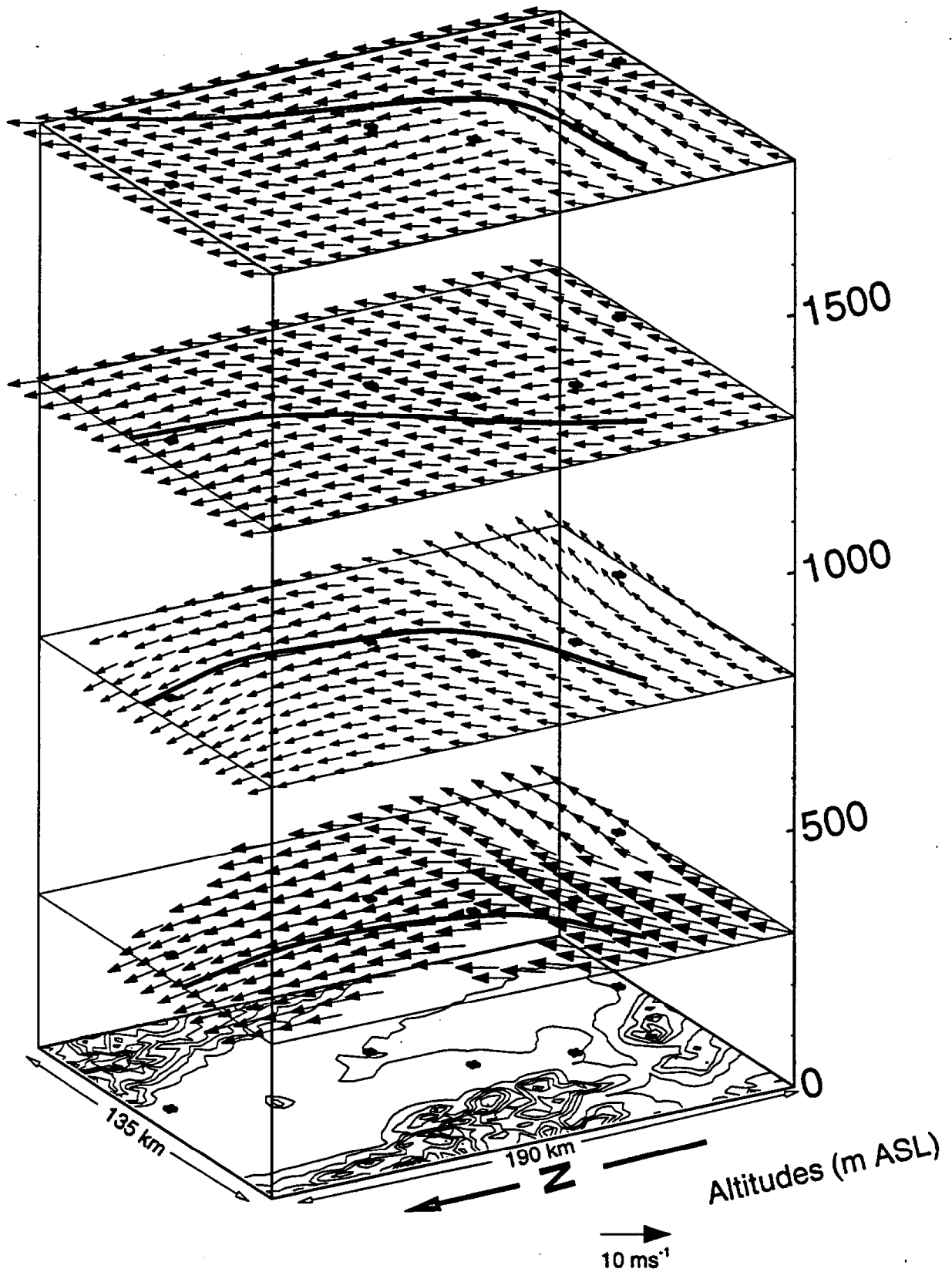


Figure 19. Vector winds for 500-mb trough cases at 1700 PDT derived from profiler data.

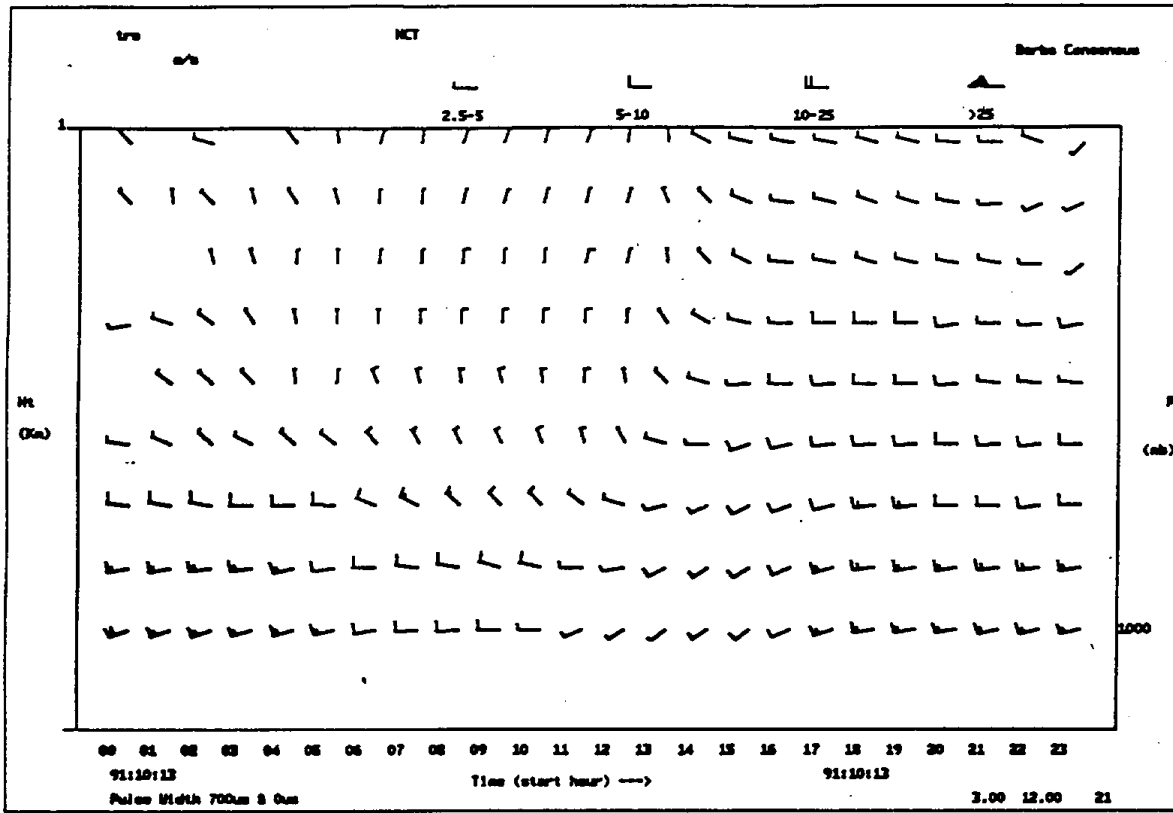


Figure 20. Ensemble average time-height (GMT) cross section of winds at TRS for high ozone cases.

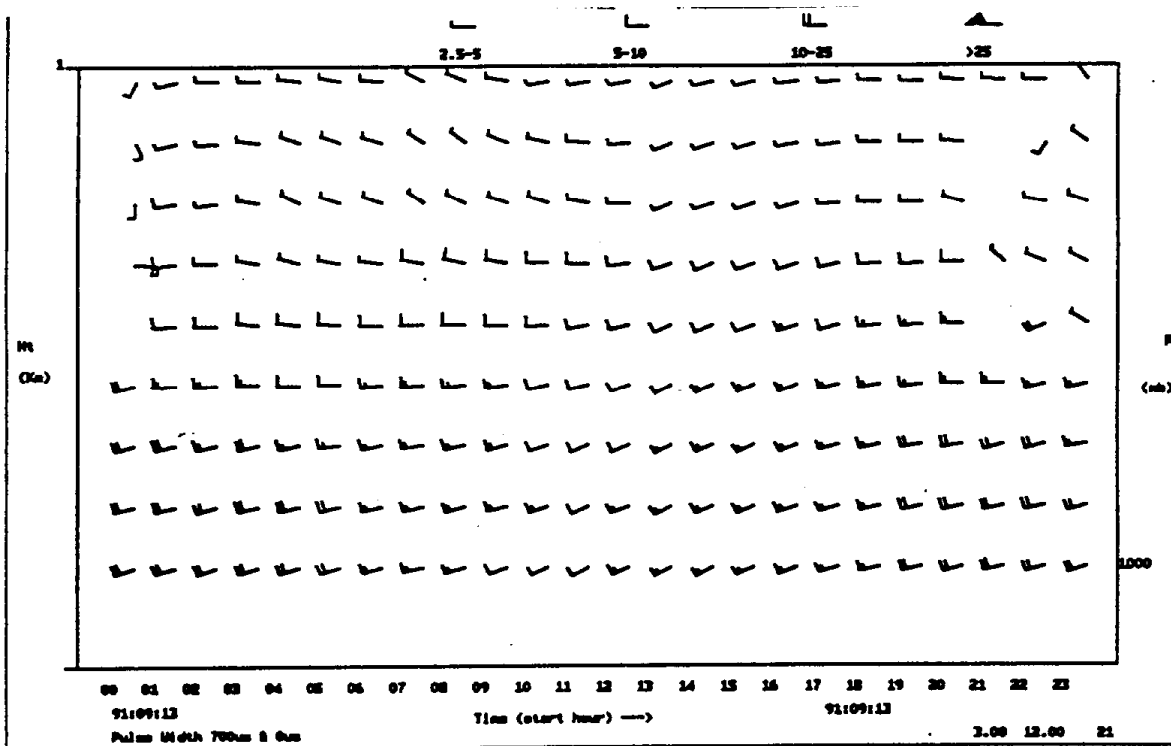


Figure 21. Ensemble average time-height (GMT) cross section of winds at TRS for low ozone cases.

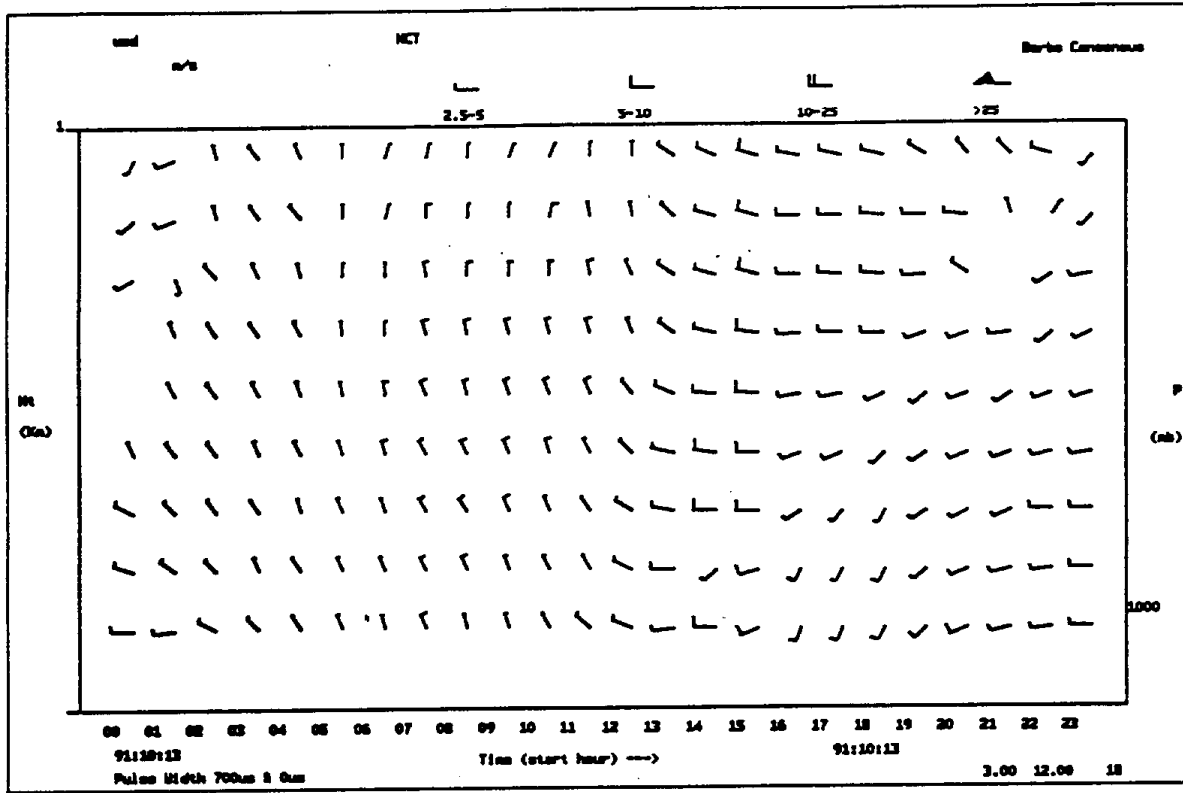


Figure 22. Ensemble average time-height (GMT) cross section of winds at UCD for high ozone cases.

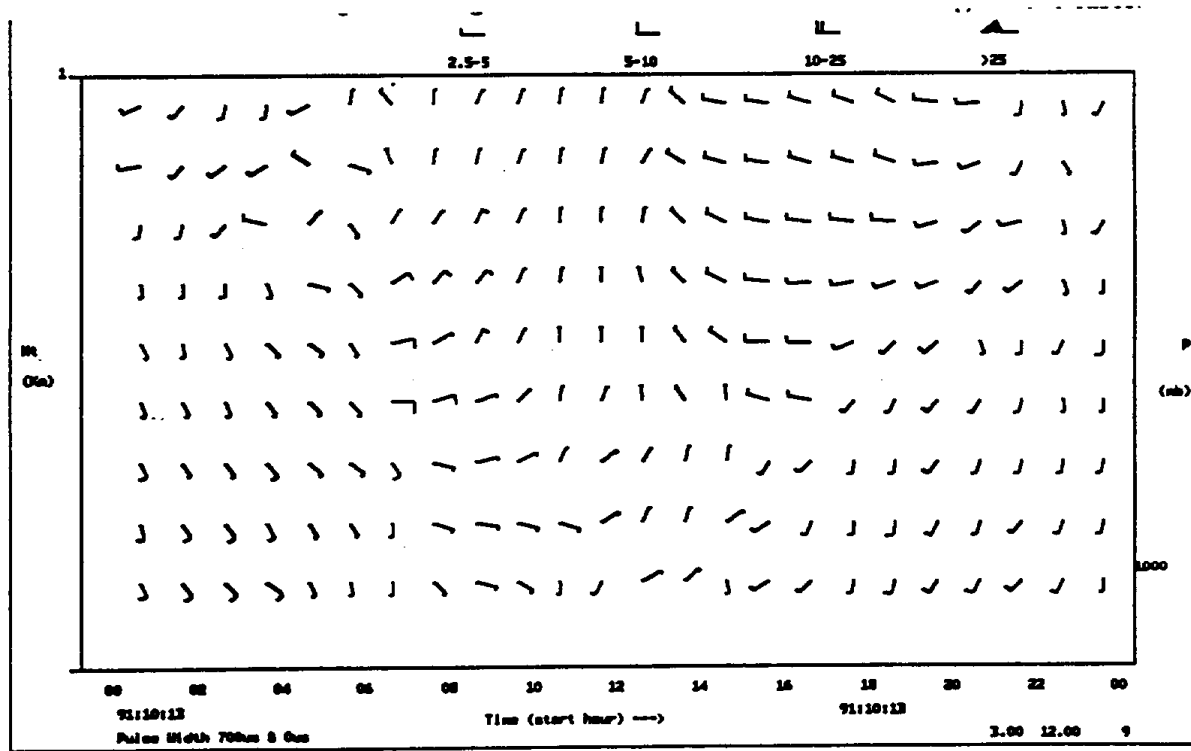


Figure 23 Ensemble average time-height (GMT) cross section for winds at PLG for high ozone cases.

10.5 Potential for Transport Between The SFBA and the Sacramento Valley Air Basins

The original goals of this part of the study were to identify the dominant synoptic-scale and mesoscale meteorological patterns associated with high ozone levels in both the San Francisco Bay area and the Sacramento Valley and to then exploit these relationships to examine the potential for transport between the SFBA and the Sacramento Valley.

During the summer and early fall of 1991, the SFBA recorded 22 violations of the NAAQS for ozone, while during the same period the Sacramento Valley recorded 49 violations. The areas most susceptible to high ozone values are those areas downwind of the major source regions with elevated terrain to the east blocking the prevailing winds. These regions typically record the highest ozone concentrations.

Days with high ozone concentrations in the San Francisco Bay Area are characterized by 500-mb ridging either over or west of California, accompanied by a well-developed thermal trough through the Central Valley, and a shallow mixed layer in the SFBA. For these days, the depth of the mixed layer was the most important variable for determining ozone levels, followed by the presence or absence of ridging at 500 mb.

Days with high ozone concentrations in the Sacramento Valley were similar to those in the SFBA, although the mixing heights within the Sacramento Valley showed little relationship to the ozone levels. For this area, high ozone values will be observed with a 500-mb ridge either over or west of California accompanied by a strong surface thermal trough through the Central Valley. The most important variable for controlling ozone levels was the 500-mb ridge, accounting for 21% of the variance in ozone levels, while the 500-mb ridge and the thermal trough strength accounted for 29% of the variance. The variables RIDG, TROFST, and TROF explained 32% of the variability in ozone levels.

Both the meteorology and topography in the SFBA are more favorable for the ventilation and transport of pollutants out of the area. The only times when ozone values in the SFBA exceed those in the Sacramento Valley occur with rather weak subsidence inversions. It was speculated that these weak subsidence inversions are destroyed in the valley because of the strong heating. An examination of profiler winds during high ozone events suggested a strong possibility for transport of ozone from the SFBA into the Sacramento Valley during high ozone days in the Sacramento Valley but only a very small probability of transport from the Sacramento Valley into the SFBA during high ozone days in the SFBA.

Profiler measured winds show that below 500 m, 500-mb patterns have only a minimal effect on the flow at sites closest to the Carquinez Straits. A profiler located near the gap between the SFBA and the Central Valley showed that for nearly all summer and early fall meteorological conditions, the flow is almost continuously from the west, suggesting the possibility of continuous transport of pollutants from the SFBA into the Central Valley. The 500-mb patterns above 500 m do, however, have a large effect on the winds.

11 ANALYSIS: THE SOUTH COAST AND SOUTHEAST DESERT AIR BASINS

Similar to the previously described central and northern California study areas, the late spring and summer climate of this region is dominated by the presence of the semi-permanent subtropical high over the eastern Pacific Ocean with a persistent thermal trough over the desert. The predominant wind direction during this time period is northwesterly. The combination of this northwesterly flow over a relatively cool ocean surface and the descending air on the eastern side of the subtropical high results in a persistent marine layer. The combination of a surface-based marine layer capped by a strong subsidence inversion within a heavily populated region on a coastal plane bounded by mountains results in a severe air pollution problem. As discussed by Keith (1980), the depth of the marine layer, defined as the height of the base of the subsidence inversion, is the most important meteorological parameter that affects the daily ozone maximum concentrations. The most effective mechanism for transporting this pollution out of the South Coast Air Basin (SoCAB) is through the major passes within the mountains surrounding the SoCAB leading into the Southeast Desert Air Basin (SEDAB). These include the Soledad Canyon, the Cajon Pass, and the Banning Pass. Transport from the SoCAB to the SEDAB has been substantiated by visual observations, by the analysis of daily wind patterns, and by contaminants measured at desert receptor areas (Keith, 1980). Sections 11.2 and 11.3 will concentrate on transport through the Banning and Cajon Passes, respectively. During the Southern California Transport (SCT) Study, wind profilers were located on both sides of these passes providing vertical profiles of winds both upwind and downwind of the passes. Historically, winds aloft data have been sparse in the SoCAB and computations of movement of polluted air have been based on surface wind data (Keith, 1980). The profilers provided the opportunity to examine the vertical structure of the wind fields in both the ozone source and receptor regions.

To examine transport through the Cajon Pass, wind profilers were located in San Bernardino and Hesperia (Fig 2). For this study, the months of July and August were investigated. During these two months, violations of the state ozone standard occurred on a majority of the days. At San Bernardino, 79% of the days violated the ozone standard while 61% of the days violated at Hesperia. A maximum reading of 24 pphm was recorded at the San Bernardino monitoring site on 15 August '92 with a reading of 18 pphm at Hesperia on the same day. Profilers located at Banning and White Water (Fig 2) measured winds both upstream and downstream of the Banning Pass during the period from 1 May through 23 June '92. During this time, six violations of the state ozone standard occurred at the Banning monitoring site. With lower level flows almost continuously from west to east through the Banning Pass, the receptor areas for pollutants from the SoCAB would likely include Palm Springs and Indio. Unfortunately, the Palm Springs monitoring site was nonoperational for 24 of the 54 study days. During the other 30 days, 8 violations of the ozone standard were recorded. At the Indio site, violations occurred on 6 of the 54 study days.

11.1 Data Sources For The South Coast Air Basin - Southeast Desert Air Basin Study

Similar to the analysis for the SFBA - Sacramento Valley study, both synoptic-scale and mesoscale data were utilized for this study. Synoptic-scale information were obtained from the NMC 00 GMT surface and 500-mb analyses. As with the NCT study, synoptic-scale patterns were classified according to the presence of a trough or ridge at 500 mb. Trough days are those days when a 500-mb trough was present between 110°-125° longitude and 30°-35° latitude. A ridge day represents those days with a 500-mb ridge in the same region. The surface pressure gradient between Los Angeles

International Airport (LAX) and Yuma was taken as the representative coast - desert pressure gradient. This gradient was used by McCutchan and Schroeder (1973) to classify meteorological patterns in southern California and was found to be the most useful predictor of summer weather patterns. Mixing depths were obtained from the profilers at San Bernardino and Banning using profiler signal strength. Mesoscale wind fields were obtained from wind profilers located on either side of the Banning and Cajon Passes. All wind profiler data are presented in GMT for this part of the study. Ozone data were obtained from the California Air Resources Board and included hourly averages from all stations in the SoCAB and the SEDAB. All statistical tests in Section 11 use significance levels of 0.01. Sections 11.2 and 11.3 use the presence of a 500-mb trough or ridge, the mixing depth, and the coast-to-desert pressure gradient as meteorological parameters for the statistical analyses.

11.2 Banning Pass Transport

This study encompasses the time period from 1 May through 23 June '92. As discussed previously, relatively few ozone violations occurred in the Banning Pass area during this period. Ozone levels were obtained from the Banning, Indio, and Palm Springs monitoring sites. A correlation analysis between the meteorological parameters and the ozone levels showed very little correlation between the variables. The only significant relationship existed between the mixing height and the pressure gradient ($r=.64$). The reasons for the lack of correlations are twofold. First, ozone levels at all three sites during the study period were relatively low with maximum levels of 11, 13, and 12 pphm at the Banning, Indio, and Palm Springs sites respectively. Also, the synoptic-scale pattern was dominated by 500-mb troughs resulting in deeper mixed layers, more clouds, and lower temperatures in the Banning area. These conditions typically result in lower ozone production. Relatively few 500-mb ridge events occurred during the study period. A comparison of maximum ozone levels at Banning and Palm Springs shows that Palm Springs maximum ozone levels average 32% greater than those at Banning. Wind profiler data from Banning (Fig. 24) and White Water (Fig. 25) shows that on high ozone days in Palm Springs, the flow of air is continuously from west to east through the Banning Pass in the lowest 500 m. This suggests that the air in the Palm Springs area originates in the SoCAB. As this polluted air is carried towards Palm Springs, photochemical reactions in the clear desert air produce ozone. These reactions may have been inhibited in the SoCAB because of cloudier conditions. The concentrations can remain high, as fewer nitric oxide sources in the desert area reduce ozone loss by nitric oxide scavenging. Fig. 26 shows a time series of average ozone levels on high ozone days in Palm Springs. Nighttime levels remain relatively high because of the lack of nitric oxide scavenging. Maximum levels occur several hours after radiational sunset. During the daytime hours, strong dispersion in this area keeps ozone levels low. In contrast, Banning ozone levels (Fig. 27) remain relatively low during the nighttime hours and peak 1 to 2 hours prior to the peaks observed in the Palm Springs data set. Overall the data set suggests that almost continuous transport from the SoCAB into the SEDAB occurs during the late spring and early summer through the Banning Pass possibly increasing ozone levels in both the Palm Springs and Indio areas.

In Figs. 24 and 25, the ensemble average winds for the profilers at Banning and White Water reveal a persistent westerly component at low levels throughout the full diurnal period. However, aloft, easterly winds develop from 0700 GMT through 1800 GMT (mid-night through early morning) descending to less than a km at times. The decrease in the height of the shear layer may result from the decrease in the coast-to-inland thermal contrast during the night and the consequent decrease in westerly airflow. Of interest is the easterly flow aloft during these episodes. Close inspection of the raw profiler moment data does not give any indication of bird contamination. However, synoptic

analyses do not support this airflow either. The absence of upper air soundings to the east limits our ability to interpret this phenomena.

11.3 Cajon Pass Transport

The months of July and August 1992 were used for this analysis. During these months, pollution monitoring stations located on both sides of the Cajon Pass violated the state ozone standard on the majority of days. As in the previous analysis, a correlation analysis between the meteorological parameters and the ozone levels was performed. The results showed statistically significant relationships between the maximum ozone levels in San Bernardino (SBO) and the SBO mixing height ($r = -0.52$), the presence of a 500-mb trough ($r = -0.48$), and the presence of a 500-mb ridge ($r = +0.53$). Also, significant correlations existed between the mixing height and the presence of a 500-mb trough ($r = +0.43$) and the presence of a 500-mb ridge ($r = -0.33$). These results suggest that high ozone days in the SBO area will occur with lower mixing heights resulting from 500-mb ridging. Troughs at 500 mb create deeper mixing depths and lower ozone values. A comparison of profiler winds at SBO during 500-mb trough (Fig. 28) and 500-mb ridge events (Fig. 29) shows very little difference in the wind fields in the lowest 2 km. Perhaps the greatest effect of synoptic forcing in this area is reflected in the mixing heights. The maximum ozone levels at Hesperia (HES) showed little relationship to any of the meteorological variables.

To examine possible transport of ozone and ozone precursors through the Cajon Pass, two data sets were created. One data set consisted of cases when the maximum daily ozone level at SBO exceeded those at HES by at least 5 pphm (Case 1). The other data set consisted of cases when the maximum ozone level at HES exceeded those at SBO on ozone violation days at HES (Case 2). For all cases, SBO and HES maximum ozone levels showed a significant relationship ($r = +0.43$). A time series of ozone levels on Case 1 days (Fig. 30) shows a peak in ozone at SBO occurring at 1500 PDT following a rapid rise in ozone levels beginning near sunrise (0600 PDT). Levels at HES exceed those at SBO during the nighttime hours. As discussed previously, this is likely related to the minimal nitric oxide scavenging in the high desert area. Ensemble wind averages from SBO (Fig. 31) and HES (Fig. 32) show transport through the Cajon Pass from SBO to HES during the daytime hours. The height of the Cajon Pass is 1250 m ASL which is 736 m higher than the SBO site.

A time series of average ozone levels for Case 2 days (Fig. 33) shows the SBO peak occurring at 1400 PDT while the HES peak occurs 1 hour later. Hesperia ozone levels exceed those at SBO for all except the mid-morning to mid-afternoon hours. This is the time when dispersion in the high desert would likely exceed that in the SoCAB. An examination of ensemble winds for Case 2 days shows some differences from Case 1 days. Afternoon winds at SBO are stronger on Case 2 days when compared to Case 1 days. The stronger winds may account for the earlier time of maximum concentration and lower ozone levels. Besides the stronger afternoon winds, Case 1 and Case 2 winds at SBO look remarkably similar. Hesperia winds are continuously through the Cajon Pass (towards HES), and stronger, on Case 2 days.

An examination of cases when SBO maximum ozone levels exceeded those at HES by at least 9 pphm (14 cases) showed an average mixing height at SBO of 695 m. The elevation difference between SBO and the top of the Cajon Pass is approximately 700 m. Perhaps for these cases, ozone and ozone precursors were trapped below the subsidence inversion and could not enter the SEDAB. For Case 2 days, mixing heights at SBO averaged just over 1100 m, a height well above the top of the Cajon Pass.

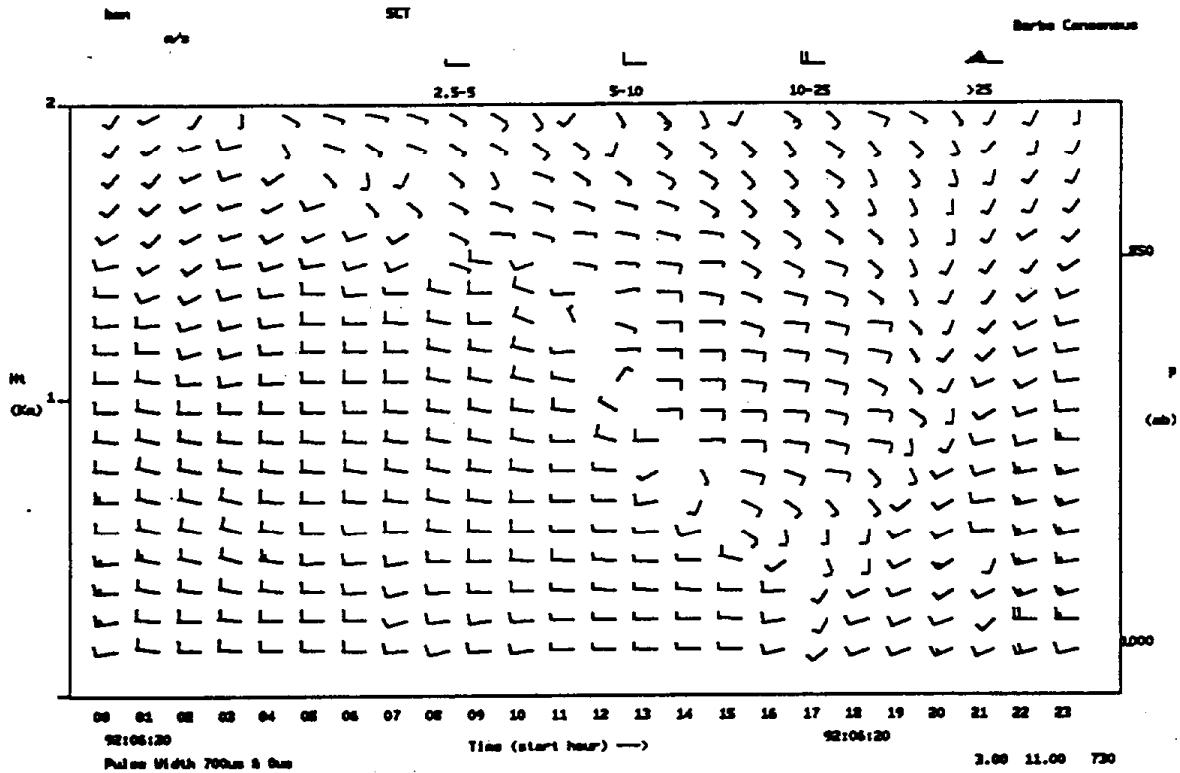


Figure 24. Ensemble average time-height cross section of winds at BAN for high ozone days in Palm Springs. Times are in GMT for comparison with synoptic maps.

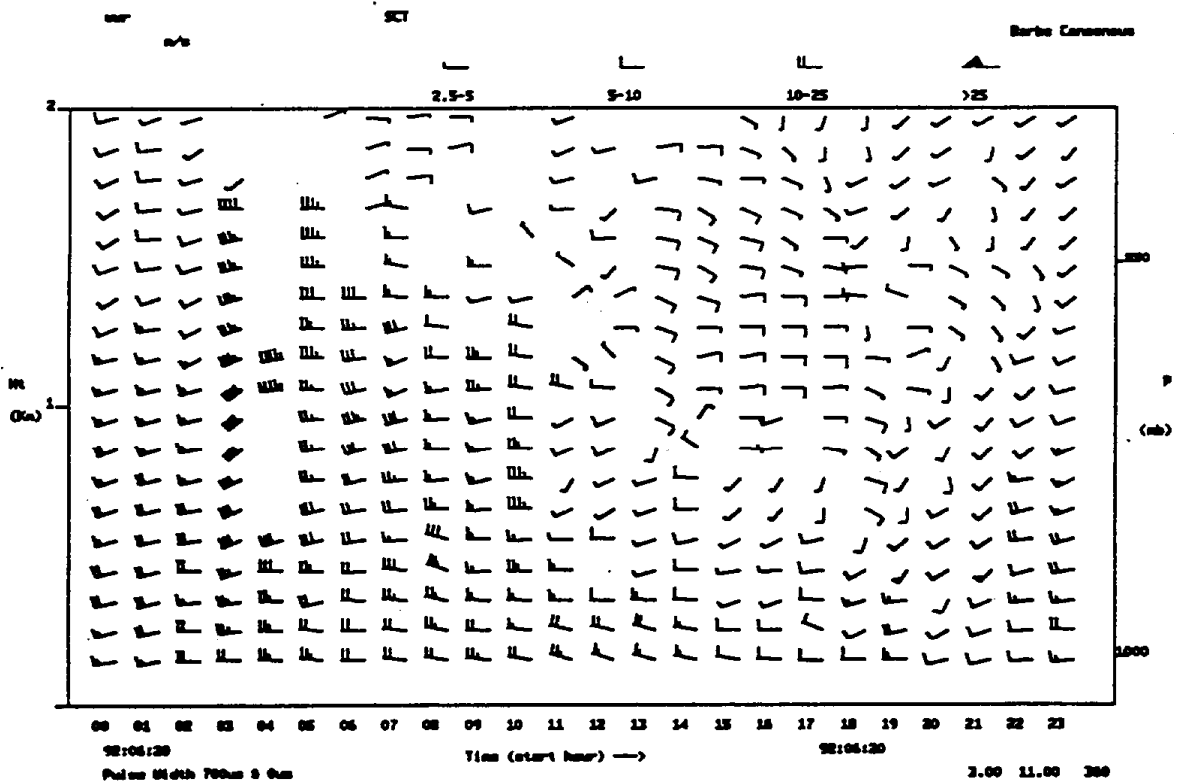


Figure 25. Ensemble average time-height cross section of winds at WWR for high ozone days in Palm Springs. Times are in GMT for comparison with synoptic maps.

Banning High Ozone Days (7 days)

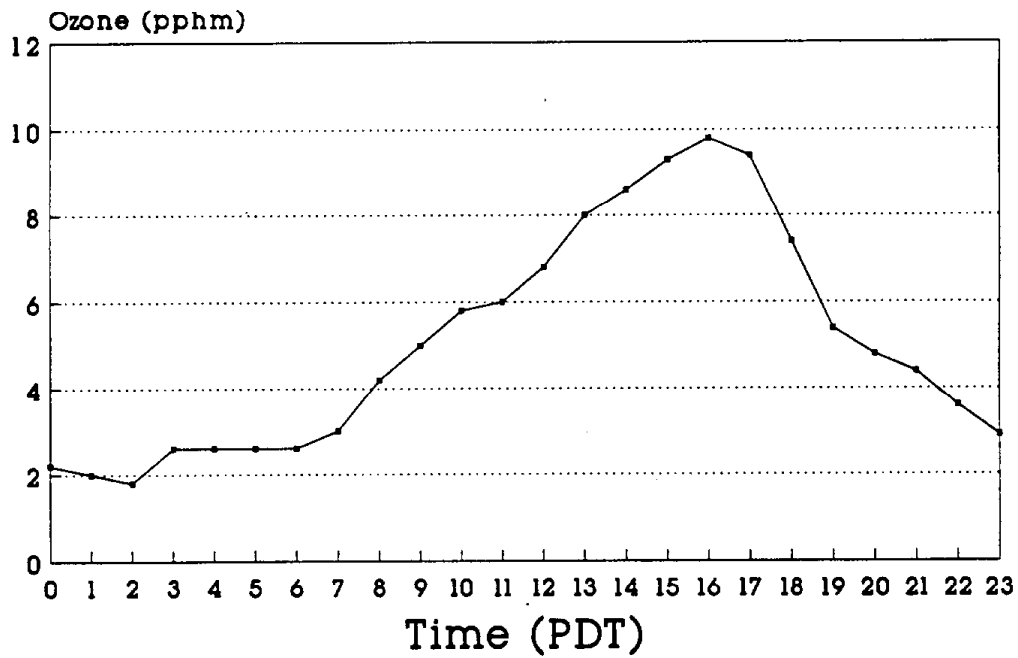


Figure 26. Time series of average ozone during high ozone days in Palm Springs.

Palm Springs High Ozone Days (7 days)

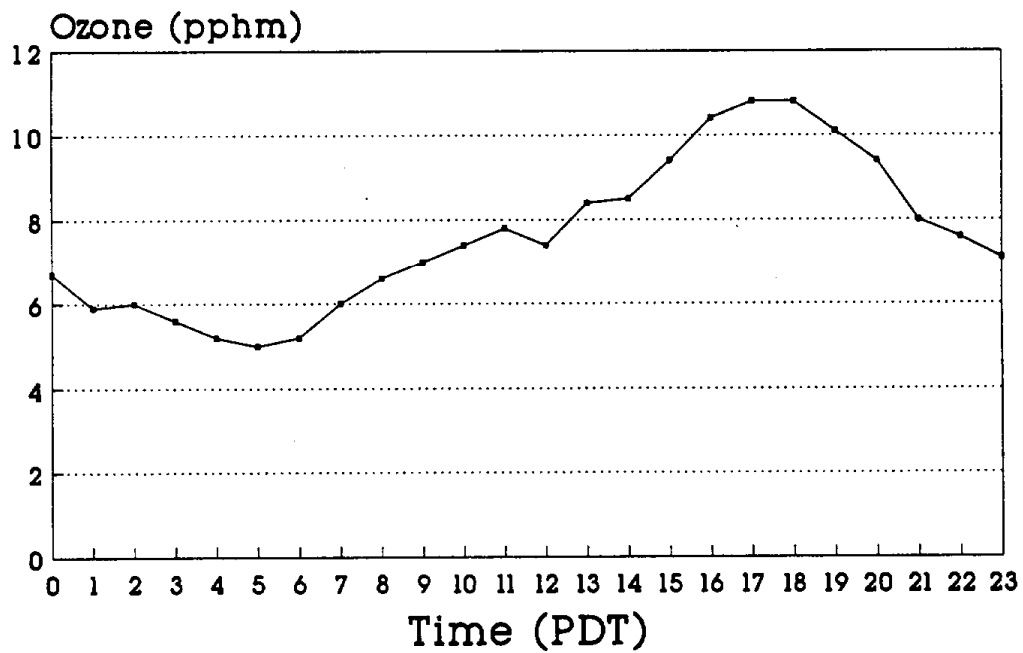


Figure 27. Time series of average ozone at Banning during high ozone days.

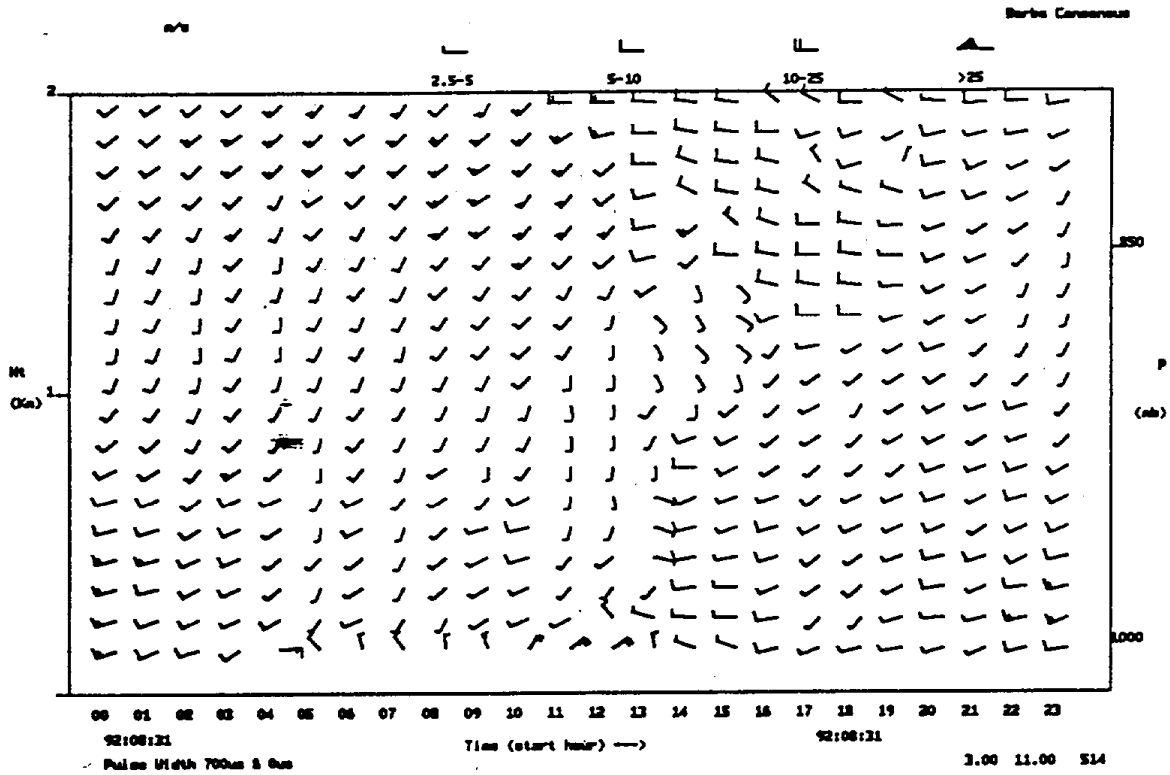


Figure 28. Ensemble average time-height cross section of winds at SBO during 500-mb trough cases. Times are in GMT for comparison with synoptic maps.

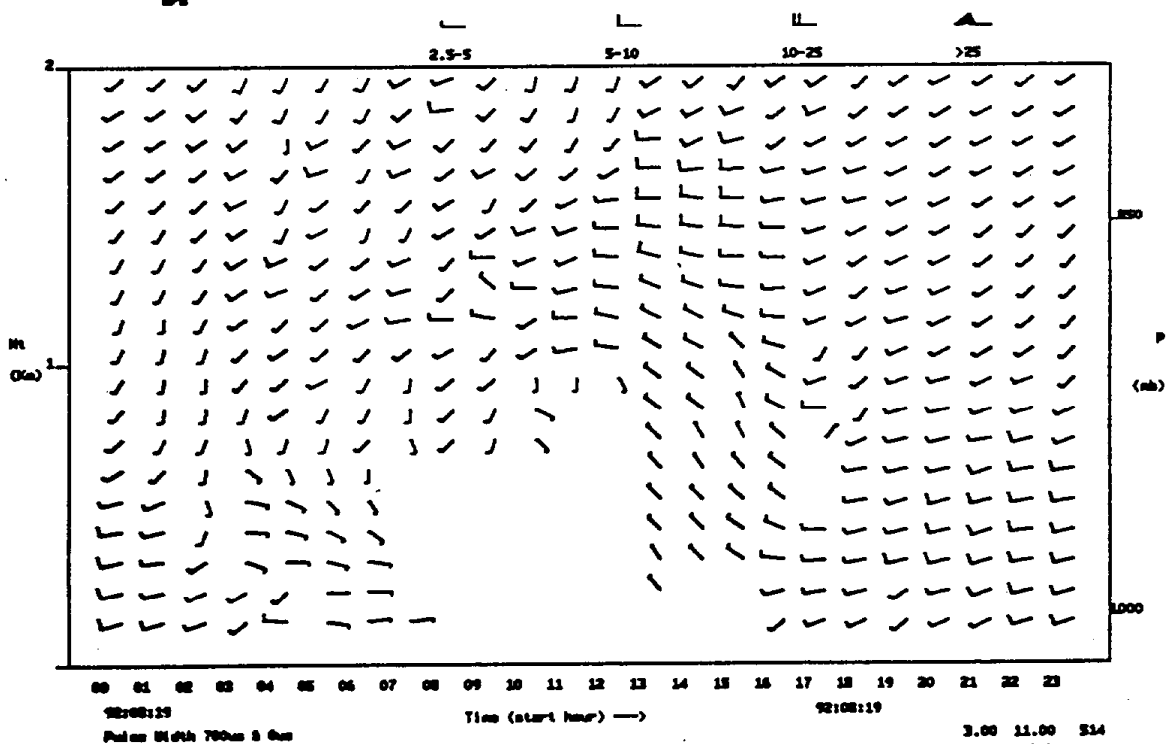


Figure 29. Ensemble average time-height cross section of winds at SBO for 500-mb ridge cases. Times are in GMT for comparison with synoptic maps.

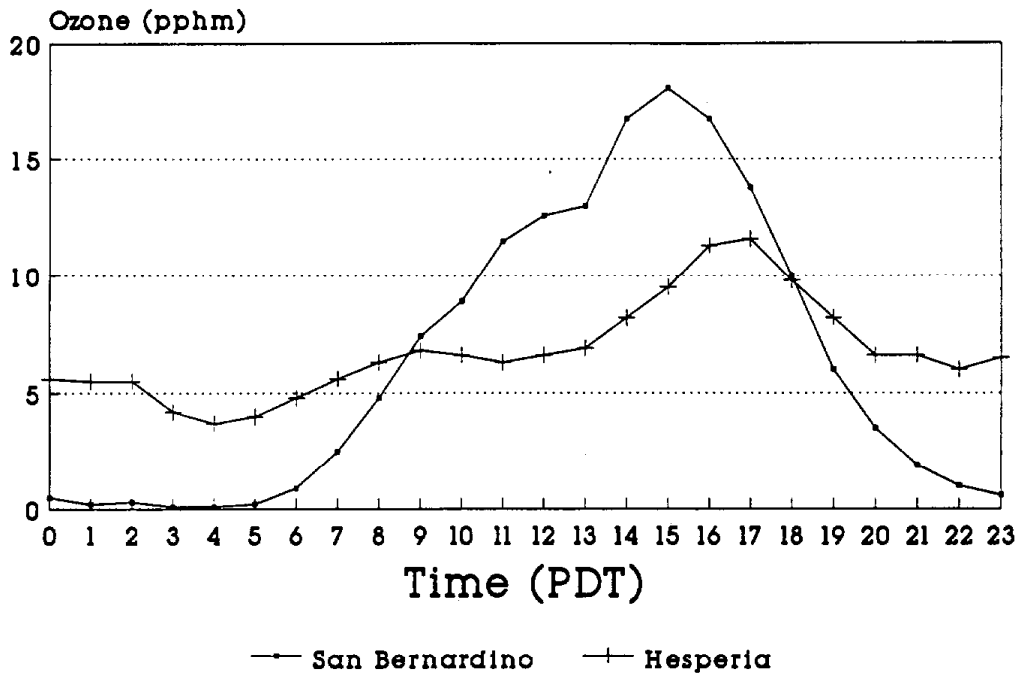


Figure 30. Time series of average ozone levels on Case 1 days at SBO and HES.

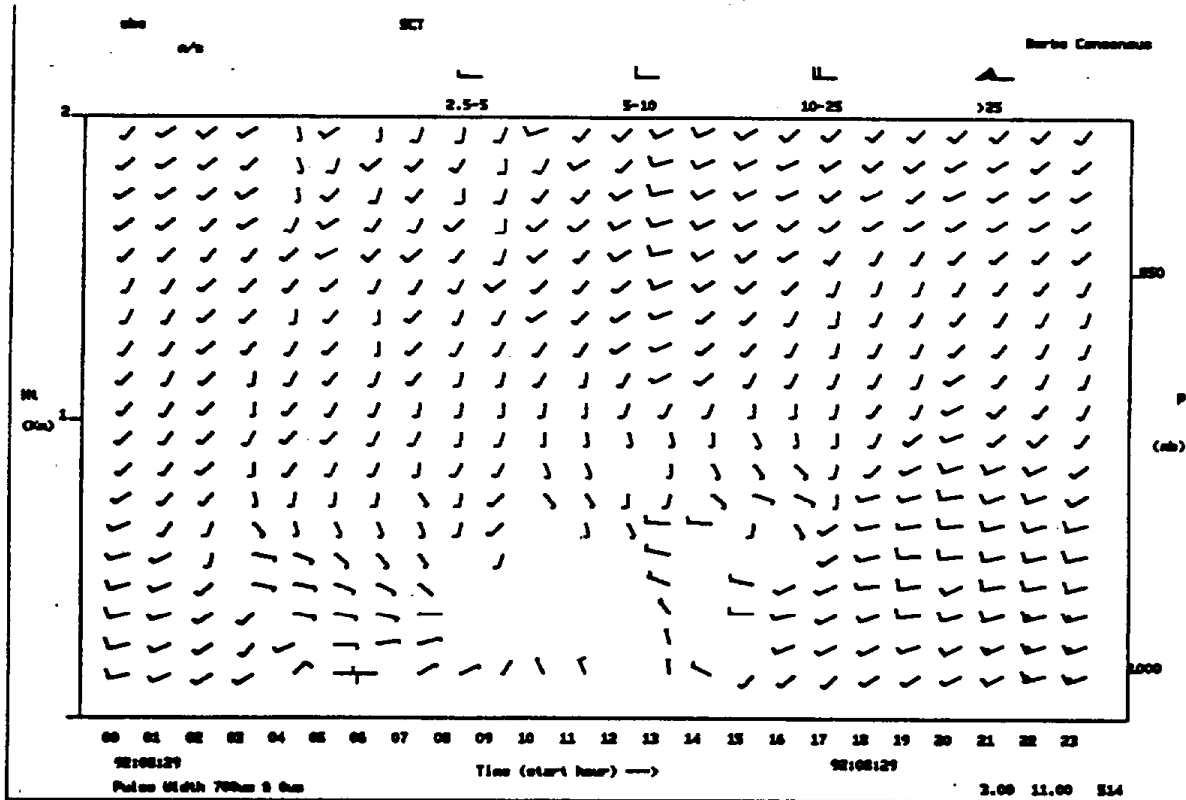


Figure 31. Ensemble average time-height cross section of winds at SBO for Case 1 days. Times are in GMT for comparison with synoptic maps.

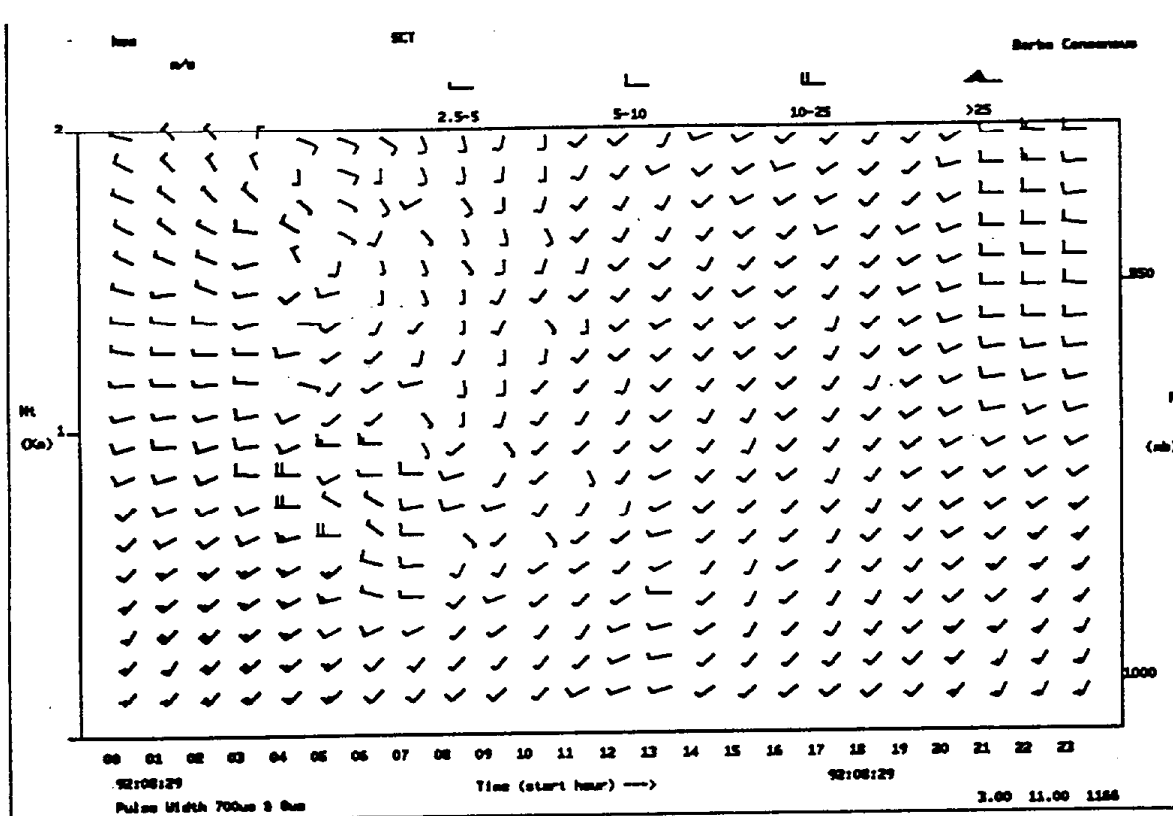


Figure 32. Ensemble average time-height cross section of winds at HES for Case 1 days. Times are in GMT for comparison with synoptic maps.

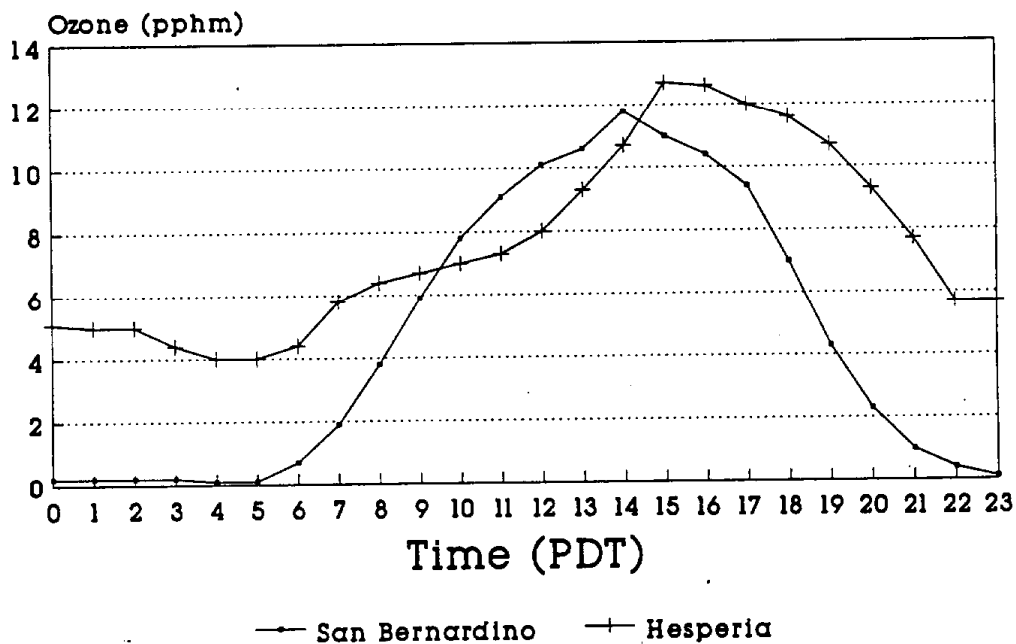


Figure 33. Time series of average ozone levels at SBO and HES for Case 2 days.

11.4 Soledad Canyon Transport

The data set was rather limited for examining the potential for transport through Soledad canyon, consisting of the profiler data obtained at Palmdale (PAL; Fig. 2), located approximately 10 km northeast of where the canyon meets the Antelope Valley. Ozone values were obtained from Lancaster, located 15 km northwest of the PAL site and 20 km north of Soledad Canyon. The data were stratified according to maximum ozone values recorded at the Lancaster monitoring station. Maximum ozone concentrations less than 8 pphm were classified as low ozone days while days with values exceeding 9 pphm were classified as high ozone days. Data from the months of July, August, and September were used for the analysis. Winds obtained at 200 m, 1000 m and 2000 m above ground level were summarized as speed distributions as a function of directional class interval for the high and low ozone days. The time period used for the analysis of transport was for the twelve hour period beginning at 1200 PDT (1900 GMT). It was assumed that most of the transport would occur during this time interval. Transport through the Soledad Canyon would appear as wind directions in the southwest quadrant at PAL. The results show that for high ozone days in Lancaster (18 days) the winds at PAL do indeed suggest transport through Soledad Canyon into the Antelope Valley. Almost all winds at 200 m AGL were within the southwest quadrant with speeds generally greater than 4 ms⁻¹. The majority of winds at 1 km AGL were also within the southwest quadrant. The wind distributions for the low ozone days (33 days) duplicated those obtained for the high ozone cases. The results suggest that almost constant transport from the SoCAB occurs in this part of the SEDAB during the summer months. Other meteorological factors must account for the variability of ozone concentrations at the Lancaster monitoring station.

11.5 Tehachapi Pass Transport

To examine the potential for transport from the San Joaquin Valley Air Basin (SJVAB) into the SEDAB through the Tehachapi Pass, profiler data obtained at the Mojave (MOJ; Fig. 2) and Barstow (BAR; Fig. 2) sites were analyzed. The MOJ site was located 10 km southeast of the Tehachapi Pass at an elevation 375 m lower than the top of the pass at the town of Tehachapi. Transport from the SJVAB into the SEDAB would appear as winds in the northwest quadrant at this site. The BAR site was 100 km east of MOJ and 125 m lower in elevation. The Barstow monitoring site may likely be impacted by transport through the Cajon Pass, Soledad Canyon, and Tehachapi Pass. As in the previous discussion, the data were stratified according to high and low ozone days, but this time for the Barstow monitoring site. The Barstow air quality monitoring station is the nearest station downwind of the Tehachapi Pass. The months of June and July were used for the analysis. For high ozone days in Barstow, MOJ winds at 200 m were almost constantly in the northwest quadrant and fairly strong (> 10 ms⁻¹). Winds at 1 and 2 km were generally in the southwest quadrant with lower speeds than those observed at 200 m AGL. These results suggest that during high ozone days in Barstow, strong transport existed through the Tehachapi Pass. Similar to the analysis for the Soledad Canyon, strong transport also existed through the Tehachapi Pass on low ozone days in Barstow. The major difference was for low ozone days, the westerly winds at MOJ were deeper and stronger than those observed on the high ozone days.

A spatial interpolation scheme (described earlier in the report) was utilized to illustrate the fate of the air transported through the Tehachapi Pass using the terrain and profilers indicated in Fig. 34. The data were again stratified according to ozone concentrations at the Barstow monitoring station. The vector plot for high ozone days is shown in Fig. 35 while the plot for low ozone days is shown in

Fig. 36. The BAR profiler site appears as a black dot in the lower right hand section of the surface plot while the MOJ site is located in the upper right hand section. The black lines originating at the MOJ site represent streamlines originating at this location. As shown in the figures, for both high and low ozone days in Barstow, an air parcel transported through or over the Tehachapi Pass from the SJVAB will be deflected towards the north, west of Barstow, and have little impact on ozone levels in the SEDAB.

By way of contrast, we also examined mixed layer behavior and vector wind patterns for conditions of high and low ozone concentrations at San Bernardino for the domain shown in Fig. 36. Because of the relative density of wind profilers in this area, consistent wind field patterns could be obtained, unlike the offshore areas influencing San Diego. Figure 37 shows the evolution of the averaged mixed layer through an entire diurnal cycle for 9 low-ozone days at San Bernardino while Figure 38 shows the corresponding vector wind averages for 1700 PDT (0100 GMT). Figures 39 and 40 show the mixed layer depth and vector wind fields for the average of 22 high-ozone days. Note that in Figs. 35-40, winds have been plotted at elevations relative to sea level whereas the mixed layer depth is relative to local ground level. This gives a better appreciation of local mixing processes in the presence of significant variations in topography; in the Sacramento Valley portion of the study this was not necessary because all the sites were close to sea level. Appendices J and K contain the hourly data for the full diurnal cycle for low- and high-ozone cases respectively.

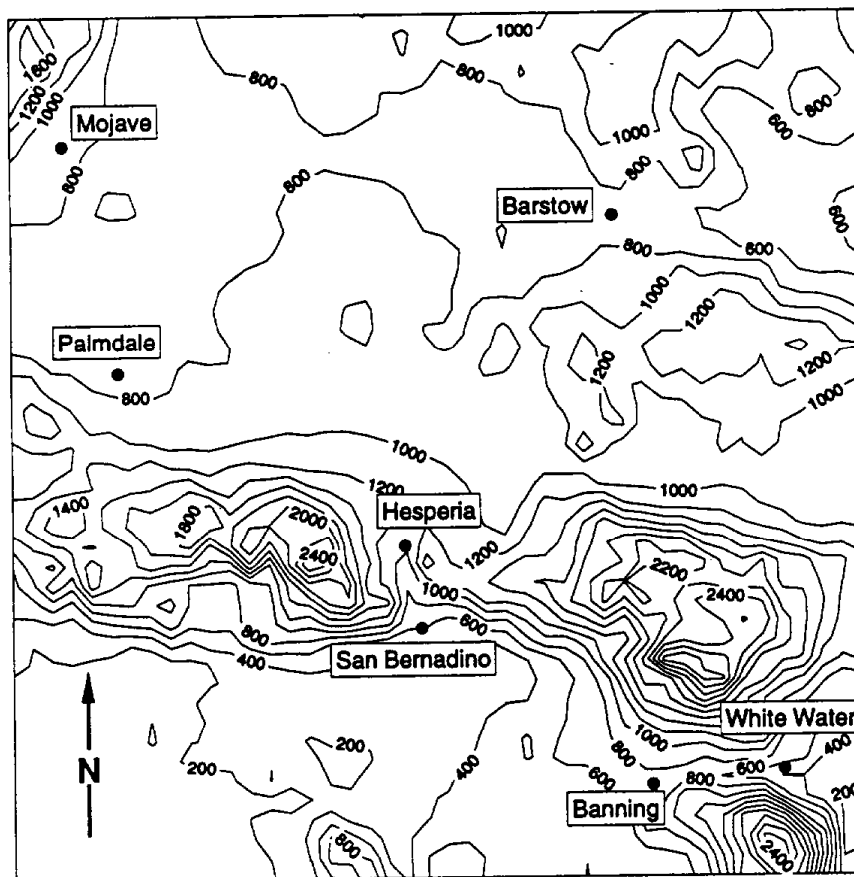


Figure 34. Terrain and profiler locations used in the determination of mixed layer depth and vector averaged wind fields for low- and high-ozone cases shown in Figs. 35-40.

0000 GMT
HIGH O3 (BARSTOW)

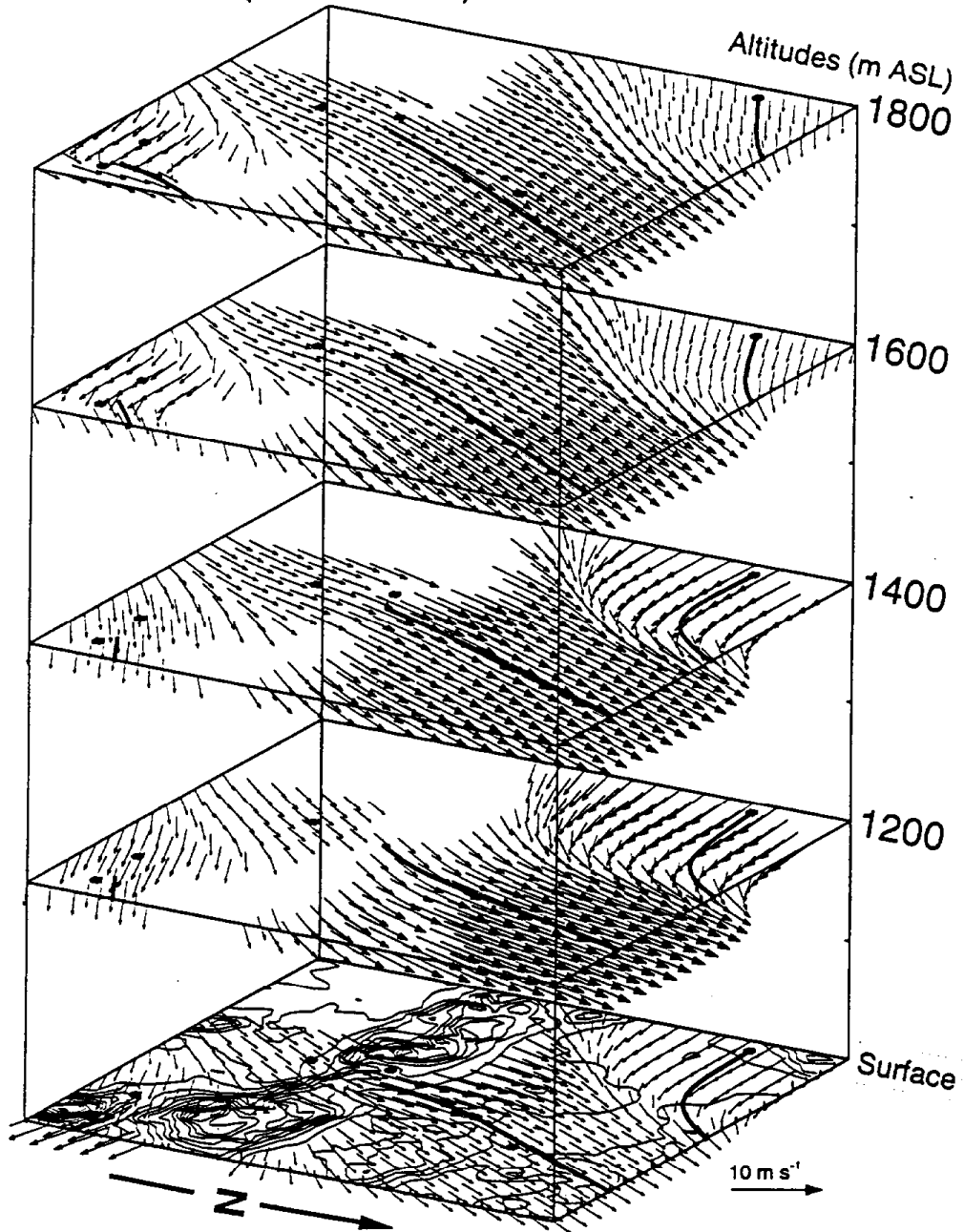


Figure 35. Vector winds for high ozone cases in Barstow. Winds were derived from 1700 PDT surface and profiler data.

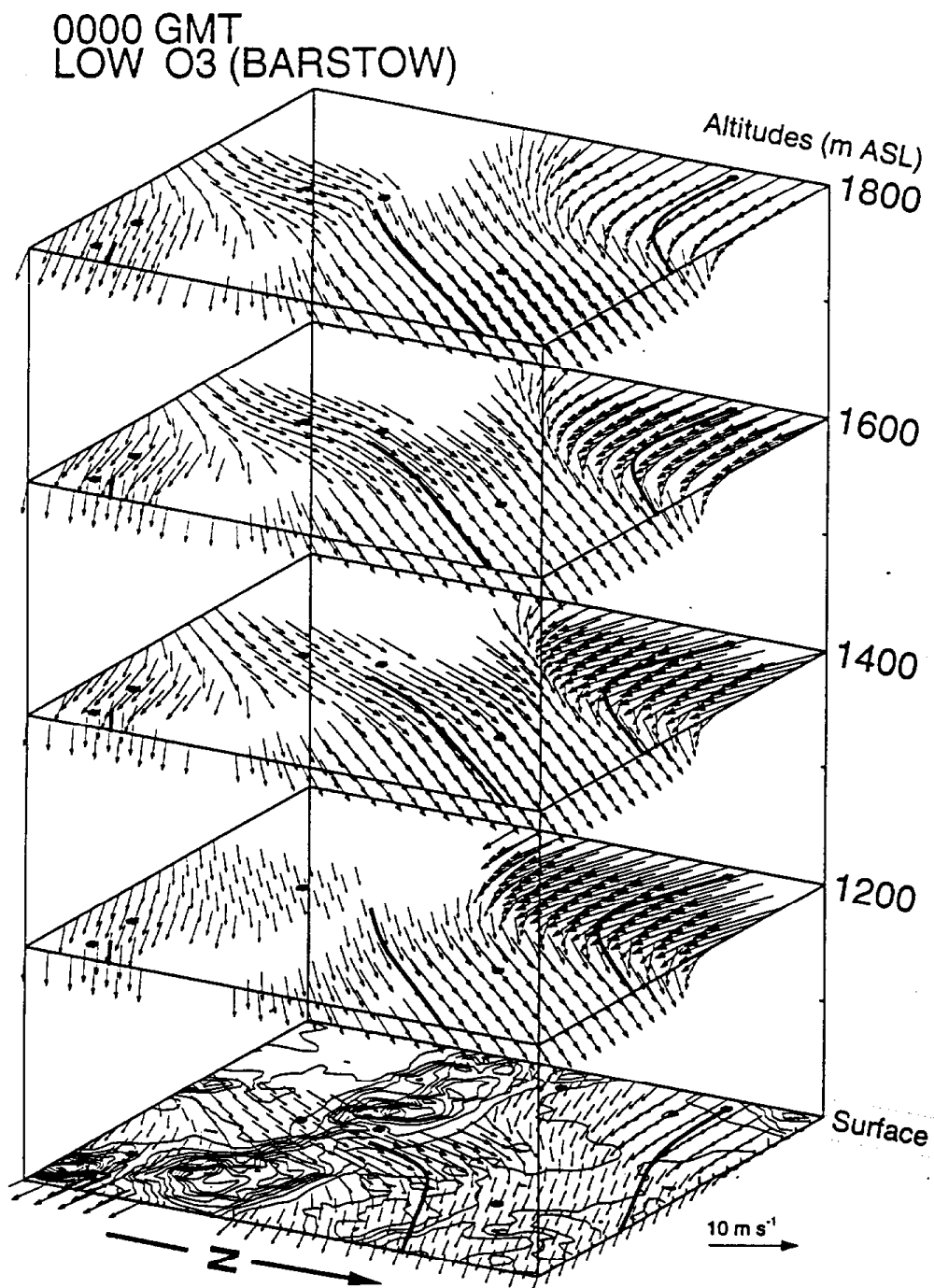


Figure 36. Vector winds for low ozone cases in Barstow. Winds were derived from 1700 PDT surface and profiler data.

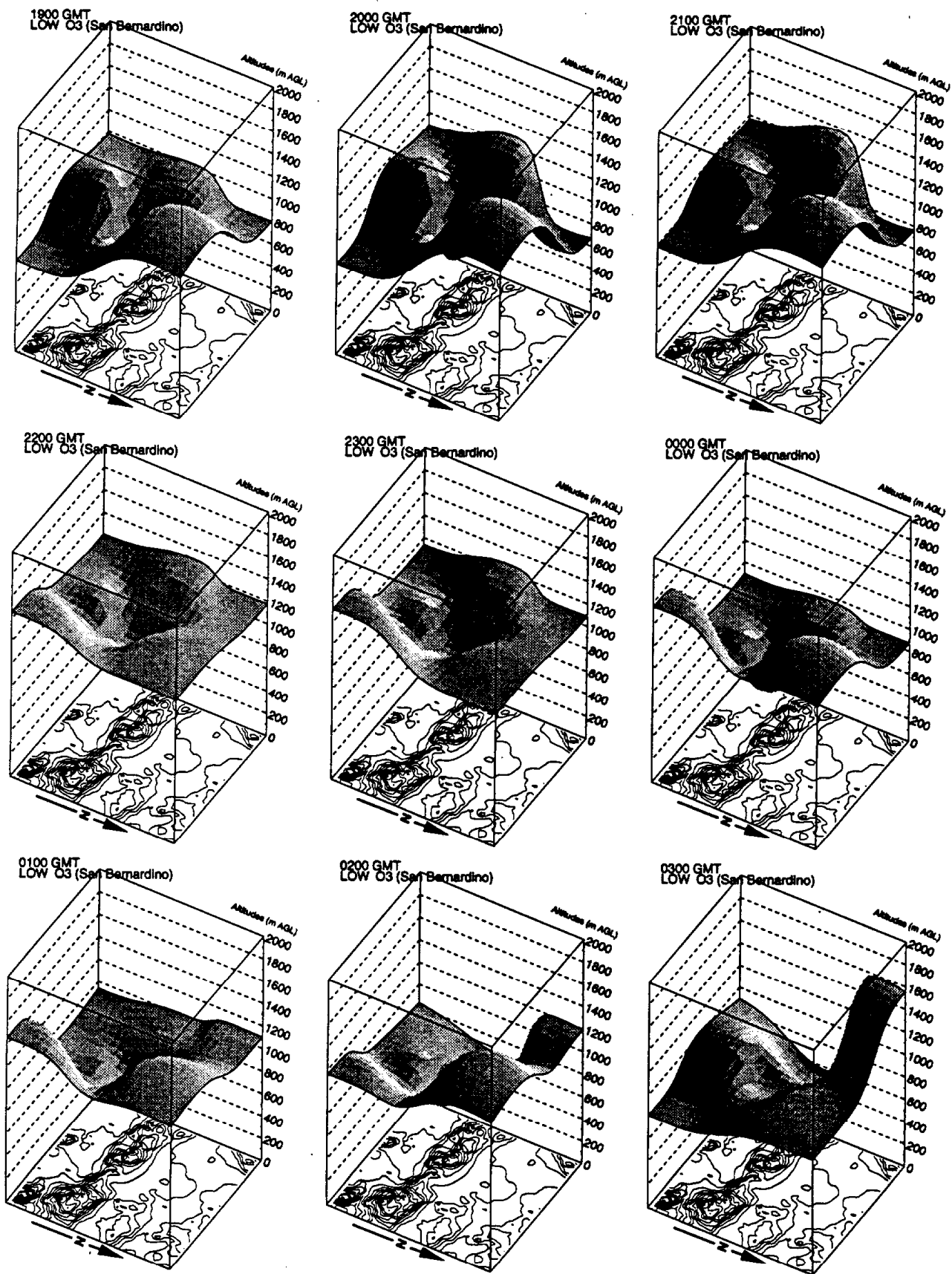


Figure 37. Mixed layer depth (m above ground level) averaged over 9 low ozone days in San Bernardino.

0000 GMT
LOW O3 (San Bernardino)

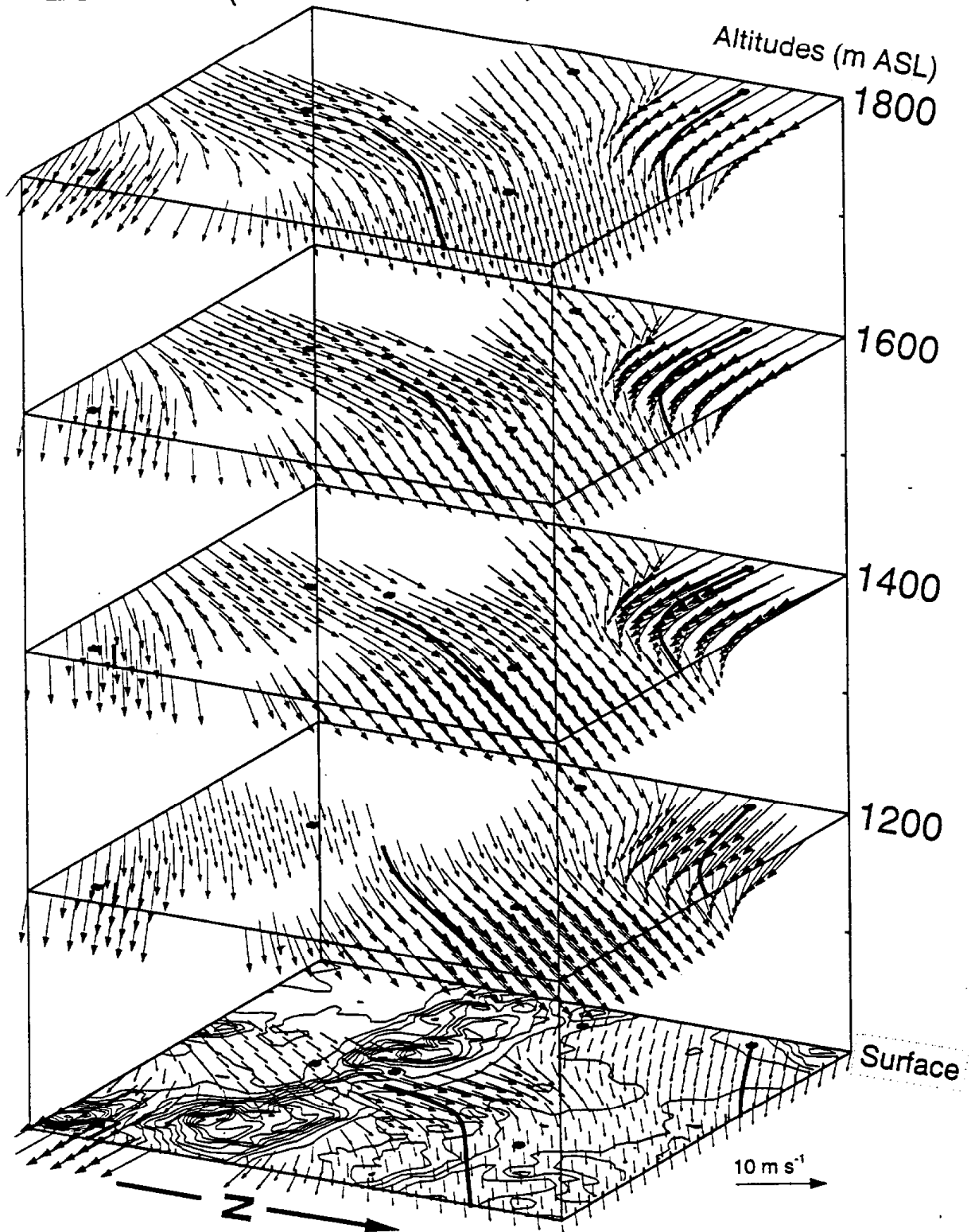


Figure 38. Vector-averaged winds for the same periods as in Fig. 36.

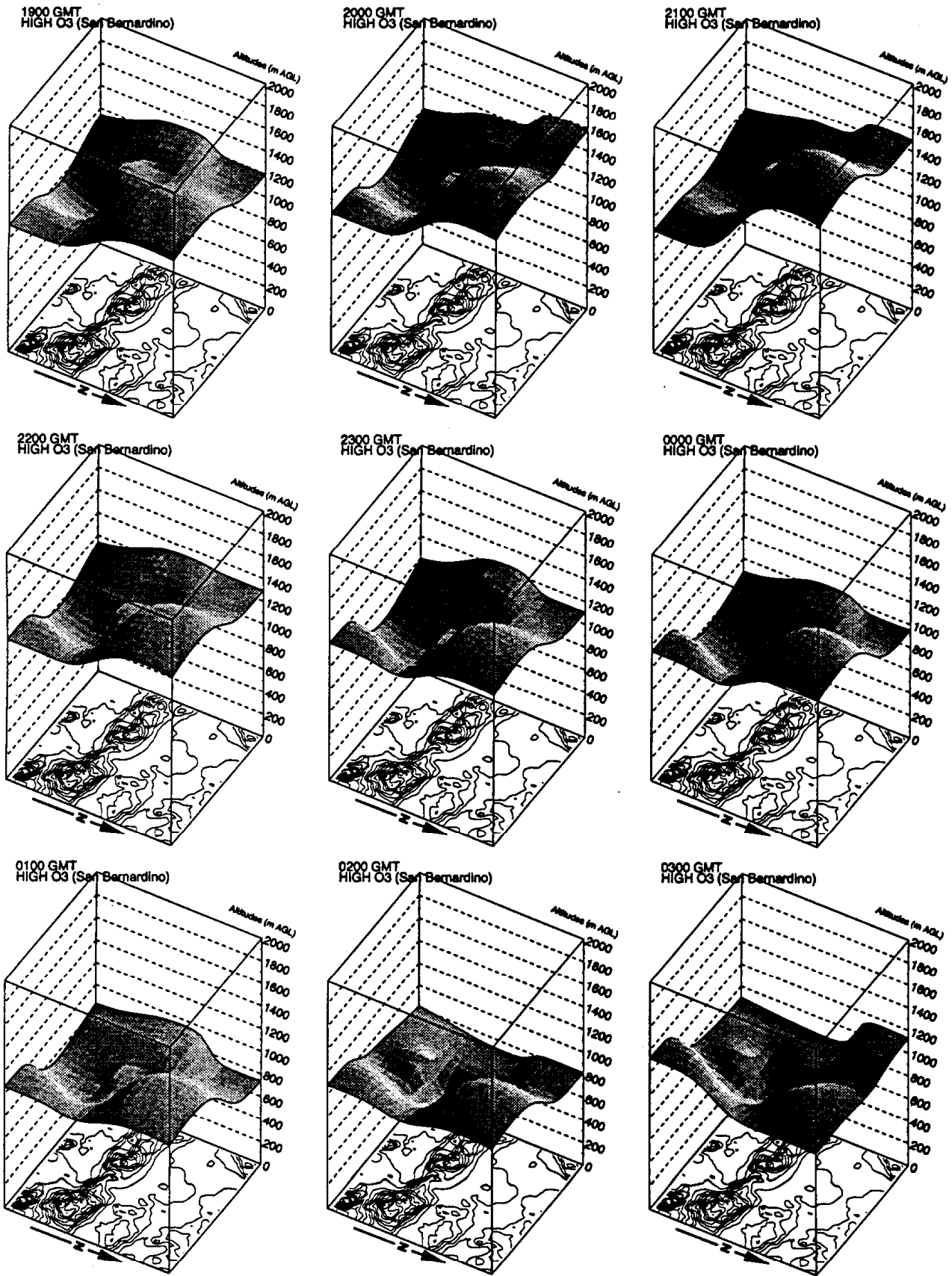


Figure 39. Mixed layer depth (m above ground level) averaged over 22 high-ozone days in San Bernardino.

0000 GMT
HIGH O3 (San Bernardino)

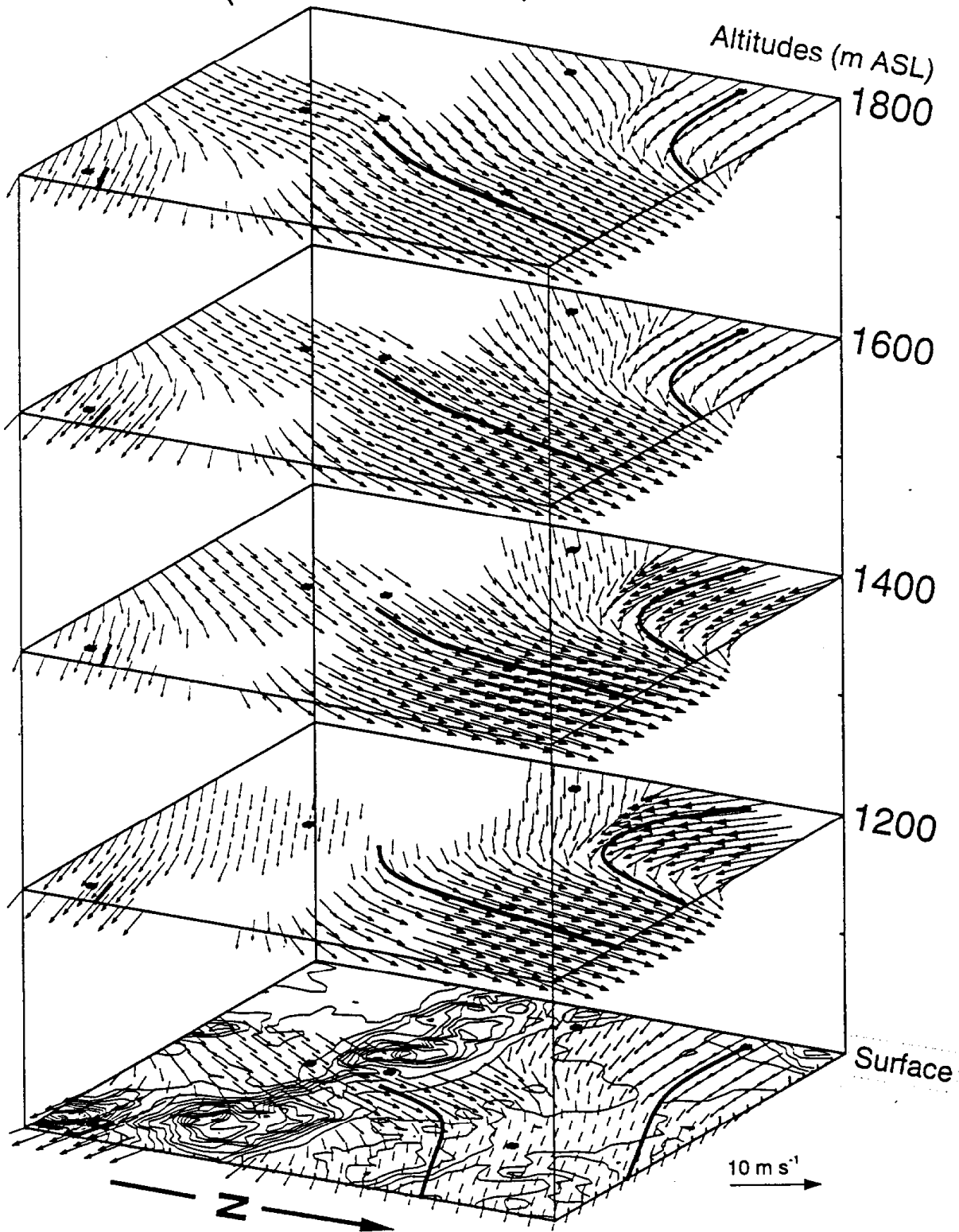


Figure 40. Vector-averaged winds for the same period as in Fig. 38.

Comparing Figs. 37 and 39 during the period from 0100 GMT to 0300 GMT shows a much more rapid growth of the mixed layer at the Mojave profiler site in the late afternoon/early evening period during low-ozone days at San Bernardino. Because this rapid growth occurs at only one site, it suggests that some caution be used in interpreting its source. Inspection of winds as shown in Appendix K indicates a much stronger westerly flow from the San Joaquin Valley over Mojave during low-ozone days in San Bernardino than during high ozone days. Similarly, the Palmdale profiler shows stronger southerly flow on low-ozone days. The apparent growth of the mixed layer in Fig. 37 may thus result from an increase convergence of air as well as decreased static stability aloft on the low-ozone days when a 500-mb trough was more likely to be present. It will be useful in future modeling exercises to return to a more detailed analysis of cases such as these.

11.6 Potential For Transport Between The SoCAB And The SEDAB

Profiler wind fields show almost continuous daytime transport in the lowest 500 to 1000 m through the Cajon and Banning Passes during the summer months. The direction of transport is from the SoCAB to the SEDAB. The synoptic weather patterns appear to have only a small influence on the wind fields in both the SoCAB and the SEDAB. The patterns do, however, have an effect on the mixed layer heights. Violations of state ozone standards at SBO are directly related to the mixed layer depth which in turn is related to the 500-mb pattern. The depth of the mixed layer appears to influence the amount of pollutants transported into the SEDAB through the Cajon Pass. Large differences in ozone levels occur between SBO and HES when the height of the mixed layer is below the height of the Cajon Pass. Ozone violations at HES occur with good transport through the Cajon Pass and with mixed layers in the SBO area exceeding the height of the pass. As illustrated in Figs. 35 and 36, during both high and low ozone days at Barstow, the flow of air in the late afternoon is from the SoCAB and the SJVAB into the SEDAB. The difference is that for high ozone days in Barstow, the flow of air at the surface and aloft is directly through the Cajon Pass towards Barstow. During low ozone days, air passing through the Cajon Pass passes south of Barstow while air passing through the Tehachapi Pass passes to the north. These patterns continue throughout the evening hours.

During the summer and early fall, the flow of air is almost continuously from the SoCAB and the SJVAB into the SEDAB. The strength and depth of this flow appears to be related to the synoptic conditions although strong relationships do not exist as they did with the NCT study. High ozone cases within the SEDAB appear to be related to the depth of the marine layer within the SoCAB and the strength and depth of the transport through the various canyons and passes.

12 REFERENCES

- Air Resources Board, Staff, 1989: Proposed Identification of Districts Affected by Transported Air Pollutants which Contribute to Violations of the State Ambient Air Quality Standards for Ozone. Meteorology Section, Modeling and Meteorology Branch, Technical Support Division, October, 1989.
- Air Resources Board, Staff, 1990: Assessment and Mitigation of the Impacts of Transported Pollutants on Ozone Concentrations within California. Technical Support Division and Office of Air Quality Planning and Liaison. June, 1990.
- Air Resources Board Staff, 1990: Technical Guidance Document: Photochemical Modeling. Technical Support Division. August, 1990.
- Air Resources Board, Staff, 1993: Assessment and Mitigation of the Impacts of Transported Pollutants on Ozone Concentrations within California. Technical Support Division, Draft Report, June 1993.
- Angevine, W.M., A.B. White, and S.K. Avery, 1994: Boundary layer depth and entrainment zone characterization with a boundary layer profiler. *Bound.-Layer Meteor.*, to appear.
- Angevine, W.M., S.K. Avery, W.L. Ecklund, and D.A. Carter, 1993: Fluxes of heat and momentum measured with a boundary-layer wind profiler radar-radio acoustic sounding system. *J. Appl. Meteor.*, **32**, 73-80.
- Beecher, E.A., 1988: Analysis of temperature and velocity microturbulence parameters from aircraft data and relationship to atmospheric refractive index structure. **M.S. thesis**, Pennsylvania State University.
- Blumenthal, D.L., T.B. Smith, D.E. Lehrman, R.A. Rasmussen, G.Z. Whitten, and R.A. Baxter, 1985: *Southern San Joaquin Valley Ozone Study, Final Report*. Prepared for Western Oil and Gas Association (WOGA), Los Angeles, Contract No. 84-8.0.05(2)-07-01 by Sonoma Tech., Inc., and Systems Applications, Inc. STI Report 94100-510-FR, 143 PP.
- Carroll, J.L., and R.L. Baskett, 1979: Dependence of air quality in a remote location on local and mesoscale transports: A case study. *J. Appl. Meteorol.*, **18**, 474-486.
- Chertock, B., C.W. Fairall, and A.B. White, 1993: Surface-based measurements and satellite retrievals of broken cloud properties in the Equatorial Pacific. *J. Geophys. Res.*, **98**, 18,489-18,500.
- Ecklund, W.L., D.A. Carter, and B.B. Balsley, 1988: A UHF windprofiler for the boundary layer: Brief description and initial results. *J. Atmos. Oceanic Technol.*, **5**, 432-441.
- Ecklund, W.L., J.L. Green, D.A. Carter, W.L. Clark, P.E. Currier, J.M. Wanock, and K.S. Gage, 1989: "Summertime observations in Illinois using two wind profilers", in *Preprints for the 24th Conference on Radar Meteorology, March 27-31, 1989, Tallahassee, FL*. American Meteorological Society, Boston, MA, 701-704.
- Ecklund W. L., Carter D. A. and Balsley B. B. (1988) A VHF wind profiler for the boundary layer: Brief description and initial results. *J. Atmos. Oceanic Technol.* **5**, 432-441.
- Ecklund W. L., Carter D. A., Balsley B. B., Currier P. E., Green J. L., Weber B. L. and Gage K. S. (1990) Field tests of a lower tropospheric wind profiler. *Radio Sci.* **25**, 899-906.

- Eckman R. M., Dubosy R. J. and Rao K. S. (1992) Spatial variability of the winds over moderately complex terrain. *Preprints, Tenth Symposium on Turbulence and Diffusion*, Portland, OR, 29 September-2 October, pp. (J4)84-(J4)87. American Meteorological Society, Boston.
- Ecklund, W.L., K.P. Moran, P.E. Currier, B.L. Weber, D.A. Carter, D.B. Wuertz, 1988: "A comparison of 915, 405, and 50 MHz wind profiling radars". *Extended Abstract Volume, Lower Tropospheric Profiling: Needs and Technologies, May 31-June 3, 1988, Boulder Colorado*, National Oceanic and Atmospheric Administration, National Center for Atmospheric Research, and American Meteorological Society, Boulder Colorado, 123-124.
- Ewell, D.M., R.G. Flocchini, and L.O. Myrup, 1989: Aerosol transport in the southern Sierra Nevada. *J. Appl. Meteorol.*, **28**, 112-125.
- Fairall, C.W., 1991: The humidity and temperature sensitivity of clear-air radars in the convective boundary layer. *J. Appl. Meteor.*, **30**, 1064-1074.
- Fairall, C.W., 1984: Wind shear enhancement of entrainment and refractive index structure parameter at the top of a turbulent mixed layer. *J. Atmos. Sci.*, **41**, 3472-3484.
- Fitzwater M. D. (1981) Summer and fall low-level mesoscale wind patterns in the Sacramento Valley, California. Ph.D. dissertation, 188 pp., Dept. of Geophysics, University of California, Davis
- Frenzel, C.W., 1962: Diurnal wind variations in central California. *J. Appl. Meteorol.*, **1**, 405-412.
- Frisch, A.S., and S.F. Clifford, 1974: A study of convection capped by a stable layer using Doppler radar and acoustic echo sounders. *J. Atmos. Sci.*, **31**, 1622-1628.
- Gaynor, J.E., Y.J. Ping, and A.B. White, 1994: Regional mixing heights and transport patterns using radar profilers. *Atmos. Environ.*, submitted.
- Gossard, E.E., 1990: Radar research on the atmospheric boundary-layer. *Radar in Meteorology*, D. Atlas, Ed., Amer. Meteor. Soc., 477-527.
- Hoehne, W.E., 1980: Precision of National Weather Service upper air measurements. NOAA Tech. Memo. NWS T&ED-16, 12pp. [Available from the National Technical Information Service (NTIS), U.S. Dept. of Commerce, Sills Bldg., 5285 Port Royal Rd. Springfield, VA 22161.]
- Intrieri, J.M., C.G. Little, W.J. Shaw, R.M. Banta, P.A. Durkee, R.M. Hardesty, 1990: The land/sea breeze experiment (LASBEX). *Bull. Am. Meteor. Soc.*, **71(5)**, 656-664.
- Isaaks E. H. and Srivastava R. M. (1989) *Applied Geostatistics*, 561 pp. Oxford University Press, New York.
- Kaimal, J.C, N.L. Abshire, R.B. Chadwick, M.T. Decker, W.H. Hooke, R.A. Kropfli, W.D. Neff and F. Pasqualucci, 1982: Estimating the depth of the daytime convective boundary layer. *J. Appl. Meteor.*, **21**, 1123-1129.
- Keith, R.W., 1980: A Climatological - Air Quality Profile. California South Coast Air Basin. South Coast Air Quality Management District, El Monte, CA, January 1980, 165 pp.

- Kessler, R.C., and S.G. Douglas, 1989: Technical Memorandum: Numerical Simulation of Summer Mesoscale Airflow in the Central Valley of California. Technical Support Study #6 prepared for the San Joaquin Valley Air Pollution Study Agency by Systems Applications, Inc., San Rafael, CA. 111pp.
- King, C.W., 1989: Representativeness of single vertical wind profiles for determining volume flux in valleys. *J. Appl. Meteor.*, 28, 463-466.
- Lewis, L.K., J.M. Wilczak, A.B. White, and L. Zhang, 1994: Newly developed X Windows tools for analyzing the boundary-layer structure. NOAA Tech. Memo., NOAA Environmental Research Laboratories, Boulder, CO, to appear.
- May, P.T., K.P. Moran, R.G. Strauch, 1989: The accuracy of RASS temperature measurements. *J. Appl. Meteor.*, 28(12), 1329-1335.
- McCutchan, M.H., and M.J. Schroeder, 1973: Classification of meteorological patterns in southern California by discriminant analysis. *J. Appl. Meteor.*, 12, 571-577.
- Miller, A. and D. Ahrens, 1970: Ozone within and below the west coast temperature inversion. *Tellus*, 22, 328-339.
- Morgan, D.L., D.R. Grose, and K.D. Hansen, 1990: Preliminary study of diurnal winds in the Sierra Nevada. Unpublished Manuscript.
- Morris, R., R. Kessler, L. Chinkin, S. Douglas, 1990: Draft Final Report: Modeling Plan for the San Joaquin Valley Air Quality Study. SJVAQS, Stage One, Phase III, SYSAPP-90/033.
- Neff, W.D., 1990: Remote sensing of atmospheric processes over complex terrain. Chapter 8 in *Atmospheric Processes over Complex Terrain* (W. Blumen, Ed.), American Meteorological Society, Boston, MA, 173-228.
- Neff, W.D., J. Jordan, J. Gaynor, D. Wolfe, W. Ecklund, D. Carter, and K. Gage, 1991: The use of 915-MHz wind profilers in complex terrain and regional air quality studies. American Meteorological Society *7th Conference on Applications of Air Pollution Meteorology, New Orleans, 1991*.
- Ochs, G.R., and R.S. Lawrence, 1972: Temperature and C_n^2 profiles measured over land and ocean to 3 km above the surface. NOAA Tech. Rep. ERL 251-ETL 22, NOAA Environmental Research Laboratories, Boulder, CO, 39 pp.
- Panofsky, H.A., and J.A. Dutton, 1984: *Atmospheric Turbulence*. John Wiley and Sons, 397 pp.
- Pitts, J.N. Jr., 1969: Environmental appraisal: Oxidants, hydrocarbons and oxides of nitrogen. *J. Air Poll. Control Assoc.*, 19, 658-667.
- Reible, D.D., J.R. Ouimette, and F.H. Shair, 1982: Atmospheric transport of visibility degrading pollutants into the California Mojave desert. *Atmos. Environ.*, 16(3), 599-613.
- Reible, D.D., F.H. Shair, and R. Aris, 1983: A two-layer model of the atmosphere indicating the effects of mixing between the surface layer and the air aloft. *Atmos. Environ.* 17(1), 25-33.
- Richter, J.H., D.R. Jensen, V.R. Noonkester, V.R. Konrad, T.G. Arnold, and J.R. Rowland, 1974: Clear air convection: A close look at its evolution and structure. *Geophys. Res. Lett.*, 1, 173-176.

- Roberts, P.T., T.B. Smith, C.G. Lindsay, D.E. Lehrman, and W.R. Knuth, 1990: Analysis of San Joaquin Valley Air Quality and Meteorology. Final Report STI-98101-1006-FR. Prepared for the San Joaquin Valley Air Pollution Study Agency by Sonoma Technology Inc. Available from California Air Resources Board, Sacramento CA.
- Seamon, N.L., 1992: Private communication. The Pennsylvania State University, Department of Meteorology, University Park, Pennsylvania.
- Strauch, R.G., B.L. Weber, A.S. Frisch, C.G. Little, D.A. Merritt, K.P. Moran, and D.o.C. Welsh, 1987: The precision and relative accuracy of profiler wind measurements. *J. Atmos. Ocean. Technol.*, **4(4)**, 563-571.
- Tanrikulu, S., and Su-Tzai Soong, 1990: A numerical simulation of summer wind flow pattern in the central valley of California.
- Ulrickson, B.L., and C.F. Mass, 1990a: Numerical investigation of mesoscale circulations over the Los Angeles basin. Part I: A verification study. *Mon. Wea. Rev.*, **118**, 2138-2161.
- Ulrickson, B.L., and C.F. Mass, 1990b: Numerical investigation of mesoscale circulations over the Los Angeles basin. Part II: Synoptic influences and pollutant transport. *Mon. Wea. Rev.*, **118**, 2162-2184.
- Wakimoto, R.M., and J.L. McElroy, 1986: Lidar observation of elevated pollution layers over Los Angeles. *J. Climate Appl. Meteor.*, **25**, 1583-1599.
- Weber, B.L., and D.B. Wuertz, 1990: Comparison of rawinsonde and wind profiler radar measurements. *J. Atmos. Ocean. Technol.* (In press).
- Weber B. L., Wuertz D. B., Welsh D. C. and McPeck R (1993) Quality controls for profiler measurements of winds and RASS temperatures. *J. Atmos. Oceanic Technol.* **10**, 452-464.
- Wesely, M.L., 1976: The combined effect of temperature and humidity fluctuations on refractive index. *J. Appl. Meteor.*, **15**, 43-49. Wuertz, D.B. And B.L. Weber, 1989: *Editing Wind Profiler Measurements*, NOAA Technical Report ERL 438-ETL 62, NOAA Environmental Research Laboratories, Boulder, Colorado 80303.
- Whiteman, C.D., 1990: Observations of thermally developed wind systems in mountainous terrain. Chapter 2 in *Meteorological Monographs: Atmospheric Processes Over Complex Terrain*. W. Blumen, Ed., Amer. Meteor. Soc., Boston, MA, 5-42.
- Wilczak, J.M., M.L. Cancillo, and C.W. King, 1992: Observations of mesoscale flows in northern California using an array of wind profilers. *Preprints: Sixth Conference on Mountain Meteorology, Portland, OR, 29 Sept-2 Oct 1992*, American Meteorological Society, Boston, MA, 222-227.
- Wilczak, J.M., and J.W. Glendening, 1988: Observations and mixed-layer modeling of a terrain-induced mesoscale gyre: The Denver cyclone. *Mon. Wea. Rev.*, **116(12)**, 2688-2711.
- Wilczak, J.M. and T.W. Christain, 1990: Case study of an orographically induced mesoscale vortex (Denver cyclone). *Mon. Wea. Rev.*, **118(5)**, 1082-1102.
- Wilczak, J.M., W.F. Dabberdt, and R.A. Kropfli, 1991: Observations and numerical model simulations of the atmospheric boundary layer in the Santa Barbara coastal region. *J. Appl. Meteorol.* (Accepted for publication).

- White, A.B., R.G. Strauch, and C.W. Fairall, 1994: A calibration for measuring C_n^2 with the NOAA/ETL/AL 915-MHz radar. NOAA Tech. Memorandum ERL-ETL-239, NOAA Environmental Research Laboratories, Boulder, CO, 11pp.
- White, A.L., C.W. Fairall, and D.W. Wolfe, 1991: Use of 915-Mhz Doppler wind profiler data to describe the diurnal variability of the turbulent mixed layer. American Meteorological Society *7th Conference on Applications of Air Pollution Meteorology*, New Orleans, 1991.
- White, A.B., and C.W. Fairall, 1991: Convective boundary layer structure observed during ROSE-I using the NOAA 915-MHz radar wind profiler. NOAA Tech. Memo. ERL ETL-205, NOAA Environmental Research Laboratories, Boulder, CO, 58 pp.
- White, A.B., C.W. Fairall, and D.W. Thomson, 1991: Radar observations of humidity variability in and above the marine atmospheric boundary layer. *J. Atmos. Oceanic Technol.*, **8**, 639-658.
- White, A.B., 1993: Mixing depth detection using 915-MHz radar reflectivity data. Preprint Vol. *Eighth Symp. on Observations and Instrumentation, Amer. Meteor. Soc., Boston*, 248-250.
- Wyngaard, J.C., and M.A. Lemone, 1980: Behavior of the refractive index structure parameter in the entraining convective boundary layer. *J. Atmos. Sci.*, **35**, 1573-1585.

